

Fabrication and Optimization of Efficient Electrochromic Electrodes and Devices

A THESIS

*Submitted in partial fulfillment of the
requirements for the award of the degree*

of
DOCTOR OF PHILOSOPHY

by
Tanushree Ghosh



**DEPARTMENT OF PHYSICS
INDIAN INSTITUTE OF TECHNOLOGY INDORE
MAY 2023**



Indian Institute of Technology Indore

I hereby certify that the work which is being presented in the thesis entitled **Fabrication and Optimization of Efficient Electrochromic Electrodes and Devices** in the partial fulfillment of the requirements for the award of the degree of **Doctor of Philosophy** and submitted in the **Department of Physics, Indian Institute of Technology Indore**, is an authentic record of my own work carried out during the time period from July 2019 to May 2023 under the supervision of Dr Rajesh Kumar, Professor, Department of Physics, IIT Indore.

The matter presented in this thesis has not been submitted by me for the award of any other degree of this or any other institute.

(22/05/2023)

Signature of the student with date
(Tanushree Ghosh)

This is to certify that the above statement made by the candidate is correct to the best of my/our knowledge.

Signature of Thesis Supervisor with date
(Professor Rajesh Kumar)

Tanushree Ghosh has successfully given her Ph.D. Oral Examination held on **27/06/2023**

Signature of Thesis Supervisor with date
(Professor Rajesh Kumar)

*Dedicated to my family and
teachers.*

Acknowledgement

PhD is not a destination, rather an unparalleled journey of learning and self-determination which can only be achieved with a cumulative effort of many individuals. I, therefore, take this propitious moment to express my heartfelt gratitude to everyone who directly or indirectly impacted my life and made this possible for me. This beautiful journey has indeed taught me a lot and made me a better human.

I am deeply indebted to my thesis supervisor, Professor Rajesh Kumar for his constant support, invaluable patience, and critical feedback. I couldn't have completed this journey without his generous knowledge and ideas and most importantly his selfless guidance. His ideologies has been a constant source of inspiration, helping me push through my limitations and achieve this feat. Additionally, this endeavor wouldn't have been possible without the valuable feedback I received from my PSPC members, Professor Suman Mukhopadhyay (IIT Indore), and Professor Krushna Mavani (IIT Indore) who patiently refined my work year and again.

Besides, I am highly thankful to Professor Pankaj Sagdeo, HOD Department of Physics IIT Indore, Professor Suhas Joshi, Director IIT Indore, and all the faculty members for continuous discussions and their valuable insights about my work. I also extend my gratitude to all my collaborators for providing me with an opportunity to work with them. I especially thank Professor Rahul Banerjee (IISER Kolkata) for his invaluable guidance and support. I thank Professor Rajneesh Misra (IIT Indore), Professor P.K Agnihotri (IIT Ropar), Dr. H.C. Jha (IIT Indore), Dr. Maxim M. Maximov (Peter the Great Saint-Petersburg Polytechnic University, Saint Petersburg, Russia), Dr. Himani Sharma (Doon University, Dehradun), Dr. Sameera (Guru Jambheshwar University, Hisar), Mr. Sayantan Sarkar, Ms. Amrita, and Mr. Vishal for all the learning exchange.

The technical staff of Physics Department, IIT Indore, Mr. Prashant, Dr. Nitin and Mr. Ved Prakash are thanked for their contributions alongside librarian Mr. Rajesh Kumar and all staff members of IIT Indore. I am very grateful to all the hospitality staff (especially, Mr. Siyaram ji), sports staff, Dr. Shilpa Raut, and medical staff of IIT Indore for providing me with all essentials during need. I would like to especially mention members of Physics club and thank Mr. Swapnesh Khade, Mr. Kulbhushan, Mr. Dushmanta, Mr. Utama, Dr. Alestine Mawrie and Dr. Onkar Game for all the learning and opportunities I received.

Any journey is incomplete without the help of friends, and mine too had a lot of them in it. I want to especially thank Mr. Tinto TD for his continuous support and boosting me throughout, Ms. Jinti Barman for her well wishes and insights, Mr. Suruj Jyoti Das for his irreplaceable motivations and Mr. Prince Kaushik for believing in me and making me stronger. Besides I want to thank my colleagues who are no less than friends, Ms. Chanchal Rani, Ms. Suchita Kandpal, Mr. Love Bansal, Mr. Deb Kumar Rath, Ms. Bhumika Sahu and my seniors Dr. Anjali Chaudhary, Dr. Manushree Tanwar, and Dr. Devesh Pathak. In the never-ending list I would finally add a few important names, Ms. Meghna Gangadharan, Dr. Krishnendu S, Mr. Debanjan Bagchi, Mr. Kranthi Panuganti, Mr. Vikas Kumar, Ms. Neha Bhadala, and Dr. Rajarshi Roy for their love and support.

I would finally and with all my heart thank my mother Mrs. Bandana Ghosh for all the non-repayable hard work she has done to make me who I am today, my father Mr. Tapan Kumar Ghosh without whose knowledge, wisdom and support this journey were an impossible matter, my sister Dr. Tapashree Ghosh who constantly believed in me and supported me and the endless love I received from my brother, Mr. Bikramjeet Ghosh. I end here by thanking the Almighty and my heartfelt thanks to all the people mentioned here and others whose names I might have omitted unwillingly.

Tanushree Ghosh

Abstract

Various aspects associated with ‘nanotechnology’ have touched almost every sphere of our day-to-day life. Some of the modern-day gadgets like supercapacitors, batteries, solar panels, electrochromic devices (ECDs) etc. are doing their bit to combat the crisis. Electrochromism or electrochromic (EC) effect is the phenomenon of displaying a visible change in optical property under electrical stimuli and the materials displaying such effect are classified as EC materials (ECM). Spanning around a large range of materials from inorganic to organic and also composites, these materials possess an ability to change their intrinsic band gap structure which visibly results in a change of color thus offering them potential industrial applications. The basic structure of an ECD has a generic five layered design wherein electrochromic materials are chosen on basis of compatibility and the resultant devices are assessed in terms of few established parameters.

In this thesis work, electrodeposition method has been chosen to obtain EC active electrodes which were then fabricated into devices. A conducting polymer, polyaniline has been established as an ambipolar EC material which functions as both p-type and n-type counter layer when sandwiched appropriately with a complimentary pair. Four different category of devices fabricated out of polyaniline confirms its versatile ability of switching in any direction without any change in its properties. An all-organic and a hybrid device has then been fabricated out of polyaniline, ethyl viologen and tungsten oxide, respectively, to further understand the relationship of the complimentary pair theory. Besides, exhibiting excellent EC activities, both the devices appeared to possess certain unique properties which were reported to be the best in their respective family of contemporaries. For example, the all-organic PANI/EV device shows multiwavelength switching starting from visible, up to NIR wavelengths along with uncompromised compatibility in flexible device. The hybrid PANI/WO₃ device on the

other hand reports highest device efficiency in the infrared region promising itself as an excellent candidate for a heat shield device.

Besides its straightforward application in display industry for producing smart windows, ECDs finds multifunctional applications such as supercapacitors, sensors even electrocatalysts. Therefore, in this work, a few electrochromic materials have been thoroughly studied in respect to two other functionalities i.e., energy storage and water splitting. A hybrid core-shell, i.e., PANI@WO₃ was electrochemically fabricated, and the successful formation was first established analyzing its morphology. Then, electrochemistry experiments performed on the core-shell resulted in observation of charge storage, electrocatalytic and electrochromic properties which were confirmed using conventional tools. In a nutshell, the thesis work reports electrochromic electrodes and devices portraying excellent switching times, contrast ratios, and higher efficiency with a scope of further improvement. Besides, it reports a multifunctional hybrid core-shell and its ability to work as an energy storing, generating, and converting electrode, which with further calibrations promises to show better results.

List of Publications:

(a) Peer reviewed journals (Thesis):

1) **T. Ghosh**, S. Kandpal, C. Rani, L. Bansal, M. Tanwar, and R. Kumar; '*Multiwavelength color switching from polyaniline-viologen bilayer: Inching towards versatile all-organic flexible electrochromic device*'. **Adv. Electron. Mater.** **2023**, **9**, **2201042**.

2) **T. Ghosh**, L. Bansal, S. Kandpal, C. Rani, M. Tanwar, and R. Kumar; '*Ambipolar All-Organic Solid-State Electrochromic Device Using Electrodeposited Polyaniline: Improving Performance by Design*' **ACS Appl. Opt. Mater.** **2023**, **1**, **473–480**

3) **T. Ghosh**, C. Rani, S. Kandal, M, Tanwar, L. Bansal, and R. Kumar; '*Chronoamperometric deposition of transparent WO₃ film for application as power efficient electrochromic auxiliary electrode*' **J. Phys. D: Appl. Phys.** **2022**, **55**, **365103**.

4) **T. Ghosh**, L. Bansal, S. Kandpal, C. Rani, D.K. Rath, B. Sahu, and R. Kumar; '*Multifunctional Electrochromic Hybrid PANI@WO₃ Core-Shell for Energy Generation and Storage*' (communicated).

(b) Peer reviewed journals (Outside thesis):

1) **T. Ghosh**, S. Kandpal, C. Rani, A. Choudhary, and R. Kumar; '*Recipe for fabricating optimized solid-state electrochromic devices and its know-how: Challenges and future*' **Adv. Opt. Mater.** **2023**, **2203126**.

2) **T. Ghosh**, S. Kandpal, C. Rani, L. Bansal, and R. Kumar; '*Electrochromic Strategies for Modulation*, **ACS Appl. Opt. Mater.** **2023**.

- 3) **T. Ghosh***, S. Kandpal*, M. Tanwar, D.K Pathak, C. Rani, T. Anusuya, V. Kumar, R. Kumar, and A. Chaudhary; '*Electrochemically reduced graphene oxide/nano-WO₃ composite-based supercapacitor electrodes for better energy storage*'. **Eur. Phys. J. Spec. Top.**, **2022**, **231**, 2927–2932
- 4) **T. Ghosh**, S. Kandpal, D.K Pathak, M. Tanwar, , A. Chaudhary, and R. Kumar; '*Aloe Vera Flower Extract as a Botanical Resistive Memory Element: A Natural Memristor!*' **ACS Appl. Electron. Mater.** **2021**, **3**, 1556–1559
- 5) **T. Ghosh**, S. Kandpal, C. Rani, D.K Pathak, M. Tanwar, A. Chaudhary, and R. Kumar '*Atypical Green Luminescence from Raw Cassia Siamea Extract: A Comparison with Red Emitting *Tinospora Cordifolia**' **ACS Appl. Bio Mater.** **2021**, **4**, 5981–5986.
- 6) **T. Ghosh**, S. Kandpal, C. Rani, D.K Pathak, M. Tanwar, S. Jakhmola, H.C. Jha, M.Y. Maximov, A. Chaudhary, and R. Kumar; '*Synthesizing luminescent carbon from condensed tobacco smoke: bio-waste for possible bioimaging*' **Can. J. Chem.**, **2022**, **100**, 545-551.

(c) Peer reviewed journals (contributory work):

- 1) S. Kandpal, **T. Ghosh**, C Rani, A. Chaudhary, J. Park, P.S. Lee, and R. Kumar; '*Multifunctional Electrochromic Devices for Energy Applications*, **ACS Energy Lett.** **2023**, **8**, 1870–1886
- 2) D.K. Pathak, **T. Ghosh**, S. Kandpal, C. Rani, and R. Kumar; '*All-polymer solid state electrochromic device for low voltage and fast modulation between primary colors*, **Opt. Mater.**, **2023**, **137**, 113519
- 3) D.K Pathak, **T. Ghosh**, and R. Kumar; '*Improved inclusive performance of bi-stacked NiO nanoflakes coated nano-Co₃O₄*

for dual function: An electrochromic-supercapacitor, **J. Energy Storage** **67**, 107643.

4) S. Kandpal, **T. Ghosh**, C. Rani, L. Bansal, M. Tanwar, and R. Kumar; *Tungsten-oxide/Polypyrrole film for hybrid solid-state electrochromic smart window*, **J. Appl. Phys.**, **2023**, **133**, 023101

5) L. Bansal*, **T. Ghosh***, S. Kandpal, C. Rani, M. Tanwar, and R. Kumar; *Exploiting Charge Storage Capabilities of NiTiO₃/TiO₂ for Achieving the Most Efficient Hybrid Electrochromic Device*, **ACS Appl. Eng. Mater.** **2023**, **1**, 577–5835

6) S. Kandpal, **T. Ghosh**, C. Rani, S. Rani, L. Bansal, M. Tanwar, R. Bhatia, I. Sameera, and R. Kumar; *MoS₂ doping and concentration optimization for application-specific design of P3HT-viologen-based solid state electrochromic device*, **J. Phys. D: Appl. Phys.**, **2022**, **55**, 375101.

7) S. Kandpal, **T. Ghosh**, C. Rani, S. Rani, D.K. Pathak, M. Tanwar, R. Bhatia, I. Sameera, and R. Kumar; *MoS₂ nano-flower incorporation for improving organic-organic solid state electrochromic device performance*, **Sol. Energy Mater Sol. Cells.**, **2022**, **236**, 111502.

8) S. Kandpal, **T. Ghosh**, C. Rani, M. Tanwar, M. Sharma, S. Rani, D.K. Pathak, R. Bhatia, I. Sameera, J. Jaybalan and R. Kumar; *Bifunctional Application of Viologen-MoS₂-CNT/Polythiophene Device as Electrochromic Diode and Half-Wave Rectifier*, **ACS Mater. Au** **2022**, **2**, 293–300.

9) S. Kandpal, **T. Ghosh**, M. Sharma, D.K. Pathak, M. Tanwar, R. Bhatia, I. Sameera, A. Chaudhary, and R. Kumar; *Multi-walled carbon nanotubes doping for fast and efficient hybrid solid state electrochromic device*, **Appl. Phys. Lett.** **2021**, **118**, 153301.

- 10) A. Chaudhary, **T. Ghosh**, D.K. Pathak, S. Kandpal, M. Tanwar, C. Rani, and R. Kumar; *Prussian blue-based inorganic flexible electrochromism glucose sensor*, **IET Nanodielectrics**, **2021**, **4**, 165-170.
- 11) B. Sahu, **T. Ghosh**, S. Kandpal, L. Bansal, C. Rani, H.C Jha, and R. Kumar; *Green and Red Luminescent Curcuma and Lawsonia Herbal Amalgam as Yellow Emission Source*, **ChemistrySelect** **2023**, **8** (14), e202204265.
- 12) C. Rani, M. Tanwar, **T. Ghosh**, S. Kandpal, D.K Pathak, A. Choudhary, P. Yogi, S. Saxena, and R. Kumar; *Raman spectroscopy as a simple yet effective analytical tool for determining Fermi energy and temperature dependent Fermi shift in silicon*, **Anal. Chem.** **2022**, **94**, 1510–1514.
- 13) C. Rani, S. Kandpal, **T. Ghosh**, L. Bansal, M. Tanwar, and R. Kumar; *Energy dispersive anti-anharmonic effect in a Fano intervened semiconductor: revealed through temperature and wavelength-dependent Raman scattering*, **Phys. Chem. Chem. Phys.**, **2023**, **25**, 1627-1631
- 14) L. Bansal, C. Rani, **T. Ghosh**, S. Kandpal, S. Chhoker, M. Tanwar, and R. Kumar; *Mesoporous Nickel Titanate–Titanium Oxide Complex Material for Enhanced Energy Storage Application*, **J. Phys. Chem. C.**, **2023**.

Table of contents

Acknowledgements.....	i
Abstract	iii
List of publications.....	v
List of tables.....	xv
List of figures.....	xv
List of abbreviations.....	xxiii
Chapter 1: Introduction.....	1-12
1.1 General background.....	1
1.2 What is electrochromism: the phenomenon	2
1.3 Active chromophores' categories	3
1.4 Electrochromic device (ECD): the concept.....	4
1.5. Device performance parameters	6
1.5.1 Switching time.....	6
1.5.2 Cyclic stability.....	7
1.5.3 Color contrast	7
1.5.4 Coloration efficiency.....	8
1.5.6 Color coordinates through CIE color chart	8
1.5.7 Color rendering index.....	8

1.6	Multifunctional applications.....	8
1.7	Main objective of work.....	10
1.8	Organization of thesis.....	11
Chapter 2: Experimental techniques		13-30
2.1	Electrode fabrication techniques	14
2.1.1	Spin coating method.....	14
2.1.2	Hydrothermal method	15
2.1.3	Electrodeposition method.....	16
2.2	Electrode Characterization techniques	18
2.2.1	Scanning electron microscopy (SEM)	18
2.2.2	Raman spectroscopy	19
2.2.3	Fourier transform spectroscopy (FT-IR).....	20
2.2.4	X-ray diffraction (XRD).....	21
2.2.5	UV-Visible spectroscopy (UV-Vis)	22
2.2.6	Photoluminescence spectroscopy (PL)	22
2.2.7	Electrochemistry.....	23
2.2.7.1	Linear sweep voltammetry	23
2.2.7.2	Cyclic voltammetry	24
2.2.7.3	Galvanostatic charge discharge	25
2.2.7.4	EIS Spectroscopy	25

2.2.7.5	In-situ absorbance spectroscopy.....	26
2.3	Device fabrication methodologies	27
2.3.1	Electrolytic gel composition.....	27
2.3.2	Flip-chip method	27
2.4	Device characterization.....	28
2.4.1	Device kinematics.....	28
2.4.2	In-situ raman spectroscopy.....	29
2.5	Software Used (Osram Sylvania)	29
2.6	Conclusion.....	30
Chapter 3: Polyaniline –based electrochromic device for ambipolar operation.....		31-49
3.1	Why polyaniline?	32
3.2	Deposition of PANI thin film.....	33
3.3	Characterization of PANI film.....	34
3.3.1	Scanning electron microscopy.....	35
3.3.2	Raman spectroscopy	35
3.3.3	Cyclic voltammetry	36
3.3.4	In-situ absorbance spectroscopy.....	38
3.4	Solid state electrochromic device and ambipolar operation	39
3.4.1	A PANI alone linear device.....	40

3.4.2	A PANI/counter ion ECD	41
3.4.3	Bi-layered solid state ECD based.....	46
3.5	Conclusion	49
Chapter 4: Polyaniline/ethyl viologen based all-organic multi-wavelength switching ECD		
51-67		
4.1	An all-organic flexible ECD.....	52
4.2	Ethyl Viologen as electrochromic layer	52
4.2.1	Linear EV solid state device	54
4.3	An ITO/PANI/EV/ITO solid-state device	55
4.3.1	Solid state device fabrication	55
4.3.2	Solid state device performance	57
4.3.2.1	In-situ absorbance spectra	57
4.3.2.2	In-situ Raman spectra.....	58
4.3.2.3	CIE color chart	59
4.3.2.4	Device performance kinematics	60
4.4	Flexible all-organic device	65
4.5	Conclusions.....	67
Chapter 5: Organic-inorganic hybrid electrochromic device using polyaniline/WO₃.....		
69-85		
5.1	Advantages of a hybrid ECD	70
5.2	Tungsten oxide.....	70

5.2.1.1	Deposition of WO ₃ film	71
5.2.2	Characterization of the WO ₃ electrode.....	72
5.2.2.1	Scanning electron microscopy...72	
5.2.2.2	X-ray of WO ₃ film	73
5.2.2.3	Raman spectroscopy	74
5.2.2.4	Cyclic Voltammetry.....	76
5.2.2.5	Absorbance spectroscopy	76
5.2.2.6	Electrode's kinematics	78
5.3	A hybrid solid state PANI/WO ₃ electrochromic device	80
5.3.1	Fabrication of the solid-state device.....	80
5.3.2	Performance characteristics of device	81
5.3.2.1	In-situ absorption spectroscopy.....	81
5.3.2.2	Device performance kinematics	82
5.4	Conclusion	85
Chapter 6: Hybrid electrochromic PANI@WO₃ core-shell for multifunctional energy application.....87-103		
6.1	Hybrid core-shell.....	88
6.2	Fabricating the PANI@WO ₃ core-shell.....	88
6.3	Characterizing the PANI@WO ₃ core-shell	89

6.3.1	Surface morphology.....	89
6.3.2	Raman spectroscopy.....	90
6.3.3	X-ray diffraction.....	91
6.3.4	Fourier transform infrared.....	92
6.4	Multifunctional application of the core-shell electrode.....	93
6.4.1	Super capacitive energy storage properties	93
6.4.2	Electrocatalytic activity.....	98
6.4.3	Electrochromic property of the electrode	100
6.5	Conclusion.....	103
Chapter 7: Conclusions and future scope.....		105-107
7.1	Important conclusions.....	105
7.2	New findings reported in the thesis	106
7.3	Possible future scope	106
7.4	Societal impact of the work	107
Appendices.....		109-111
Appendix A.1	109
Appendix A.2	110
Appendix A.3	110
References.....		113
Annexures.....		131-132

List of tables:

Table No.	Description	Page No.
Table T1	Table showing comparison between various combinations of PANI and EV ECDs.	62
Table T2	Comparison of charge storing abilities, energy, and power densities among various material compositions.	97

List of figures:

Figure No.	Description	Page No.
Figure 1.1	Schematic of a five layered ECD with its incident and transmitted light, defining all of its components.	5
Figure 1.2	Schematic showing various device designs of an ECD.	6
Figure 1.3	Some applications of ECDs in buildings, aircraft, eye wear and as sweat sensors.	9
Figure 2.1	Schematic showing the spin coating mechanism.	14
Figure 2.2	Schematic showing various parts of hydrothermal method.	15
Figure 2.3	Schematic showing three electrode cell setup.	16
Figure 2.4	Schematic showing various parts of an electron microscope	18

Figure 2.5	Schematic showing basic mechanism of Raman spectroscopy.	19
Figure 2.6	Schematic showing basic working mechanism of an FT-IR spectrometer with its inset showing a benzene infrared spectrum.	20
Figure 2.7	Schematic of an X-ray diffractometer.	21
Figure 2.8	Schematic of an UV-Vis spectrometer.	22
Figure 2.9	Schematic explaining emission phenomenon.	23
Figure 2.10	Typical LSV and CV curves of Ferrocene.	24
Figure 2.11	Different shapes of the GCD curves belonging to different material types.	25
Figure 2.12	Typical pattern of Bode and Nyquist plots	26
Figure 2.13	Schematic showing the set up for in-situ absorbance spectroscopy.	27
Figure 2.14	Schematic showing step by step method of flip-chip technique.	28
Figure 2.15	A typical CIE chart wherein various colors has been assigned certain specific co-ordinates.	30
Figure 3.1	Molecular structures of the three different redox state of PANI represented in their corresponding colors.	33
Figure 3.2	Schematic showing redox process of PANI	34
Figure 3.3	SEM images recorded at indicated scale from the PANI film.	35
Figure 3.4	Raman spectrum recorded from the PANI film with inset showing actual image of the as deposited film.	36

- Figure 3.5** CV curve of PANI film obtained in a 0.5M H₂SO₄ electrolytic solution and inset showing actual images of the film at three different bias conditions. 37
- Figure 3.6** CV curves of the PANI electrode recorded in 0.5M H₂SO₄ electrolytic solution at 50mV/s scan rate in two scan directions (a) negative to positive and (b) positive to negative. 38
- Figure 3.7** In-situ absorbance spectra of PANI film recorded in a 0.5M H₂SO₄ electrolytic solution. 39
- Figure 3.8** In-situ absorbance device kinematics showing (a) absorption spectra at three different biases and (b) switching time calculated at 600nm whilst applying a bias of $\pm 1.5V$. 40
- Figure 3.9** Schematic showing molecular structures of PCBM and TTF. 41
- Figure 3.10** (a) Schematic of pPCBMed device fabrication and (b) In-situ transmittance of the device recorded between 2V (ON) and -2V(OFF). 42
- Figure 3.11** In-situ device kinematics of pPCBMed showing (a) potential and current v/s time (b) stability of device (c) switching time and (d) coloration efficiency, all measured at 800nm wavelength. 43
- Figure 3.12** The CIE diagram of the device with color coordinates (u, v, w) along with actual photographs of the device (insets). 44
- Figure 3.13** Schematic of pTTFed device fabrication (a) and (b) In-situ transmittance of the device recorded between 2V (ON) and -2V(OFF). 45

Figure 3.14	In-situ device kinematics of pTTFed showing (a) potential and current v/s time (b) stability of device (c) switching time and (d) coloration efficiency, all measured at 800nm wavelength.	46
Figure 3.15	In situ device kinematics of pP3HTed device at $\pm 1.5V$ showing (a) in-situ absorbance spectra (b) switching time (c) potential and current v/s time graph and (d) coloration efficiency of the device.	48
Figure 3.16	Stability (a) and (b) CV curve of pP3HTed device.	48
Figure 4.1	Schematic showing molecular structure of Viologen.	52
Figure 4.2	CV curve recorded from $EVClO_4$ solution in ACN, recorded at 50mV/s scan rate, showing actual color change of material over an ITO glass slide as inset images.	53
Figure 4.3	In-situ absorbance spectra (a) and device kinematics (b) of a mono layer EV device.	55
Figure 4.4	Schematic showing the fabrication of pEVed device (a) and subsequent colors original device in ON (b) and OFF (c) states.	56
Figure 4.5	Bias dependent in-situ absorbance spectra of pEVed with inset showing images of actual device.	58
Figure 4.6	Bias dependent in-situ Raman spectra of pEVed with inset showing zoomed part the spectrum.	59
Figure 4.7	A CIE chart indicating color co-ordinates of the device.	60
Figure 4.8	In-situ device kinematics recorded at 600nm wavelength	62

Figure 4.9	In-situ device kinematics recorded at 800nm and 1000nm wavelengths.	64
Figure 4.10	Schematic showing device fabrication steps using flexible PET substrates and inset image showing photo of actual device.	65
Figure 4.11	Kinematics recorded from the flexible pEVED device showing (a) in-situ absorbance spectra (b) stability (c) switching times and (d) current and potential v/s time graphs.	66
Figure 5.1	Schematic showing molecular structure of tungsten oxide.	70
Figure 5.2	SEM images from WO ₃ film showing nano flower like structure.	72
Figure 5.3	SEM image showing cross sectional view.	73
Figure 5.4	XRD pattern of WO ₃ film.	74
Figure 5.5	Raman spectrum of WO ₃ film.	74
Figure 5.6	Cyclic voltammograms recorded from WO ₃ films at (a) 100mV/s with inset images showing actual photo of electrode and (b) showing scan rate dependent CV curves.	75
Figure 5.7	In-situ bias dependent absorbance spectra of WO ₃ film.	75
Figure 5.8	Electrode kinematics showing (a) switching time and (b) stability.	77
Figure 5.9	Graph showing current response for voltage v/s time.	78
Figure 5.10	Schematic showing PANI/WO ₃ device fabrication.	79

Figure 5.11	In-situ absorbance spectra of device with inset showing actual photos of device at indicated biases.	80
Figure 5.12	Device kinematics showing (a) voltage pulse and simultaneous current response (b) absorbance response to applied pulse (c) switching times (d) coloration efficiency.	81
Figure 5.13	Switching times reported at (a)700 and (b) 500nm wavelength.	83
Figure 5.14	Devices' stability (a) and CV curve (b)	84
Figure 6.1	Schematic showing core-shell electrodeposition process.	88
Figure 6.2	Images showing SEM micrographs recorded from individual PANI and WO ₃ electrode and PANI@WO ₃ core-shell at indicated scales.	90
Figure 6.3	Raman spectra of (a) PANI@WO ₃ core-shell and (b) WO ₃ and (c) PANI electrode.	91
Figure 6.4	XRD pattern of PANI@WO ₃ core-shell electrode and inset showing the pattern for individual WO ₃ film for comparison.	92
Figure 6.5	FT-IR spectrum for PANI@WO ₃ core-shell electrode.	93
Figure 6.6	(a) Cyclic voltammograms recorded at three different scan rates and (b) peak current v/s square root of scan rate graph.	94
Figure 6.7	(a) CV curve showing electrodes' stability at 1 st and 50 th cycle and (b) Nyquist plot recorded in range 0.1 Hz to 1MHz.	95

Figure 6.8	(a) GCD curves under varying current densities and (b) corresponding current densities v/s areal capacitance with Ragone plot (inset).	95
Figure 6.9	(a) capacitive retention and areal capacitance v/s no. of cycles with stability shown in inset and (b)coulombic efficiency calculation.	98
Figure 6.10	LSV curves recorded from the PANI@WO ₃ electrode at a scan rate of 5mV/s showing (a) HER and (b) OER reactions with inset showing actual bubble formation.	99
Figure 6.11	Tafel plot for (a) OER and (b) HER reactions.	100
Figure 6.12	Electrochromic properties of PANI@WO ₃ electrode on an FTO substrate showing (a) CV curve (50mV/s) along with actual photographs of the electrode (inset) and (b) in-situ bias dependent absorbance spectra recorded at $\pm 0.5V$.	101
Figure 6.13	Electrode kinematics showing (a) current response against bias of $\pm 0.5V$, switching times calculated at (b) 600nm and (c) 1000nm and (d) stability recorded for 1000s	102
Figure A1	Comparison of CV curves obtained from as- prepared and chemically reduced (doped) Aloe Vera flower extracts(a) and (b) solution-state I-V curves under different memory states. (c) Schematic showing switching between two different resistance states using a resistive circuit. (d) I-V curves for 16 consecutive cycles showing on/off switching between two distinct resistive states (inset).	109

Figure A2 Schematic showing the presence of abundant 110 compounds in Cassia and Giloy leaves (a, b) and possible green and red emission process in Cassia and Giloy leaves (c, d), respectively.

Figure A3 Excitation wavelength dependent PL recorded at 111 400, 500, and 550 nm excitation sources. (b) Schematic showing relative red shift in PL emission due to a shift in excitation wavelength, a signature of the giant red-edge effect.

List of abbreviations

Abbreviations	Full forms
ACN	Acetonitrile
CE	Counter Electrode
CV	Cyclic Voltammetry
DCB	Dichlorobenzene
DI water	Distilled Water
EC	Electrochromic
ECD	Electrochromic Device
EIS	Electrochemical Impedance Spectroscopy
EV	Ethyl Viologen
FT-IR	Fourier Transform Infrared
FTO	Fluorine Tin Oxide
GCD	Galvanostatic Charge Discharge
H₂O₂	Hydrogen Peroxide
H₂SO₄	Sulfuric acid
HER	Hydrogen Evolution Reaction
HNO₃	Nitric acid
IR	Infrared
ITO	Indium Tin Oxide
LiClO₄	Lithium Perchlorate
NIR	Near Infrared

OER	Oxygen Evolution Reaction
P3HT	Poly(3-hexyl)thiophene
PANI	Polyaniline
PEO	Polyethylene Oxide
PL	Photoluminescence
RE	Reference Electrode
SEM	Scanning Electron Microscopy
SR	Scan Rate
UV	Ultra-violet
WE	Working Electrode
WO₃	Tungsten Oxide
XRD	X-Ray Diffraction

Chapter 1

Introduction

1.1. General Background

Ever since the beginning of the era of nano science and technology, the field of technological development have seen an upward steep rise. Thanks to Sir Richard Feynman for introducing the concept back in the year 1959, the applications of ‘Nanotechnology’ has crippled almost every sphere of our day-to-day lives[1]. The better understanding of low dimensional structures have not only landed us with supercomputers and gadgets but also helped eradicate some diseases and fight others like cancer, quite potentially[2–5].

While marching forward with available resources is essential, an eye must be kept to not exhaust them such as to invite an energy crisis soon. Some of the modern-day gadgets like supercapacitors, batteries, solar panels, and electrochromic devices are doing their bit to combat the crisis[6–10]. The latter, however, is of our particular interest as the technology behind smart windows is catching eyes of not just material scientists all over but also companies like ‘Chromogenics AB’, ‘Compagnie De Saint-Gobain’ and ‘Hitachi Chemical Co. Ltd’ marketing etc., who are continuously upgrading and selling windowpanes, automobile glasses and even displays fabricated using this technology.

Electrochromism is becoming a promising area in smart devices, including energy related ones, and is occupying a significant place in industry as well hence it becomes important to understand the “know-how” of the composition, fabrication, and optimization to keep updated with the field which has been summarized here in this thesis work.

1.2. What is Electrochromism: the phenomenon

Electrochromism or electrochromic (EC) effect is the phenomenon of displaying a visible change in optical property under electrical stimuli and the materials displaying such effect are classified as EC materials (ECM)[11,12]. With its advent during early 1960s, the field has seen tremendous research in the last few decades where scientists have come up with new materials, new device paradigms and performance optimization through different approaches like complementary electrode combinations and multifunctional application aspects[13,14]. It is well understood that any electrochemical system is governed by two types of current, the faradic and the electric double layer capacitance (EDLC) type. The basic mechanism of ECM is however dictated by faradic process as the redox reactions at the electrode-electrolyte interface leads to the color change of these materials[15].

Since ECM are mainly governed by redox reactions therefore the basic working principle of an ECD includes bias manipulation to achieve optical modulation which may extend beyond the visible range spanning from UV to IR and NIR wavelengths[16,17]. The bias, used for color modulation in the device, drives the electrons to-and-fro through the electrochromic layers between the electrodes and with the help of ions present in the electrolyte the overall process accomplishes a visible change in color thus leading to optical switching[18,19].

By choosing materials effectively, the entire spectral range can be tuned to obtain output colors of interest. Among a very broad category of ECM, which has been listed later on, the color switching mechanism of inorganic and organic materials can be understood separately as (a) in case of inorganic materials, the basic principle governing color change is intervalence charge transfer, and (b) in case of conducting organic polymers however, dynamic doping is responsible for the color change. In the latter, the π - π^* electronic transition between the HOMO-LUMO band gap induced by doping changes the neutral state of the polymer to polaronic and subsequently a bipolaronic state causing spectral changes

in them. The proper understanding of color switching mechanism is one of the most important aspects as it helps one in designing an appropriate ECD for targeted (multifunctional) application(s)[20].

To achieve application-oriented results, the ECMs are expected to show reversible behavior, i.e., to-and-fro switching among the colored/bleached states; highly responsive to bias along with showing long stability and durability[21,22]. These parameters have been thoroughly calibrated to arrive at better performance results. Conventionally a solid state ECD is made up of five layers comprising of an EC layer, an ion storage layer, and an electrolyte gel, all fit in between two transparent conducting substrates. Although the trivial design encompasses the basic requirements of a traditional ECD, a few applications however demand different device structure with additional components which will be discussed later on.

1.3. Active chromophores' categories

The intrinsic behavior of a class of materials, in response to an external voltage, amidst an appropriate surrounding makes them EC active and are termed as chromophores and the phenomenon of such bias induced color switching is commonly known as the electrochromism. For the display of Electrochromism, the fundamental process requires these materials to start an electron flow, followed by an associated color switching, which must be reversible on bias polarity reversal. It is this basic phenomenon that needs to be facilitated in the device form to exploit it for any real-life application. Incorporation of nano materials into electrodes or the ion transport layer provides an added advantage of active reaction surface area thus improvising parameters. Plenty of materials are available that can be used to fabricate devices that show different performance as measured using parameters discussed later.

Though not exclusively, ECMs are broadly categorized into organic and inorganic and mainly includes oxides of transition metals (TMO) like tungsten, vanadium, chromium, cobalt, iron, manganese, molybdenum, nickel, niobium, palladium, titanium etc. and conducting polymers

(CPs)like polyaniline (PANI), polythiophene(P3HT), PEDOT: PSS, polypyrrole (PPy), polyindole (PI) etc. [23–35]. Belonging to the big family of viologens (a bipyridine derivative), in their molecular and polymeric forms, many species have been studied and found to be EC active mainly due to the multiple redox states commonly present in all of them.

Hexacyanometalates, for example Prussian Blue (PB), is another class of ECM due to its high redox active nature and possibility to exist in three colored states namely green, blue, and white[36–42]. Metallopolymers form yet another class of ECMs where chromophore properties arise due to metal-to-ligand charge transfer. Various Ferrous and Copper based metallopolymers have been reported to have long term stability, good switching time, and better efficiencies. Well-defined layers of metal polypyridyl complexes and a palladium (II) salt can be alternatively spin coated to form EC films with high chromophore density.

In the most recent development, various types of materials like microporous metal/covalent organic framework (MOFs/COFs), organic-halide hybrid perovskites and even MXenes have been proven to behave as functionally active ECMs[43–45]. Other than these, composites consisting of two or more ECMs in the form of pure or hybrid structures also serve as emerging new materials in the domain of ECM. Overall, the library of ECMs is huge that lists materials with multiple color, multiple origin-spanning from natural to artificial and different functionality to choose from. These materials, once identified, can be used to fabricate ECDs of desired performance as quantified using various parameters defined in the next section.

1.4. Electrochromic Device (ECD): the concept

The basic structure of an ECD consists of up to five layers, starting with two transparent conducting substrates, typically made of Indium/Fluorine Tin Oxide (ITO/FTO) coated glasses, serving as outer layer for applying bias. The chromophores are deposited onto one (or

both) of these substrates with the help of varied deposition techniques like spin coating, spray casting, hydrothermal or electrodeposition which results in thin films termed as EC electrodes. The other substrate is loaded with an ion-storage layer and finally the two electrodes are integrated together with a gel electrolyte in between them (shown in Figure 1.1 below).

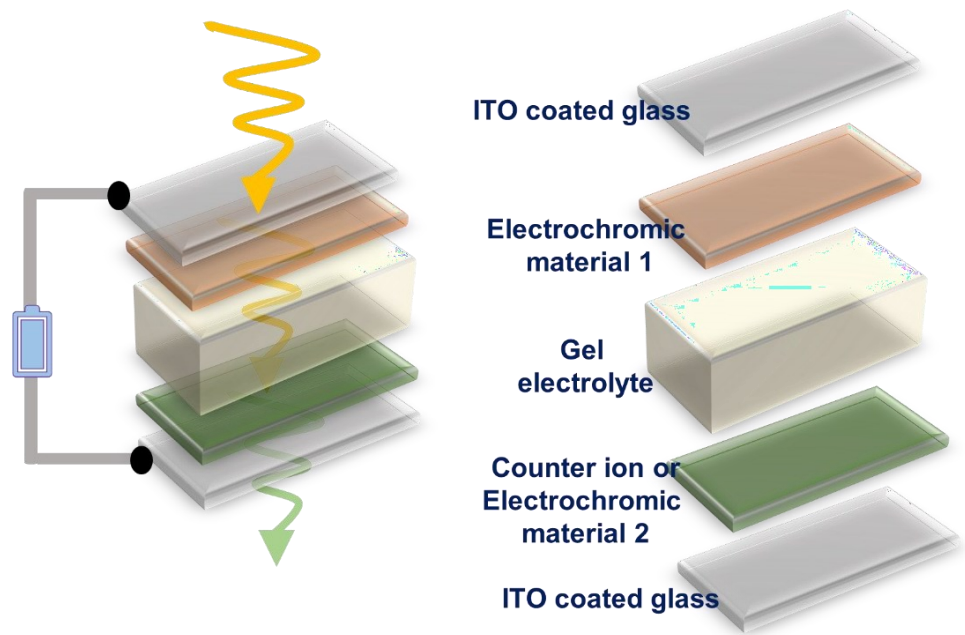


Figure 1.1: A schematic of a five layered ECD with its incident and transmitted light, defining all of its components.

Employing the flip-chip method, a sturdy ECD is obtained with its two ends ready to be connected to a power supply. The gel electrolyte possessing highly mobile ions like assists the movement of electrons leading the device change its color around the active electrode. Using this methodology either of the two types of ECD can be fabricated, i.e., transmissive which or reflective depending on the type of ECMs. In case of a reflective type ECD the second substrate is usually a shiny material instead of transparent glass. Additionally, to make these devices flexible/stretchable, the glass substrates are usually replaced with appropriate electrodes like PET (polyethylene terephthalate).

However, in deviation to the general convention of a five layered structure, there has been several reports of other device designs too. Modifications in terms of either number of layers or types of substrates are required as per necessity and applications. Initially, measurements are carried out in an EC electrode to understand its various properties. Then joining a blank substrate to it, a Monolayer ECD is fabricated and similarly joining two layers we obtain bi-layer ECDs. Finally, there exists a category of all-in-one EC gel, which are devoid of any proper layered pattern (Figure 1.2).

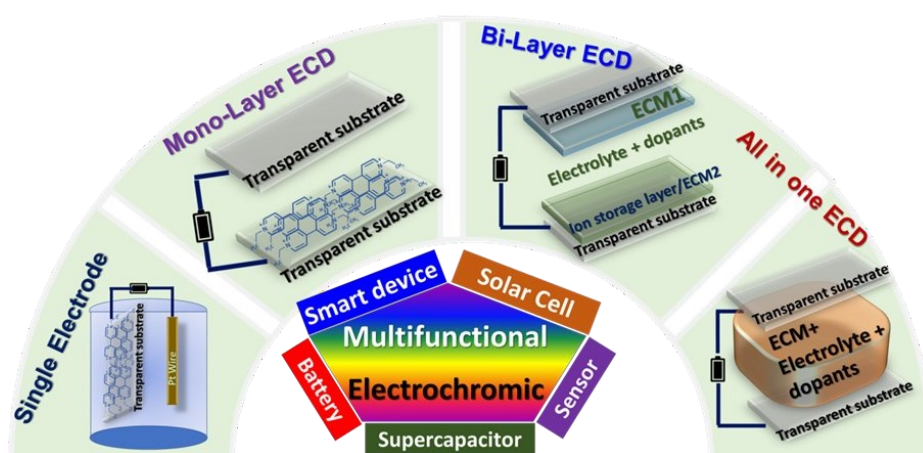


Figure 1.2: Schematic showing various device designs of an ECD.

1.5. Device performance parameters

Prior to be used as an end product, the performance of a solid-state ECD fabricated as per device schematic (Figure 1), needs to be thoroughly assessed using a few parameters listed below in order to judge its performance.

1.5.1 Switching time

When a voltage is applied, the ECD switches from a given optical state to another one after a certain time reversibly often named as coloration and bleaching. The time required to do so is roughly defined as the switching time which is the time recorded as against a maximum of 90% change in absorbance while going from bleached to colored state, which is termed as coloration time (τ_c) and the time taken, estimated for

corresponding 90% change while getting bleached, is known as the bleaching time(τ_b). Though these two values are approximately of same order but not necessarily equal as the two processes (coloration and bleaching) are governed by two different processes at microscopic level.

1.5.2 Cyclic stability

The ECDs are intended for multiple switching cycles hence cyclic stability needs to be measured. The cycle life of a device is investigated by applying a continuous voltage pulse of particular time duration and thus recording its optical output response to check for any loss in contrast value. A good device should show little variation in the colored states even after large number of coloration/bleaching cycles.

1.5.3 Color contrast

An apparent change between the different states of the device should be clearly visible and differentiable. The maximum difference in values of absorbance recorded by an ECD in its colored state against the bleached state is calculated as color contrast using the following equation (Eq. 1.1):

$$CC = \frac{A_f - A_i}{A_f}, \quad (1.1)$$

where, A_f and A_i denote the maximum and minimum values of absorbance corresponding to any particular wavelength and the final value of CC is expressed in %.

1.5.4 Coloration efficiency (CE)

It can be said to be the most important parameter which gives the information about the power efficiency of the device. The CE value, ' η ' is expressed in cm^2/C units and is calculated using the following formula (Eq. 1.2):

$$\eta = \frac{\Delta OD}{q}, \quad (1.2)$$

where, ΔOD is the change in optical density/optical contrast, i.e., the difference between the maximum and minimum absorbance value and Q is the amount of charge intercalated/deintercalated by the device to induce the above change in optical density. The physical value is calculated from the slope of a curve drawn to estimate the variation of optical density (OD) v/s charge (Q).

1.5.5 Color co-ordinates through CIE color chart

A typical chromatograph plotted using programmable software allows one to locate color co-ordinates in the form of a three-dimensional color space. This gives a somewhat mathematical estimation of the output color(s) of a device against a range of available colors, also theoretically verifying the color mixing theory. This is especially important when one explores the specific color output, like RGB etc.

1.5.6 Color rendering index

It is rather less often used parameter but useful if one wants to summarize the consolidated result through one quantity/parameter.

1.6. Multifunctional applications

Electrochromic devices widely finds application as smart switchable windows in buildings; automobiles, for example windowpanes of Boeing 767; rear view mirror to avoid glaze; as curtains in hospitals, in eye gears, and in displays such as sign boards etc. Figure 1.3 below shows a few daily examples of easily available ECDs. Most of these applications are already adapted by many companies to produce user friendly end products.



Figure 1.3: Some applications of ECDs in buildings, aircraft, eye wear and as sweat sensors[46,47].

Although a lot of work is still required to address a few problems like cost, efficiency durability etc. The need of the hour is thus to fabricate electrodes and devices which can serve us more than one general purpose. Besides these trivial applications, ECDs nowadays are reported to be multifunctional in nature. Enough literature exists that suggests that EC materials possesses a few properties other than optical ones, like charge storage, sensing, memory, and catalysis to name a few.

Supercapacitors are one such category of electrical device which stores larger amount of charge as compared to the conventional ones governed by higher surface area and thinner dielectrics[47–54]. Among them, electrochemical supercapacitors enjoy the reputation of superiority owing to higher energy densities and lower input requirement, which are again of two types, EDLC and pseudo capacitor. The former display pure capacitive nature, whereas the latter works on the principle of redox mechanism. A few EC materials have been reported to possess excellent charge storage capacities and typically exhibit the pseudo nature of capacitance because of their intrinsic redox behavior.

Electrolysis of water is another very popular study of recent times owing to its crucial step towards sustainability. In the process of water

splitting, oxygen is produced at the anode, and results in a simultaneous production of hydrogen at the cathode which can be stored and made use as substitute to fossil fuels[55–59]. A few properties like high conductivity, electrochemical stability and larger surface area are desired for both applications of a good electrocatalyst and a good electrochromic material. Thus, in this study, using the same EC material, all the three functionalities i.e., charge storage capacity, electrocatalysis along with electrochromism has been established.

1.7. Main objectives

- Introducing electrochromism and its various aspects starting from selecting materials to device fabrication strategies, assessing performance parameters, and discussing its various direct and indirect applications.
- Discussing various deposition and characterization methods used to fabricate and analyze the samples/devices using morphological, optical, and electrochemical techniques.
- Establishing chronoamperometry as one of the most suitable techniques to deposit thin films owing to reasons like control over thickness, high uniformity, and less time-consuming process resulting in sturdier films.
- Choosing various organic and inorganic EC materials such as polyaniline (PANI), ethyl viologen diperchlorate (EVCLO₄) and tungsten oxide (WO₃) and using them in combination of complimentary pairs to obtain various applications.
- Establishing polyaniline as an ambipolar electrochromic material, meaning it changes color in both positive and negative applied bias and therefore can be used in combination with either p-type or n-type color changing EC materials.
- Fabricating an all-organic device of PANI in combination with a n-type color changing EC i.e., EV to obtain properties like multiwavelength switching, very high performance and also incorporation of flexibility.

- Fabricating a hybrid combination of device with PANI and WO_3 films deposited on separate electrodes using electrodeposition, to obtain enhanced performance results.
- Designing a PANAI@ WO_3 core shell electrode using chronoamperometry and studying the electrode for three different types of energy applications

1.8. Organization of thesis

Chapter 1:

This chapter provides a brief introduction on the requirement of energy saving gadgets, from a viewpoint of electrochromic devices, and their current state of the art in terms of materials, applications, and performance parameters.

Chapter 2:

In this chapter various fabrication and characterization techniques that were used throughout the thesis have been discussed in detail, with much emphasis being laid on electrodeposition and electrochemical characterization methods.

Chapter 3:

The ambipolar electrochromic nature of polyaniline has been established in this chapter by fabricating four individual ECDs and assessing all of them to confirm that PANI can work with either categories of p-type or n-type EC materials

Chapter 4:

In this chapter, ethyl viologen being a n-type electrochromic material was used along with PANI to give rise to an all organic PANI/EV device which displayed multiwavelength switching in visible as well as NIR regions with good speed, contrast, and efficiency. Also, a flexible ECD was fabricated and tested to display all the EC parameters quite well.

Chapter 5:

Tungsten oxide was chosen this time to fabricate a hybrid ECD and check its performance parameter by fabricating a full ECD with PANI in the structure of PANI/WO₃. The device reportedly shows excellent performance parameters in terms of switching time, efficiency, contrast, and device stability.

Chapter 6:

In this chapter, using PANI and WO₃ a PANI@WO₃ core shell was fabricated using chronoamperometry to obtain high quality film which displayed multifunctional applications namely charge storage, electrocatalysis and electrochromism.

Chapter 7:

Finally, in this chapter a thorough conclusion and summary has been presented of all the work done so far along with a short sketch of future scope for extension.

Chapter 2

Experimental techniques

This chapter deals with all the fabrication and characterization methods that were made use of throughout the thesis. A broad discussion about the possible electrode fabrication methods with higher emphasis laid on the electrodeposition method has been presented. Next, morphological, optical, and electrochemical methods of characterizing the fabricated samples have been discussed at length followed by discussion about a software being used for further analysis. All the chemicals used throughout the study i.e., aniline monomer, ethyl viologen doperchlorate, poly (3-hexyl thiophene-2,5 diyl), sodium tungstate dihydrate ($\text{Na}_2\text{WO}_4 \cdot 2\text{H}_2\text{O}$), lithium perchlorate (LiClO_4), [6,6]-phenyl-C61-butyric acid methyl ester (PCBM), tetrathiafulvalene (TTF) polyethylene oxide (PEO), nitric Acid (HNO_3 , 38%), hydrogen peroxide (H_2O_2) and sulfuric acid (H_2SO_4 , 98%) were purchased from Alfa Aesar and all analytical grade reagents such as acetone, 1, 2-dichlorobenzene (DCB, anhydrous), acetonitrile (ACN, anhydrous, 99%), ethanol, methanol, and iso propyl alcohol (IPA) were all purchased from Sigma AldrichTM and were used as received.

2.1 Electrode fabrication techniques

Substrates namely Indium Tin Oxide (ITO) and Fluorine Tin Oxide (FTO) coated glasses and Carbon cloth (CC), were purchased from Macwin India, and were used by slicing them into pieces of 2X1 cm² area. The motivation behind choosing ITOs and FTOs as the substrate of interest lies with the fact that they are highly conducting and transparent which is the basic requirement for EC devices. These substrates were then made into electrodes by depositing the EC material of interest on them following one of the below mentioned techniques which are all bottom-up approaches.

2.1.1 Spin coating method

Considered as one of the simplest methods of sample deposition over flat surfaces, spin coating technique ensures quite uniform thin films over the entire area of a substrate[60]. The basic principle follows the material with a certain density to be spread across the substrate with the help of centrifugal force and eventually coat it (Figure 2.1).

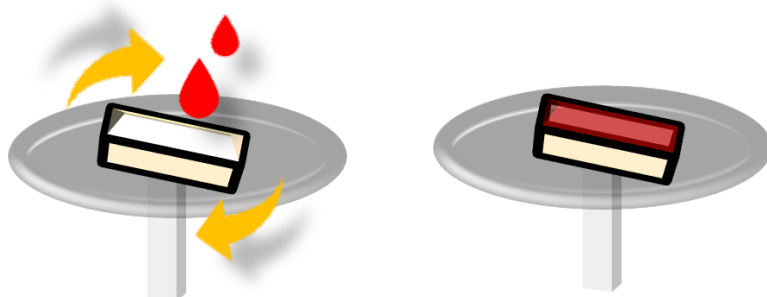


Figure 2.1: Schematic showing the spin coating mechanism.

Step by step method includes:

1. Placing the substrate over the sample holder inside the spin coater machine and attaching it using a vacuum pump.
2. Next, a preferred amount of solution (generally 10-50 μ l) is poured over the substrate.
3. The deposition then takes place at a fixed spin rate for a particular interval of time to obtain a thin film.

4. The deposited films are then dried at 80° -100° C to remove any excessive solvent.

The advantages of this method of fabrication include easy fabrication process, uniform coating, and control over thickness. Organic materials and polymers are mostly coated using this method.

2.1.2 Hydrothermal method

As the name suggests, this very conventional method makes use of higher temperature and water as its basic ingredient for film deposition. The schematic (Figure 2.2) shows the step-by-step procedure[61].

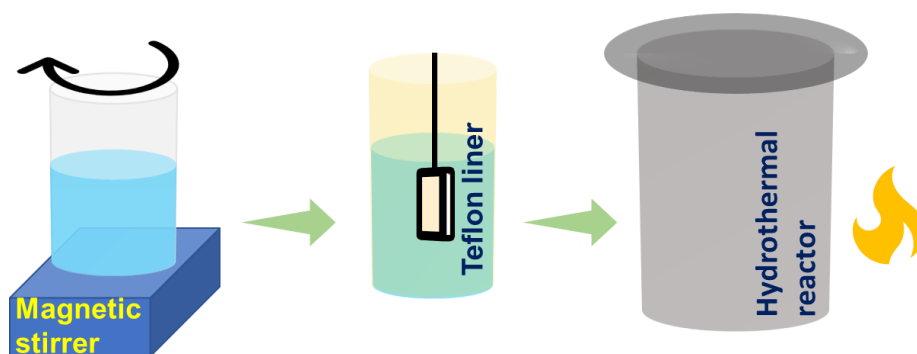


Figure 2.2: Schematic showing various parts of hydrothermal method.

Step by step method includes:

1. A precursor solution is prepared by mixing required chemicals to appropriate amount of DI water and is stirred continuously.
2. This solution is then poured into a teflon coated autoclave and the substrate is attached inside.
3. The entire solution containing autoclave is then placed inside a stainless container and is sealed very properly to avoid exchange of any air.
4. The film deposition then occurs by placing the whole set up inside a furnace and applying a very high temperature for a longer time interval.

The basic principle involves boiling off the water part of the precursor solution and a subsequent deposition of the remaining material onto the

attached substrate. The advantage of this method includes feasibility of growing large crystals without compromising on obtaining a good composition of films.

2.1.3 Electrodeposition method

The method of using bias to deposit thin films over any conducting substrate is popularly known as electrodeposition or electroplating and widely finds application in corrosion industry[62]. The basic advantage of this method lies in the complete control over uniformity and thickness. Besides, the films grown through this method form a very strong bond with the substrate and are found to be very sturdy and stable.

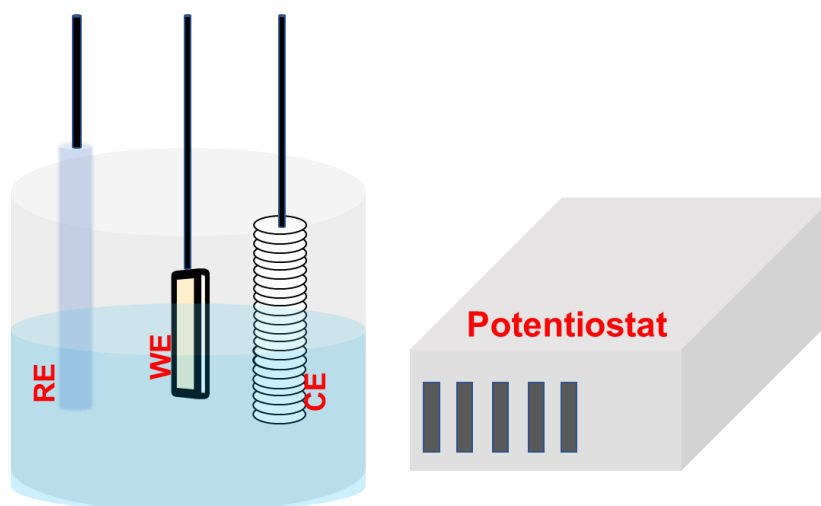


Figure 2.3: Schematic showing three electrode cell setup.

The machine used throughout the study was a dual channel Metrohm Autolab potentiostat and the set up comprises of a three-electrode cell system (Figure 2.3), filled with an electrolytic solution. The three electrodes are:

- Working electrode (WE): The substrate is usually treated as the working electrode onto which the material is to be deposited.
- Reference electrode (RE): Silver chloride electrode i.e., Ag/AgCl (in 3M KCl) being one of the most common options has been made use of owing to its simplicity and stability. Its

requirement lies in the fact that it provides a stable reference potential for electrochemical measurements.

- Counter electrode (CE): Also known as auxiliary electrode, the basic job of a counter electrode is to allow the current passage through the WE thus separating its path from the RE. Typically inert metals like Platinum coil (or sheet) is used as the CE such as to avoid any chemical reaction with the electrolytic solution.

Step by step deposition method includes:

1. Preparing a precursor solution by mixing required chemicals into suitable electrolytic solution.
2. Then the three above mentioned electrodes are fixed inside the cell and the setup is connected to the Potentiostat.
3. A thin film is then deposited over the substrate fixed as WE by applying a constant bias (/current) for a limited time interval.
4. The electrode is then properly washed to remove any excess remaining solution and used for further analysis.

The basic methodology involves redox reaction taking place in the electrolytic solution due to the externally applied bias (/current). The movement of electrons within the electrolyte and to fro through the outer layer of the substrate eventually leads to deposition of the film over it. One of the three following methods are used to carry out the film deposition.

- ❖ **Chronoamperometry**: A constant voltage is applied to the system and the simultaneous current response v/s time is recorded. The material is deposited over the substrate in requisite time and its thickness depends largely on the applied potential or the time interval[63].
- ❖ **Chronopotentiometry**: Similarly, when current is held fixed, we obtain a response of potential v/s time leading to chrono potentiometric deposition.
- ❖ **Cyclic Voltammetry**: In this method of deposition, a potential range is fixed which is allowed to run for numerous cycles and

this deposits the material depending on the scan rate provided[64].

Choosing any of the above-described methods depends on the sample type, and mostly involves the application of the sample thereafter.

2.2 Electrode characterization techniques

After successfully fabricating the electrodes through either of the methods discussed above, the next step is to characterize them for further analysis. This is a very crucial step prior to device fabrication because a few parameters give us a very fair idea about what sort of EC device combinations are to be adopted.

2.2.1 Scanning Electron Microscopy (SEM)

Morphological study provides us with a fair idea about the electrodes' reactive surface area including information about uniformity, phases, homogeneity, crystallinity, grain sizes etc. Electron microscopy makes use of a very high-power electron beam to produce a micrometer-nanometer scale image of the samples' outer surface[65]. A JEOL-7610F Plus Scanning Electron Microscope was used to record SEM micrographs throughout the thesis.

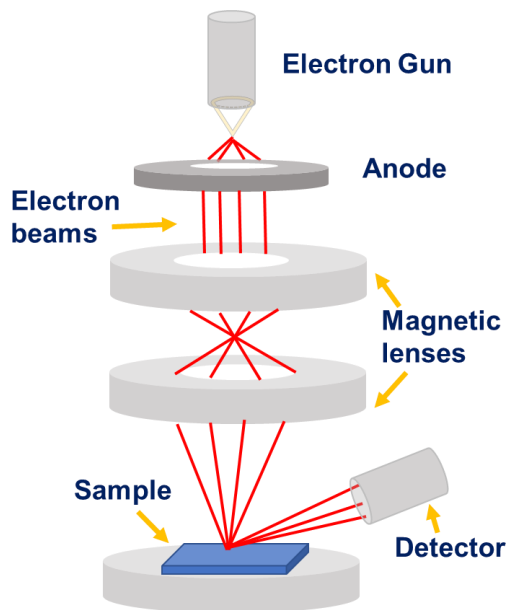


Figure2.4: Schematic showing various parts of an electron microscope

As can be observed (Figure 2.4), a high-power electron beam is released from the electron gun and is directed towards the sample placed vertically downward. Anode helps in accelerating the beam and the magnetic lenses are kept in place to allow a proper vertical direction to the rushing electrons. The moment the electrons hit the sample, collision takes place with the surface electron and as a result the electrons are scattered and reach the detector which then converts this signal into an electric signal and releases the morphological image.

2.2.2 Raman spectroscopy

Raman spectroscopy is an analytical spectroscopic method to determine the vibrational modes of a molecule which ultimately gives information about the structural fingerprint[66,67]. A HORIBA-JY LABRAM-HR spectrometer with excitation wavelengths of 532nm, 633nm and 785nm were used to record the Raman spectra for this study.

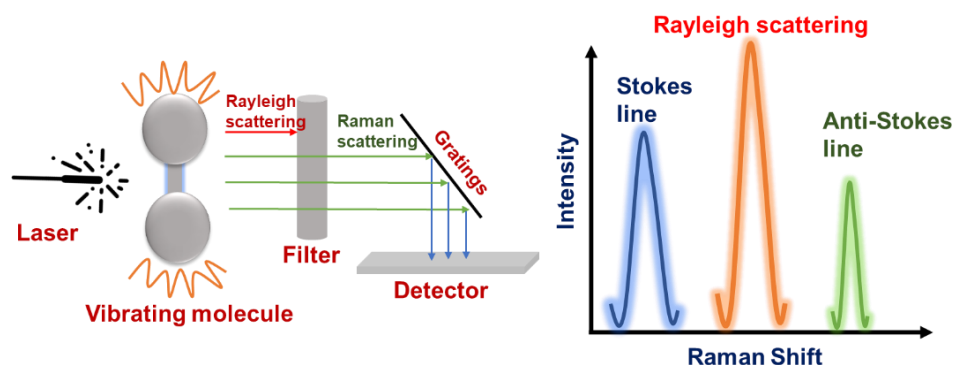


Figure 2.5: Schematic showing basic mechanism of Raman spectroscopy.

Initially, the sample is excited with a light of suitable wavelength which scatters off from the molecule leaving it in a higher excited state. The molecular vibration when returned to its ground state emits three types of photons, one with the same energy as initial (rayleigh scattering) and other two with higher (anti-stokes) or lower (stokes) energy as compared to the initial photon (Figure 2.5). It is evident that the intensity of stokes line is more than that of anti-stokes. Raman spectroscopy is a non-corrosive spectroscopic technique and the

corresponding Raman shifts are typically expressed in terms of wavenumbers.

2.2.3 Fourier transform infrared spectroscopy (FT-IR)

In FT-IR spectroscopy the sample is treated with an IR radiation which passes through the sample giving out a spectrum which is basically a molecular fingerprint of the sample[68]. Information about composition, bond vibrations and is largely obtained from this technique. For our study we have used PerkinElmer's spectrum II spectrometer to record the spectrum.

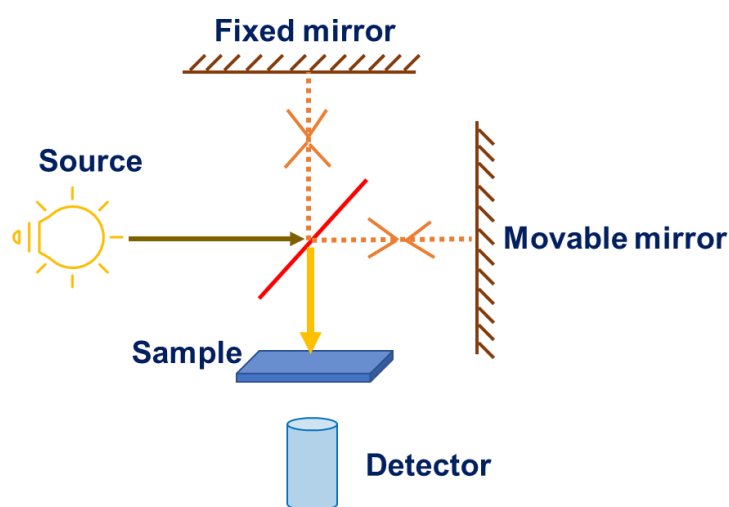


Figure 2.6: Schematic showing basic working mechanism of an FT-IR spectrometer with its inset showing a benzene infrared spectrum.

A source emits IR radiation typically in the range of 4000 and 400 cm^{-1} wavenumbers (Figure 2.6). The beam, after passing through a spectrometer and a set of mirrors hits the sample which absorbs some of the radiation and emits the rest. The resultant beam is then recorded by a detector which gives out an interferogram consisting of the detector signal as function of time. The FT-IR spectra obtained following this method is then matched with existing data to analyze various kinds of bonds obtained.

2.2.4 X-ray diffraction (XRD)

X-ray diffraction method used X-rays as the prime source of irradiation to obtain information about the chemical composition and crystallographic structure of the sample[69]. This non-destructive technique makes use of constructive interference of monochromatic X-rays. All the spectra, for this study, were recorded using a Bruker's AXA D8 Advance X-ray diffraction spectrometer.

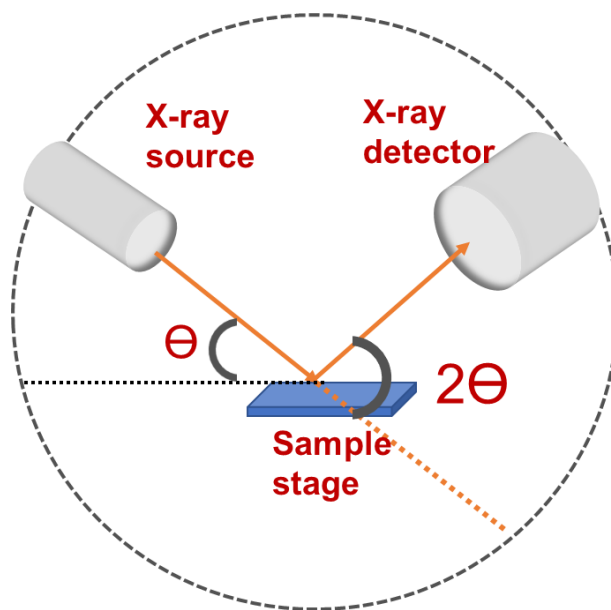


Figure 2.7: Schematic of an X-ray diffractometer.

The X-ray source, usually a cathode ray tube, is attached to a filter which produces monochromatic radiation that hits the sample in a colinear fashion (Figure 2.7). The rays which are incident at an angle Θ interact with the sample and produce constructive interference following the Bragg's equation. The diffracted rays are then collected by the detector which analyses and produces the result in the form of an XRD pattern.

Optical characterization method helps us in understanding the optical properties of the sample like band structure, electronic properties etc. It is of particular interest to us since ECDs are mostly opto-electronic devices. We have mainly used UV-Vis and PL spectroscopy in our study and therefore only these two methods have been discussed.

2.2.5 UV-Visible spectroscopy (UV-Vis)

This spectroscopic technique measures the amount of light absorbed (or transmitted) by a sample from the range of visible wavelengths, which is generally calculated in terms of a reference or blank sample called the baseline[70]. Tungsten and deuterium lamp are the common sources of light used in the visible and UV region respectively. We have made use of a Lambda 365 spectrophotometer (PerkinElmer) for the measurements throughout this study.

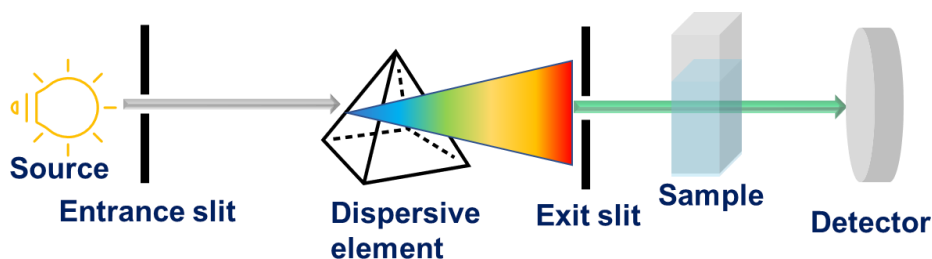


Figure 2.8 Schematic of an UV-Vis spectrometer

As shown in Figure 2.8, the entrance slit collimates with the incoming light from the source and a dispersive element breaks it into multiple components. The sample then absorbs suitable wavelength and passes on the signal to the detector. The ‘absorbance’ is basically a logarithm of the ratio of intensity of light before and after passing through the sample. However instead of absorbance sometimes, the spectrum is represented as transmittance (in %) v/s wavelength mostly for transparent liquid samples.

2.2.6 Photoluminescence spectroscopy (PL)

Also known as emission spectroscopy, this method provides us with information about the emission behavior and thus about band gap of the sample. It is a non-contact and non-destructive method of probing a sample[71]. The PL studies were accomplished using a PerkinElmer LS-55 spectrometer.

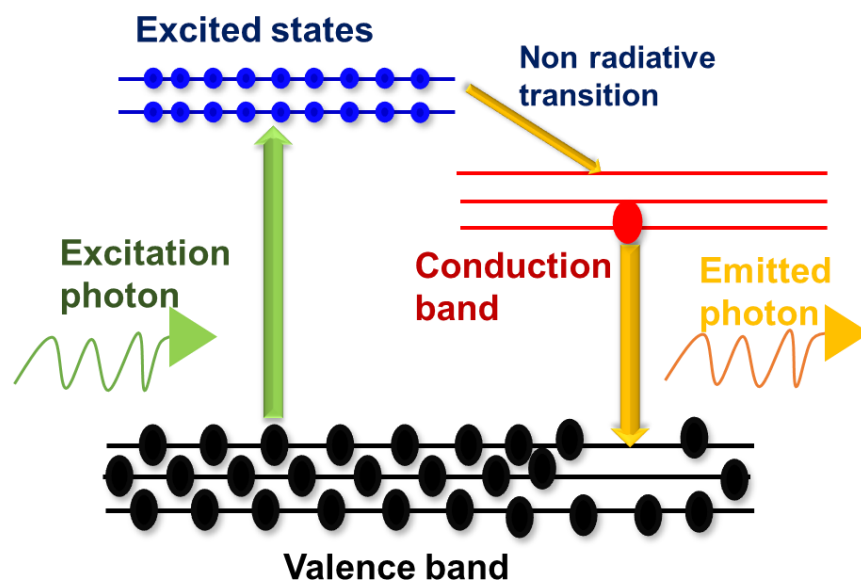


Figure 2.9 Schematic explaining emission phenomenon.

The basic methodology involves the sample absorbing energy in the form of a photon and excited electrons moving from valence band to conduction band. The electrons when they return from the conduction band back to the valence band, they emit photons, and this process is known as emission. The emitted photon is typically of lower energy than the one which was used for excitation. During the process the electron is held at a metastable state for a very small amount of time from which the electron jumps back through a non-radiative transition. Figure 2.9 demonstrates the working mechanism of PL spectroscopy.

2.2.7 Electrochemistry

Electrochemistry is the study of the chemical properties obtained against an applied current/bias. To understand the properties like redox behavior, electron/mass transport phenomenon etc., we need to perform electrochemical studies to consolidate the discussion about the sample characteristics. This method uses a three-electrode cell setup (section 2.1.3), an electrolytic solution and the experiments were performed partly in a Keithley-2450 source meter and partly in a Metrohm Autolab Potentiostat.

2.2.7.1 Linear sweep voltammetry (LSV)

As the name suggests, in this electrochemical method the sample is swept linearly from a lower potential to a higher potential limit i.e., from V_1 to V_2 ($V_2 > V_1$). The current response is then plotted as a function of voltage at a specific scan rate (expressed in volts per second).

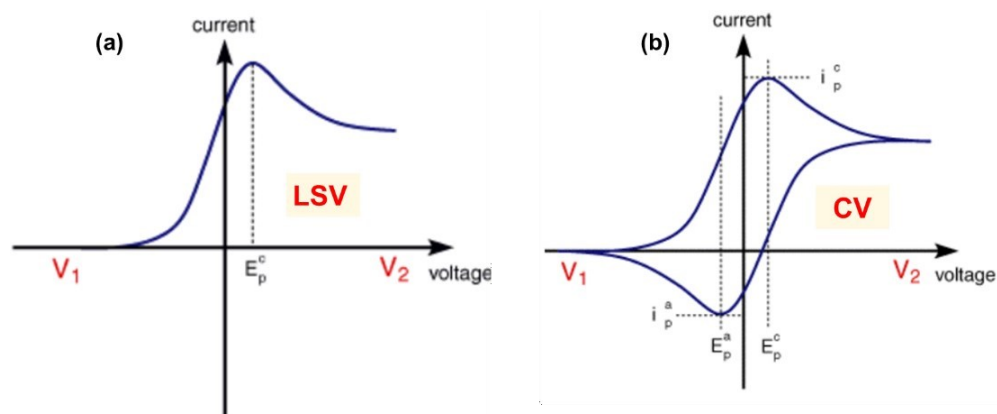


Figure 2.10: Typical LSV and CV curves of Ferrocene*

Figure 2.10a shows a typical LSV graph of ferrocene recorded at a single scan rate. Using LSV we can calculate the peak current (i_p), the potential at the peak current (E_p) and the half peak current ($E_{p/2}$) prior to reaching the peak. This method is of particular interest for irreversible systems, where a reverse sweep would not add any more information.

2.2.7.2 Cyclic voltammetry (CV)

Similar to LSV, in CV too the voltage is swept between two values, besides this time as soon as the scan reaches V_2 , the direction is reversed, and the voltage is scanned back to V_1 thus completing one full scan cycle. CV is the most common tool for electrochemistry and gives us information about the oxidation and reduction peak positions, stability of the sample, reversibility, current response etc. The area under the CV curve also denotes how well the sample can store charge.

* <https://www.ceb.cam.ac.uk/research/groups/rg-eme/Edu/linear-sweep-and-cyclic-voltammetry-the-principles>

Figure 2.10b shows a typical single scan CV from the ferrocene sample. The first part of the scan is similar to LSV with obtaining the same cathodic peak (i_p^c). However, the anodic peak (i_p^a) is obtained in the reverse scan, giving us corresponding values of peak voltages. Increasing the scan rate increases the current value and thus the peak currents are proportional to the square root of scan rates establishing the system as redox active. The electron transfer rates can be estimated by observing the peak position corresponding to shifts in scan rate.

2.2.7.3 Galvanostatic charge discharge (GCD)

In this method, a constant current is applied, and the sample is allowed to charge (or discharge) over a period of time. It is widely used to characterize the material which shows capacitive or pseudo-capacitive behavior.

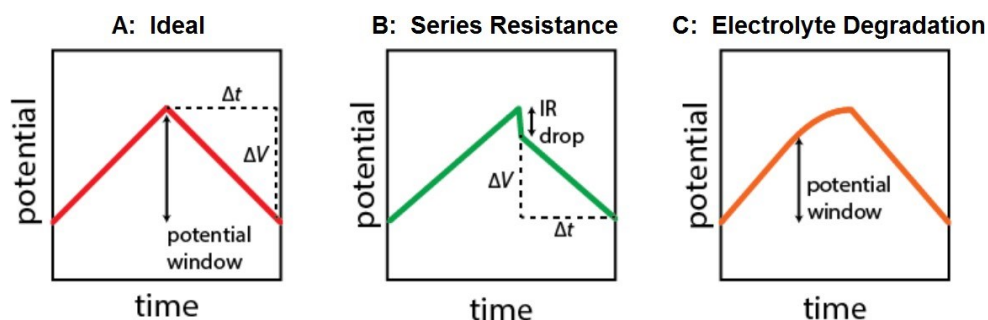


Figure 2.11: Different shapes of the GCD curves belonging to different material types*

The longer the discharge time, the better the charge storing capacity of the material and consequently better is its capacitive properties. Figure 2.11 shows the general pattern for obtaining the GCD curve depending on the type of the material.

2.2.7.4 Electrochemical impedance spectroscopy (EIS)

This is a tool to measure the impedance of a sample which is recorded by applying AC potentials. Information such as electron transfer

* <http://cleanenergywiki.org/index.php?title=File:Charge-discharge.png>

resistance, double layer capacitance, etc. are obtained using EIS. Generally, it is expressed in terms of Bode and Nyquist plots.

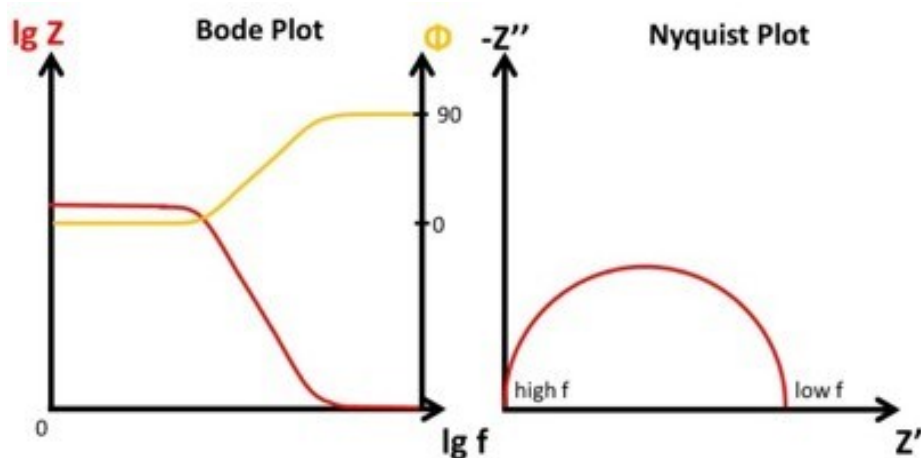


Figure 2.12 Typical pattern of Bode and Nyquist plots *

Bode plot: It is obtained by plotting Log of impedance in Y-axis v/s Log of Frequency in the X-axis and provides information about the phase of the sample.

Nyquist plot: To obtain the Nyquist plot, the imaginary part of the impedance (Z'') is plotted against the real part (Z') and a lot of circuit parameters can be directly obtained from this plot or by fitting it using an electrical circuit.

2.2.7.5 In-situ absorbance spectroscopy:

This is a special technique wherein electrochemistry is carried out inside the cuvette of the UV-Vis spectrometer (Figure 2.13) and hence the name in-situ. This method helps us record the absorbance v/s wavelength and current v/s time spectra simultaneously for an applied bias. It is particularly useful when we ought to study the kinematics of an electrode. Herein the RE and CE are generally fused, and WE is the electrode of interest.

* <https://www.palmsens.com/knowledgebase-article/bode-and-nyquist-plot/>

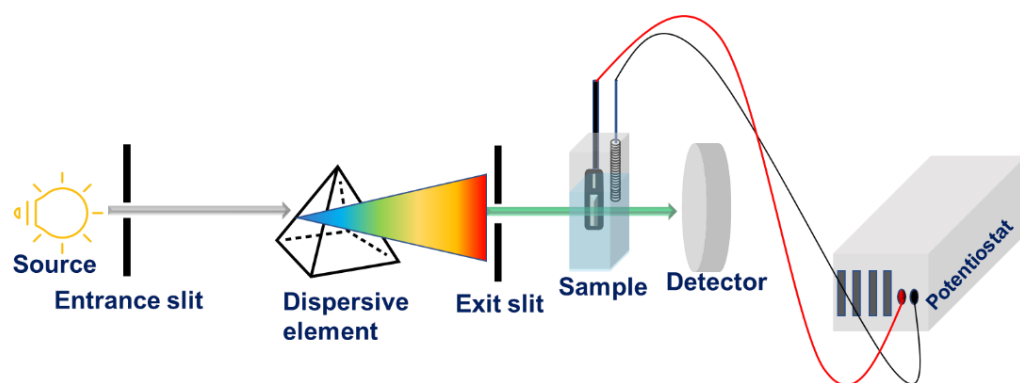


Figure 2.13: Schematic showing the set up for in-situ absorbance spectroscopy.

2.3 Device fabrication methodologies

After systematically characterizing the electrode, the next step is to fabricate it into a full-fledged device. Usually, two individual EC electrodes are chosen based on their compatibility and are stitched together as explained below. The important step is identifying what electrolyte goes inside the device as it has to be compatible with both the EC materials.

2.3.1 Electrolytic gel composition

The electrolyte is generally added to a semi solid gel structure which helps in holding the two electrodes together by providing a cushion between them. Usually polyethylene oxide (PEO), polyvinyl alcohol (PVA), poly-vinyl difluoride (PVDF), nafion etc. are used as gel binders in devices depending on the reactivity. We have used PEO gel as the binder and its step-by-step fabrication recipe is as follows:

- Amount of 5wt% PEO is dissolved in acetonitrile (ACN) and is stirred continuously for 5-6 hours along with heating.
- To it, 1M solution of LiClO_4 in ACN is added in a ratio of 2:1 (2 parts of PEO against 1 part of electrolyte).
- The mixture is then thoroughly stirred using a vortex to obtain the final gel electrolyte which has a thick consistency.

2.3.2 Flip-chip method

The electrodes are then stuck together with the help of flip-chip technique as explained below (Figure 2.14).

- To one of the electrode's, double sided tape is pasted onto the conducting facing side such that there is a window created at the center.
- Around 10-50 μ l of electrolytic gel solution is then dropped cast onto the vacant window.
- The second electrode is then placed on top of this arrangement, with its conducting side facing downwards to obtain the final device.

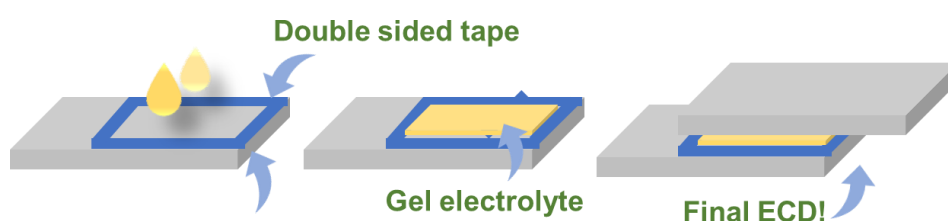


Figure 2.14: Schematic showing step by step method of flip-chip technique

Before using the final ECD, copper tapes are attached to the outward facing conducting areas of the device such that they can be connected to two terminals of a battery/power supply.

2.4 Device characterization

The as prepared solid-state devices (ECDs) are then further characterized for device parameters (section 1.5) after applying to it a suitable bias. It is generally noticed that as compared to a single electrode, a complete device requires higher bias and has an increased level of complexity.

2.4.1 Device kinematics

Device kinematics include measuring the absorbance spectra of the solid-state device, recording its switching time, stability etc. whilst applying a voltage pulse to it. The device is attached inside the

spectrometer and connections are made similar to in-situ absorption measurement of the electrode. The obtained data is further analyzed to obtain the various device parameters.

2.4.2 In-situ raman spectroscopy

Similarly, measuring in-situ Raman requires the device to be placed inside the spectrometer while simultaneously being connected to an external bias source. The detector then picks up signal from the device in both ON and OFF state giving us required Raman spectra.

2.5 Software used

Other than the various characterizing instruments and tools, a software was used to analyze the color co-ordinates of the ECDs, as explained below.

Osram Sylvania

The color space was first mathematically defined by the International Commission on Illumination (CIE) which refers to the quantitative relation between the visible wavelengths of the electromagnetic spectrum and the colors perceived by human eye[72–74]. Figure 2.15 shows a conventional CIE chromatograph and the triangle representing RGB co-ordinate denotes the “tristimulus values” also known as the Long(420-440nm) Middle(530-540nm) Short(560-580nm) or the LMS color space. These spaces don’t necessarily represent real colors but are fabricated mathematical constructs required to explain the color mixing theory. As every color has been assigned to certain co-ordinates, the addition of two colors results in a third co-ordinate and the same can be verified from the chart.

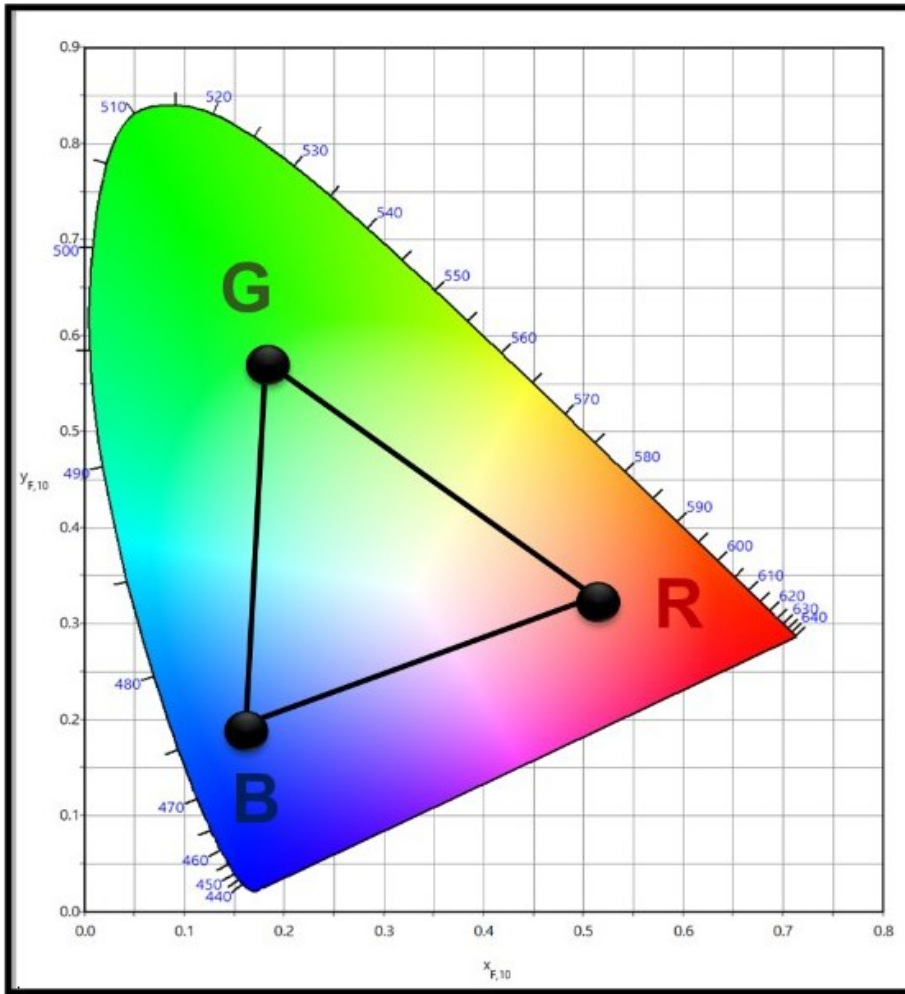


Figure 2.15: A typical CIE chart wherein various colors has been assigned certain specific co-ordinates.

2.6 Conclusion

Several experimental methods discussed in this chapter has been made use to fabricate and characterize the samples and devices.

Chapter 3

Polyaniline – based electrochromic device for ambipolar operation

In this chapter the ambipolar nature of polyaniline, a highly conducting polymer, has been exploited in its electrochromic domain to establish it as a versatile electrochromic material*. Studies carried out on electrodeposited PANI electrode show its ability to behave as an n-type as well as p-type material. Furthermore, two electrochromic devices with PANI as the electrochromic layer and two opposite kinds of counter ions TTF (Tetrathiafulvalene) and PCBM ([6,6]-phenyl-C61-butyric acid methyl ester), were fabricated and subsequently characterized. High contrast value (~50%), smaller switching time (~1s) and moderate coloration efficiency values (~100cm²/C) were obtained from the device which establishes the ambipolar electrochromic aspect of PANI based solid state electrochromic devices. To demonstrate versatile nature of PANI further, two more devices were fabricated using n- and p-type electrochromic active layer as well which furnished similarly good results.

*Ghosh. T. et. al., ACS Appl. Opt. Mater. 2023, 1, 473–480

3.1 Why polyaniline?

Conjugated Polymers (CPs), a unique class of organic materials, finds application widely in the world of electronic materials and devices mostly because of their highly conducting nature[75–77]. Most common CPs such as polythiophene (P3HT), polyaniline (PANI), polypyrrole (PPy) finds considerable application in displays, photovoltaics, energy storage as well as electrochromism among others, owing to its ease of processibility, tunable electronic and optical properties and high stability[78–82].

However, among all, PANI carries additional advantages like high conductivity, tunable working potential window and good thermal stability. Additionally, the multi-functional polymer possesses three distinct oxidation states: partially oxidized emeraldine (EM), fully oxidized pernigriniline (PG) and fully reduced leucoemeraldine (LM), each of them bearing different colors and conductivities (Figure 3.1)[83,84]. Among these, EM state being the most conducting and highly stable is extensively used over LM or PG; however, all the three states are inter-convertible among each other.

The color of PANI film depends strictly on the bias value if the aniline monomer has been polymerized electrically or on the oxidants in case of chemical polymerization[85]. Since, a given oxidation state of the polymer is responsible for its optical appearance, a bias induced color modulation can be achieved by dynamically doping it thus may find a place in designing solid state electrochromic devices and the same can be explored. The effect of chromism in a PANI film is governed mainly by reversible redox processes taking place as a response to external bias[86].

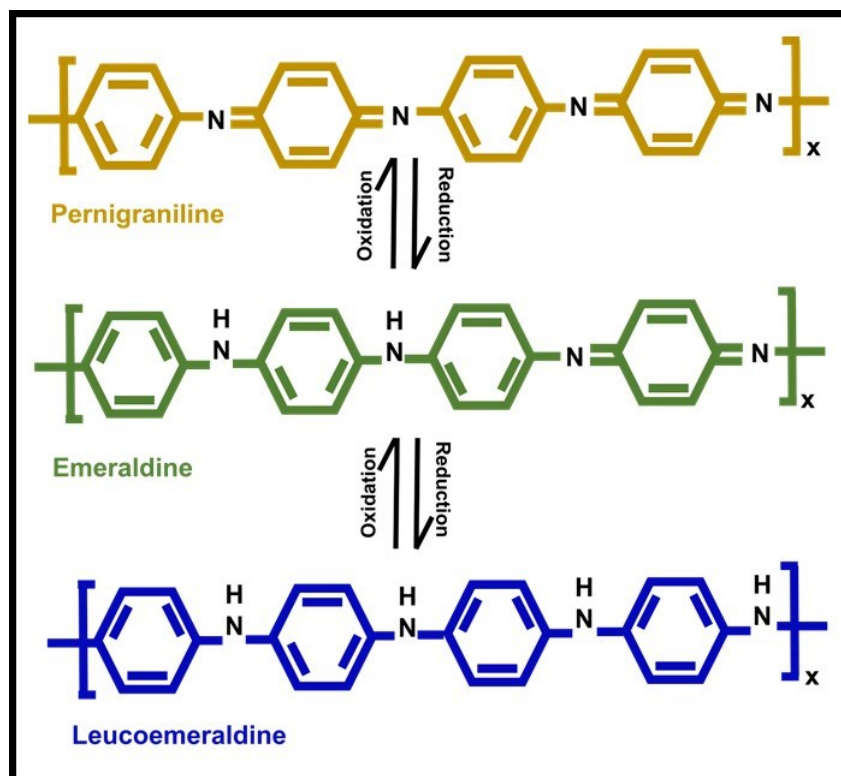


Figure 3.1 Molecular structures of the three different redox state of PANI represented in their corresponding colors.

A well-established property exhibited by PANI which also makes it an interesting polymer is its behavior to function as an ambipolar material. This unique ability of the polymer to respond to both the polarities of an applied bias has been extensively exploited in electronic devices such as Organic Field effect transistors (OFETs) and Field effect transistors (FETs) etc.[87–90]. Besides, PANI is also a well-studied electrochromic material due to its multicolor appearance at different biases along with its ease of processibility and highly stable nature. In this chapter the ambipolar nature of PANI has been utilized to fabricate ECD where electrochemically deposited PANI film has been combined with different counter layers to validate the versatile nature of these devices.

3.2 Deposition of PANI thin film by electrodeposition

The aniline monomer has been electrochemically polymerized, directly on the conducting transparent electrode, which yields a uniform green

film of PANI over ITO substrate and is basically the partially oxidized EM state as it has been obtained at a bias of 0.9V[91–93]. Accomplishing any of the other oxidized (PM) or reduced (LM) state strictly depends on the bias applied during the deposition process. All the three states are easily reversible among each other with application of a small potential; however, the EM state is chosen for potential applications mainly because of its highly stable and conducting nature as opposed to the other redox states. Switching between these states take place through bias induced dynamic doping process, which involves loss of an e⁻ and a Hydrogen atom from a monomer unit during the oxidation process and vice versa for the reduction (as shown in the schematic below)[94,95].

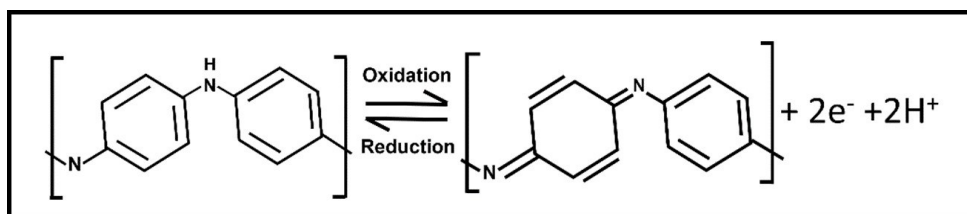


Figure 3.2 Schematic showing redox process of PANI

Steps for Electrodeposition of PANI electrode:

- To prepare the precursor for electrodeposition 0.1M aniline monomeric solution was added to DI water under constant stirring and to it 1M H₂SO₄ was added dropwise.
- Slides of ITO (size 2cm x1cm) were then thoroughly cleaned with a 1:1:1 solution of acetone, IPA, and ethanol for 30 minutes under ultrasonication process before using them.
- By applying a constant voltage of +0.9V to ITO coated glass substrates for a time interval of 30-50s, a green film was deposited using electrochemical deposition, in a three-electrode cell system, as explained in section 2.1.3.

3.3 Characterization of PANI film

Prior to be used further for device fabrication, the PANI film was thoroughly characterized. The films were found to be uniform and very sturdy and the same were characterized using SEM and Raman to understand its morphology and molecular vibrational properties.

3.3.1 Scanning electron microscopy (SEM)

The morphology of the electrodeposited PANI electrode was studied using SEM which shows a uniform film deposition onto the electrode surface (as observed from Figure 3.3). The inset image shows fiber like structures, at 100nm, covering the whole substrate. This scaly pattern allows maximum area of contact thus making the PANI film highly conducting besides making it store a large amount of charge. The uniformity of the film also dictates that electrodeposition is a very suitable method that was chosen.

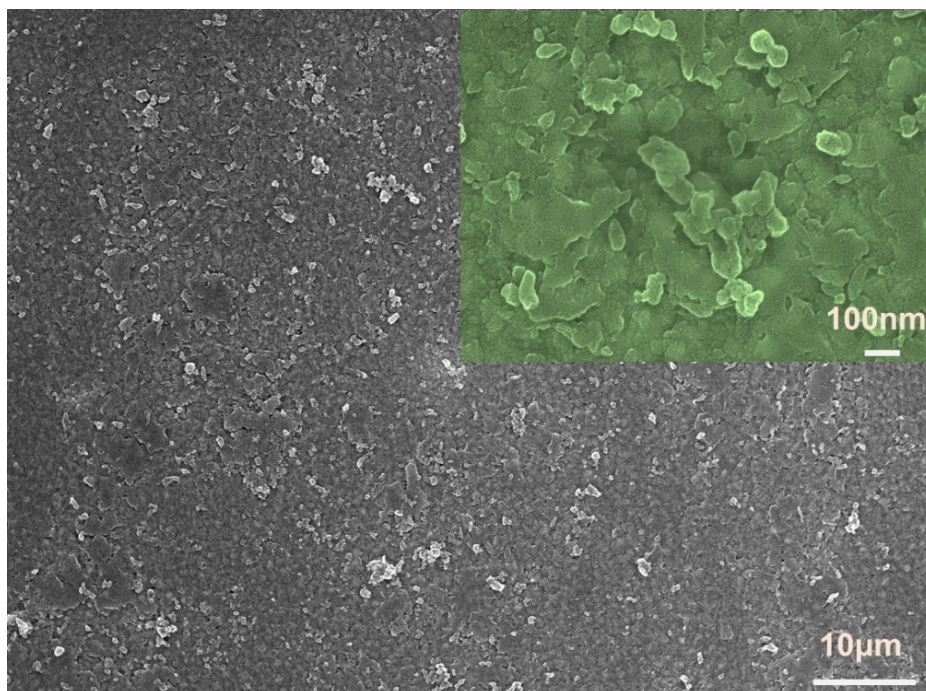


Figure 3.3 SEM images recorded at indicated scale from the PANI film.

3.3.2 Raman spectroscopy

Figure 3.4 shows the Raman spectrum with characteristics peaks appearing at 1161 cm^{-1} (C-H bending vibration), 1330 cm^{-1} (C-N⁺ vibration of de localized polaronic structures), 1472 cm^{-1} (C=N

stretching vibration) and 1586 cm^{-1} (C-C stretching vibration)[27,96–98]. This confirms the successful formation of PANI film through electrodeposition. The as-deposited film appears green (inset, Figure 3.4) throughout the substrate further confirming the complete coverage on the substrate, a must for making good quality device.

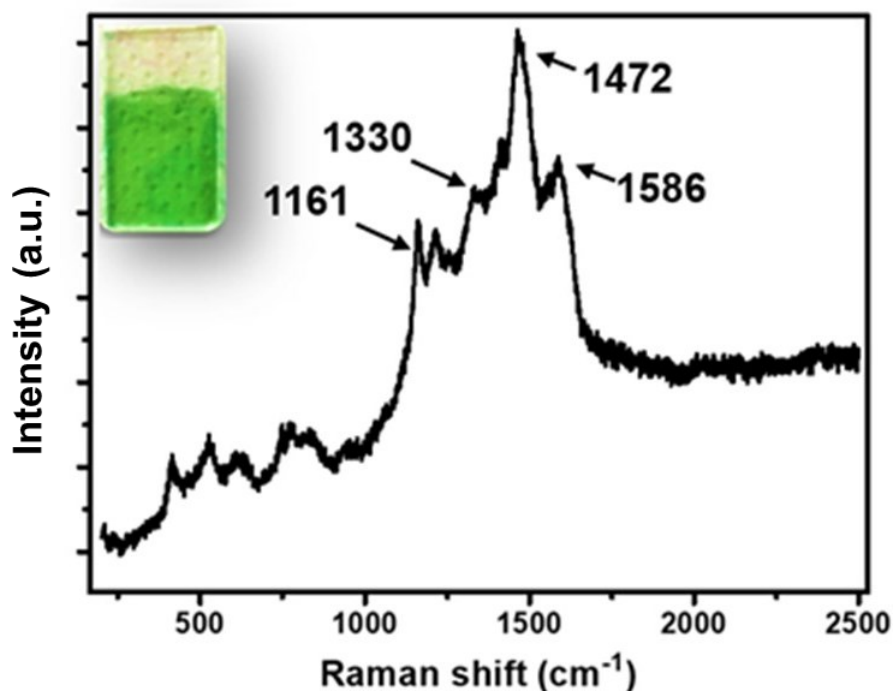


Figure 3.4: Raman spectrum recorded from the PANI film with inset showing actual image of the as-deposited film

After confirmation of proper film formation in the EM state, electrochemical studies were performed on the PANI film to investigate redox behavior and corresponding optical behavior therein.

3.3.3 Cyclic voltammetry

Using the setup explained in section 2.1.3, CV curves were recorded for the PANI electrode by dipping it in a $0.5\text{M H}_2\text{SO}_4$ electrolytic solution. Figure 3.5 shows the CV curve recorded in the range of 1V to -0.5V at a scan rate of 50mV/s . The peak at A1 represents the oxidation peak of PANI occurring when the phase changes from partially oxidized EM to fully oxidized PG state. The second peak C1 however appears due to reduction into LM state of PANI[99]. The color of the PANI film also

changes during this CV scan and inset (Figure 3.5) shows the respective colors of the three conduction states of PANI electrode at indicated biases.

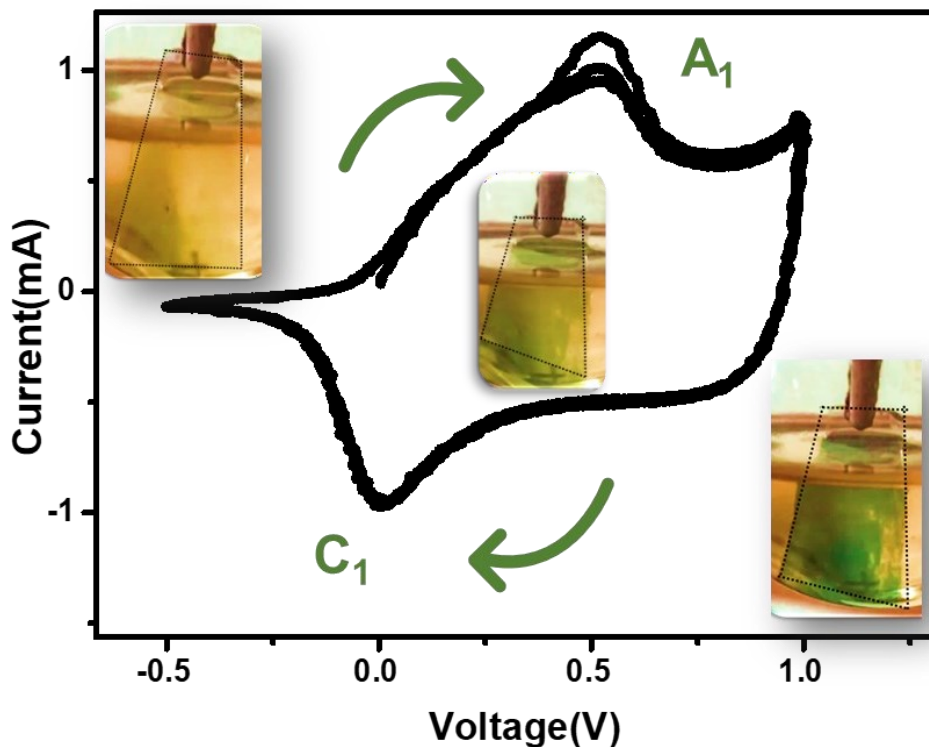


Figure 3.5 CV curve of PANI film obtained in a 0.5M H₂SO₄ electrolytic solution and inset showing actual images of the film at three different bias conditions.

The CV data can be understood as follows. The as-deposited green PANI film (Figure 3.5, inset) reversibly change between yellowish transparent (LM state) at negative bias to dark greenish blue color (PG state) in more positive bias. In other words, possession of a given color signifies one of the three states of PANI, as described earlier, and strictly depends on the applied voltage.

The EM salt state which is obtained at a potential of 0.9V is the most conducting among them i.e., the LM and PG and thus used in this study. Interestingly, it was observed that the PANI film responds and exhibits color change in both positive and negative biases. This hints towards the ambipolar electrochromic nature of PANI. To confirm the same, CV

curves were recorded in the same electrolytic solution and same potential range but in two opposite scan directions (Figure 3.6 below).

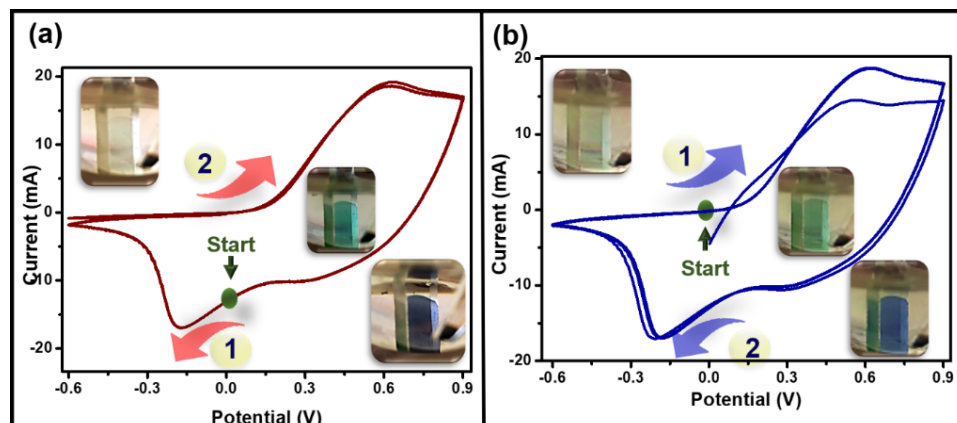


Figure 3.6 CV curves of the PANI electrode recorded in 0.5M H₂SO₄ electrolytic solution at 50mV/s scan rate in two scan directions (a) negative to positive and (b) positive to negative.

The PANI film (inset, Figure 3.6a) originally green in color, has been scanned first from 0V to -0.6V in the negative direction changing its color to yellowish then coming back to greenish at around 0.3V and then proceeded to bluish color corresponding to +0.9V. On the opposite scan direction, i.e., clockwise (Figure 3.6b), however, the original greenish film first changes to blue at around the same potential as former and then turns yellowish transparent at the negative scan, after passing through the intermediate green state.

The scan direction independent CV curves hint at the ambipolar nature of PANI meaning it is capable of responding to positive as well as negative bias. In other words, it meant PANI has the ability to be used as n-type and p-type material as per requirement. To further confirm the observation, bias dependent in-situ absorption spectroscopy was performed.

3.3.4 In-situ absorbance spectroscopy

Figure 3.7 shows the absorbance curve recorded at three different biases using the cell set up (section 2.2.7.5). The black curve shows the initial EM state which is evident from the dip at around 500nm in the

absorbance spectra and the peaks at $\sim 400\text{nm}$ and the broad hump at around $\sim 750\text{nm}$ is considered to occur due to π -polaron and π^* -polaron transition respectively[80,100]. The electrode is then switched between 1.5V (PG) and -1.5V (LM) to achieve a color contrast of $\sim 40\%$ at a wavelength of 600nm.

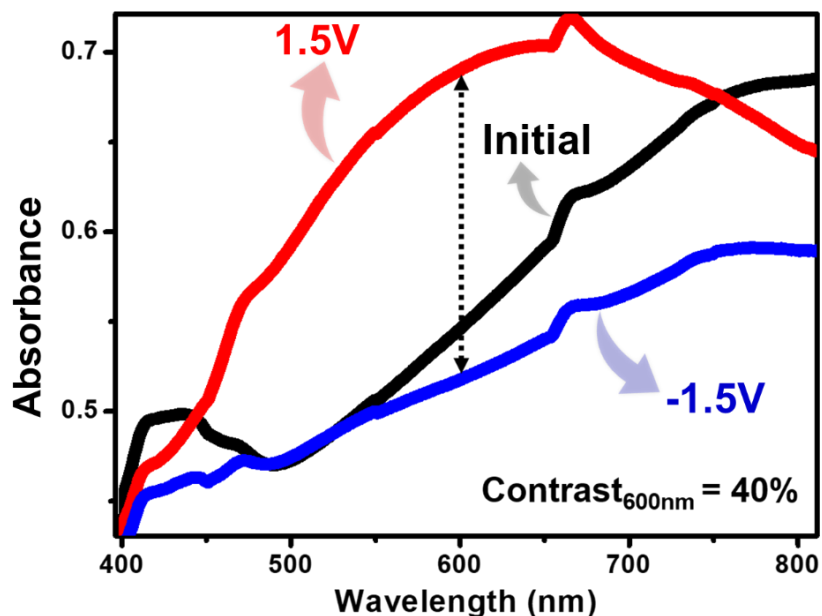


Figure 3.7: In-situ absorbance spectra of PANI film recorded in a 0.5M H_2SO_4 electrolytic solution.

The switching between LM and PG state is reversible without any loss of contrast which confirms the ambipolar electrochromic nature of the PANI film. Such an ambipolar capability, if retained in in appropriately designed solid state electrochemical cell, it can be utilized to make an ambipolar solid state electrochromic device as has been demonstrated later on.

3.4 Solid state electrochromic device and ambipolar operation

The well characterized PANI films were used to fabricate solid state ECD using the flip-chip technique. Devices in three different combinations were tested to study the ambipolar nature first using a monolayer ECD of PANI and a suitable electrolyte. Next, electrochromic passive counter ions were added to the electrolyte and

finally, a bi-layered ECD with two other EC layers was fabricated and tested.

3.4.1 A PANI alone linear device

Initially a monolayered PANI ECD was fabricated and checked for its individual performance. For that a 0.1M LiClO₄ gel electrolyte was made use of which was sandwiched between a PANI coated ITO and another blank ITO to formulate the final device structure. Following this step, the as prepared device was characterized by feeding it with a bias of $\pm 1.5V$ and subsequently its in-situ absorbance spectra was recorded (shown below in Figure 3.8). The original device appeared to be green in color due to its initial EM state.

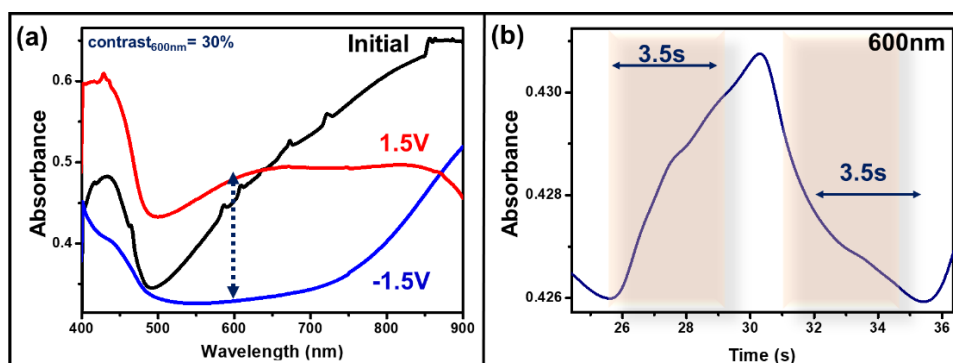


Figure 3.8: In-situ absorbance device kinematics showing (a) absorption spectra at three different biases and (b) switching time calculated at 600nm whilst applying a bias of $\pm 1.5V$.

The black curve (Figure 3.8a) shows the absorbance of the device in the initial state, prior to application of any bias and the peak at around 400nm corresponds to the typical EM state. The device was fed with -1.5V, and the color changed from green to yellow leading to a reduced absorbance value as confirmed from the absorbance spectra (blue curve). Next, feeding a bias of +1.5V led it to change its color to dark greenish leading to a higher absorbance value, red curve.

However, feeding the device with a bias of -1.5V again did not display any change in the absorbance value. A voltage pulse of 5s of $\pm 1.5V$ was provided to the device and its subsequent absorbance change was

recorded (as shown in Figure 3.8b) which confirms the poor contrast value leading to a rather poor switching time of 3.5s. This implies that the devices' reversibility is very poor, and the probable reason could be due to the linear nature of the device in absence of a counter ion or second electrochromic layer. This problem can however be solved by adding a counter ion layer as will be explained in the next section.

3.4.2 A PANI/counter ion based solid state ECD

Electrochromic passive counter ions can be used to make a solid state ECD that can easily switch color reversibility. To establish the ambipolar nature of PANI in ECDs two separate devices were fabricated by combining a PANI film with an n-type phenyl-C61-butyric acid methyl ester (PCBM) and a p-type Tetrathiafulvalene (TTF) material[101,102]. Figure 3.9 represents the molecular structure of these two materials which would serve as counter electrodes.

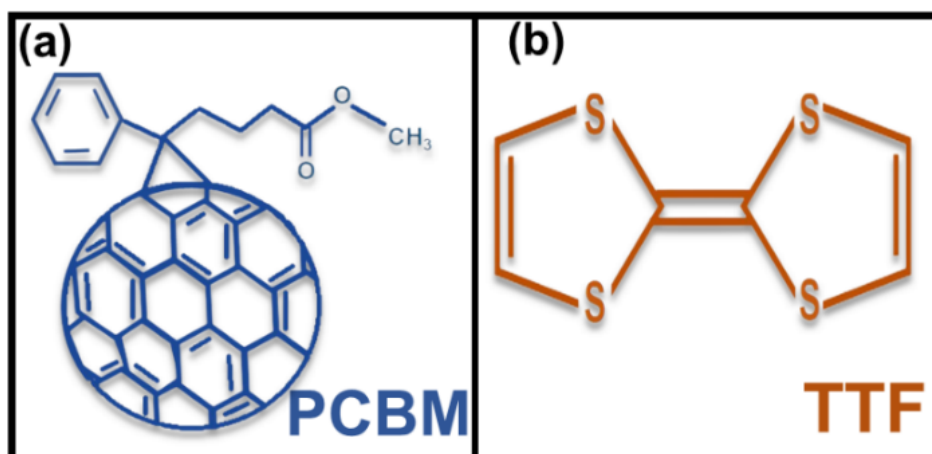


Figure 3.9: Schematic showing molecular structures of PCBM and TTF

A step-by-step fabrication recipe of these two devices of the structures ITO/PANI/PCBM/ITO and ITO/PANI/TTF/ITO is explained below and were named pPCBMed and pTTFed respectively.

- The ITO coated glass substrates, used as electrodes, were first properly cleaned under ultrasonication process.

- Onto one of the ITOs, a layer of PANI was coated by following the recipe mentioned in section 3.2.
- A 4 wt% solution of TTF in Acetonitrile and PCBM in 1, 2-Dichlorobenzene were added to PEO gel matrix (5 wt%) and the solutions were separately drop casted on to blank ITO glass slides which was pre patterned with a double-sided tape
- The two ITO glass slides were then joined together using flip-chip method to obtain the final device, pPCBMed (as explained in the schematic of Figure 3.10a) and the same for pTTFed (as explained later on).

❖ **ITO/PANI/PCBM/ITO device**

In this device combination, PCBM, an electron acceptor material has been used along with PANI. Thus, in this case, PANI behaves as the p-type material, owing to the fact that PCBM is an n-type material. It is important to mention that it is the counter ion layer that enforces the PANI to automatically act as a n- or a p-type electrochromic active layer which it chooses depending on whether the other layer is p-type or n-type respectively.

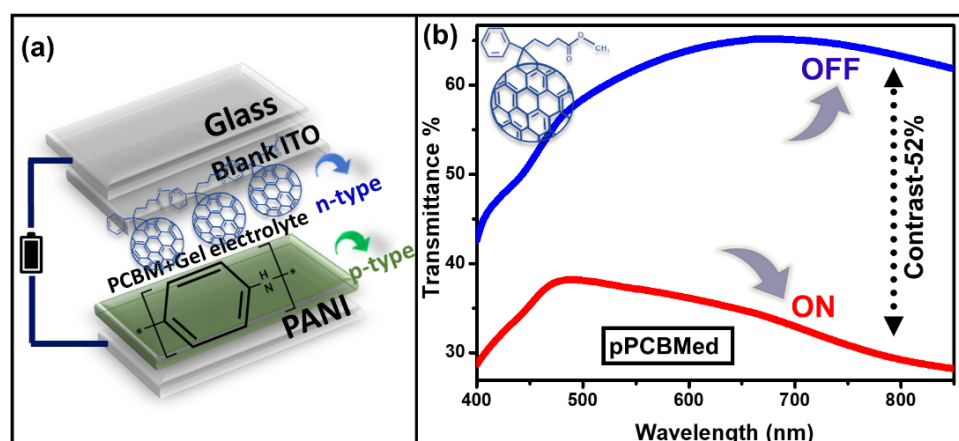


Figure 3.10: (a) Schematic of pPCBMed device fabrication and (b) In-situ transmittance of the device recorded between 2V (ON) and -2V(OFF).

To understand whether the PANI film is automatically able to switch its role in a solid-state device or not, the abovementioned device has

been characterized by applying a $\pm 2V$ bias and measuring any change in its optical properties (as shown in Figure 3.10b). An in-situ transmittance spectra of the devices have been recorded while keeping in an ON (+2V) and OFF (-2V) state. Since PANI is the only electrochromic active layer the device switch color between blue (ON state) and yellowish (OFF state).

The yellow and blue colors are attributed to the reduced (LM) and oxidized (PG) state of the as-obtained polymer layer. It is evident from the in-situ optical spectra that a maximum color contrast ratio (CR) of approximately $\sim 52\%$ for pPCBMed has been obtained corresponding to a wavelength of 800nm. Such an encouraging CR value mostly depends on the thickness of PANI layer and is quite independent of any effect of the counter ions.

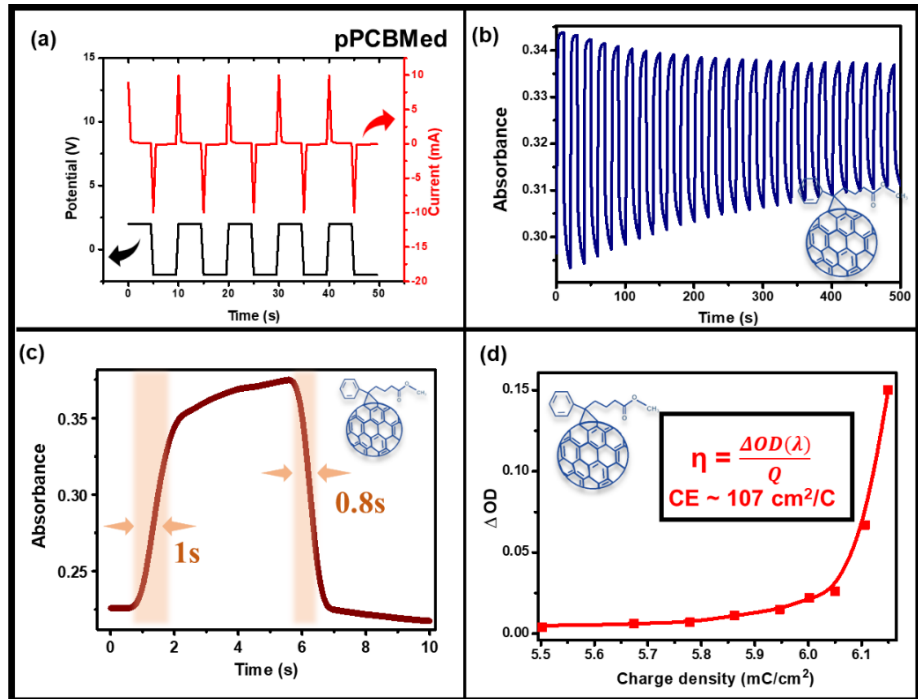


Figure 3.11: In-situ device kinematics of pPCBMed showing (a) potential and current v/s time (b) stability of device (c) switching time and (d) coloration efficiency, all measured at 800nm wavelength.

Additionally, in-situ device kinematics has been performed to investigate the devices' performance at length. The device was fed with a voltage pulse of $\pm 2V$ for 5s (as shown in Figure 3.11a) and the

corresponding absorbance response of the same was recorded for 50cycles (Figure 3.11b). Coloration (τ_c) and bleaching (τ_b) time has been estimated for 77% and 67% change in total absorbance (800nm wavelength) and a value of 1s coloration time and 0.8 s bleaching time was recorded (Figure 3.11c). CE (η) value of $107 \text{ cm}^2/\text{C}$ was obtained using equation 1.2 (chapter 1), from the slope of the ΔOD v/s Q curves (Figure 3.11d) which represents moderate power efficiency from a solid-state electrochromic device from the family of PANI. However, the devices' stability was found to be compromised.

A CIE chart showing co-ordinates of respective colors displayed by the device during the ON/OFF switching has been shown in Figure 3.12. The devices' colors in initial (0V), ON (2V) and OFF(-2V) states can be indicated by co-ordinates 'u' (0.15,0.77), 'v' (0.18,0.12) and 'w' (0.45, 0.39) respectively. The inset images show the actual photographs of the device showing color change between yellowish during OFF and bluish during ON state as also observed from the transmittance spectra (Figure 3.10b). From the CIE map it is evident that the device possesses visibly good contrast between its ON and OFF states.

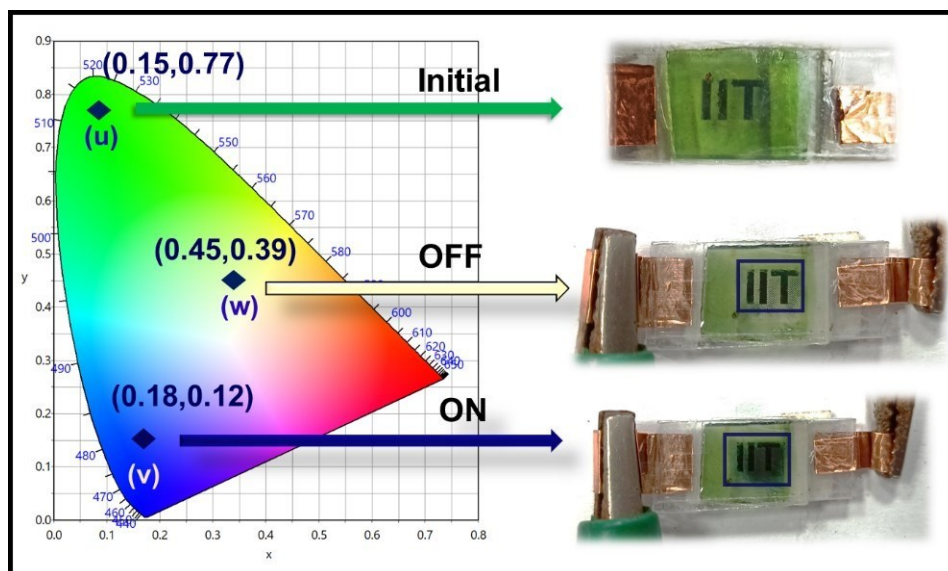


Figure 3.12: The CIE diagram of the device with color co-ordinates (u, v, w) along with actual photographs of the device (insets).

❖ ITO/PANI/TTF/ITO

Similarly, using TTF, a p-type, electron donor material, the entire above-mentioned drill has been repeated only to establish that PANI in this case can act as an n-type EC material. The ECD was fabricated in a very similar fashion with the TTF material being incorporated with the gel electrolyte (as shown below in Figure 3.13a).

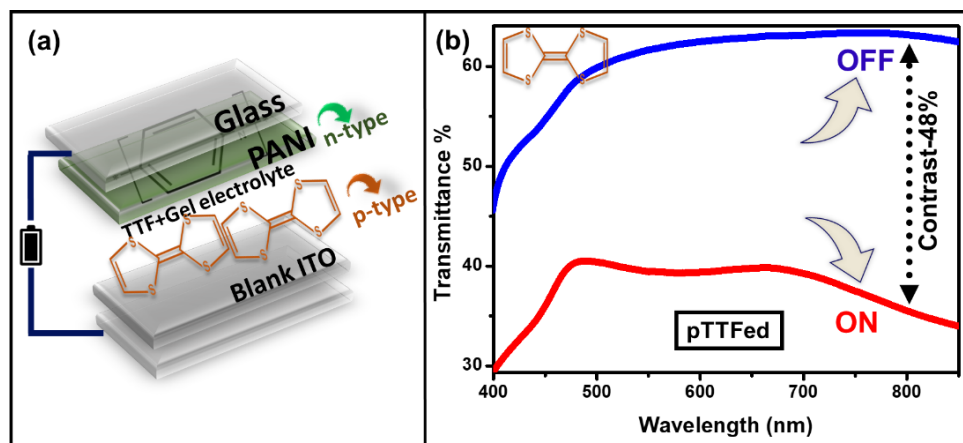


Figure 3.13: (a) Schematic of pTTFed device fabrication and (b) In-situ transmittance of the device recorded between 2V (ON) and -2V(OFF).

The in-situ absorbance spectra in Figure 3.13b shows a very impressive contrast ratio of 48% between the ON and the OFF state thereby now removing the disadvantage of a poor contrast displayed by the linear device (as discussed in section 3.4.1). The basic reason being the counter ion(s), although not adding anything to the color of the device, helps retaining the color of PANI by maintaining the electron exchange. The in-situ absorbance results obtained from pTTFed is quite similar to pPCBMed and is also what is quite expected since there is no interference of any properties of the counter ions.

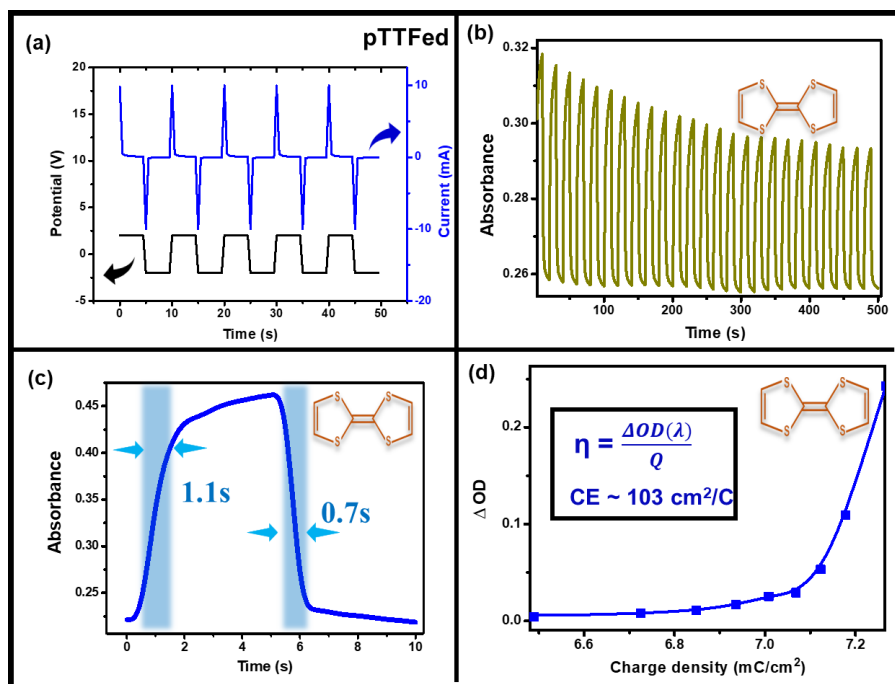


Figure 3.14: In-situ device kinematics of pTTFed showing (a) potential and current v/s time (b) stability of device (c) switching time and (d) coloration efficiency, all measured at 800nm wavelength.

Kinematic activity of the ECD recorded in a similar way reveals that the device possess all the characteristics i.e., a good switching time of almost 1s and a decent CE value of $103\text{cm}^2/\text{C}$. The CE values obtained from the two PANI only devices is one of the best reported values. However, the decreasing value of absorbance (Figure 3.14b) suggests that although the counter ions are helping in improving the device performance, it still performs poorly when it comes to retention of stability. This loophole can be curtailed using a second EC layer, instead of the counter ions which, in addition to providing a support to the PANI layer, would themselves change color too. The next section deals with the same idea wherein we choose a p-type and an n-type EC material in combination with PANI.

3.4.3 Bi-layered solid state ECD based on PANI

To exhibit the complete generic nature of the ambipolar behavior of PANI, two very well-known electrochromic materials polythiophene (P3HT) which is a p-type and ethyl viologen diperchlorate (EVC10_4)

an n-type material has been used to further fabricate two more ECDs and have been thoroughly characterized.

❖ **ITO/PANI/P3HT/ITO**

A conducting polymer, P3HT is another class of electrochromic material which is found to change color when fed with a positive bias making it behave like a p-type material[103–105].

Step-by-step recipe for fabricating the ECD:

- A solution of 0.5 wt% P3HT in 1, 2- dichlorobenzene was first prepared by stirring in a vortex.
- The solution was then spin coated onto the conducting side of a blank ITO at 600rpm for 120s and then the electrode was dried off at 80° C for an hour.
- The P3HT deposited electrode was then sandwiched with the PANI electrode along with LiClO₄ electrolyte embedded in 5wt% PEO gel matrix between them to obtain the final ECD.

Performance of the device namely pP3HTed (ITO/PANI/P3HT/ITO) has been further characterized (Figure 3.15). The in-situ bias induced transmittance spectra of the said device exhibit a very good contrast ratio, a maximum of 60% at 500nm along with a faster color switching response of less than half a second indicating excellent electrochromic activity.

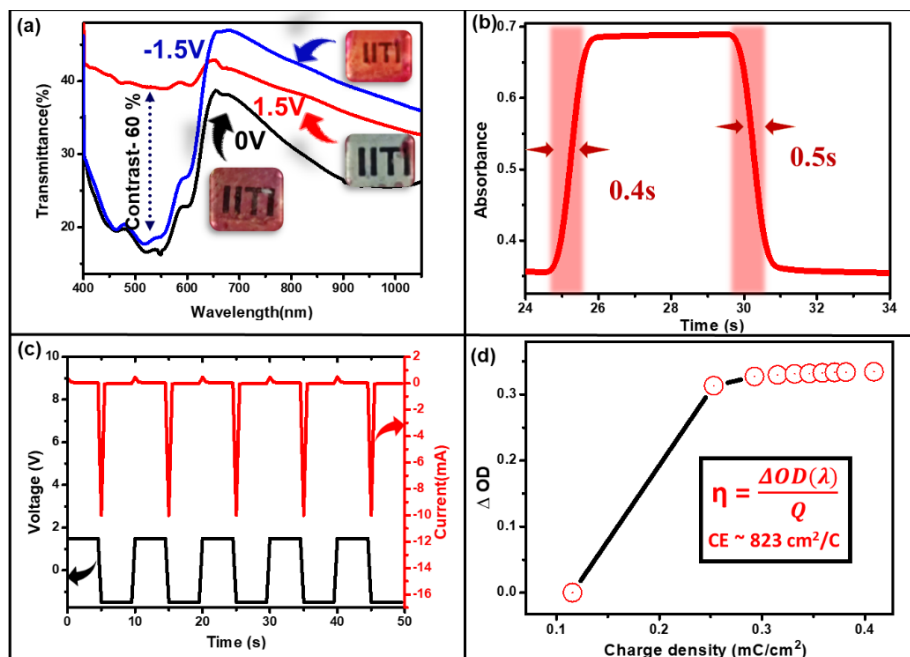


Figure 3.15 In situ device kinematics of pP3HTed device at $\pm 1.5V$ showing (a) in-situ absorbance spectra (b) switching time (c) potential and current v/s time graph and (d) coloration efficiency of the device.

An excellent CE value of $823\text{cm}^2/\text{C}$ obtained using Eq. 1.2 (chapter 1) and the corresponding current v/s time graph further validates the complimentary electrode theory indicating excellent performance portrayed by PANI/P3HT ECD combination. Additionally, longer cyclic stability ($>500\text{s}$) and devices' CV curve (Figure 3.16) also suggests that the aforementioned disadvantage of a monolayer ECD has been taken care of thereby establishing that in case of the pP3HTed device PANI acts well as an n-type material.

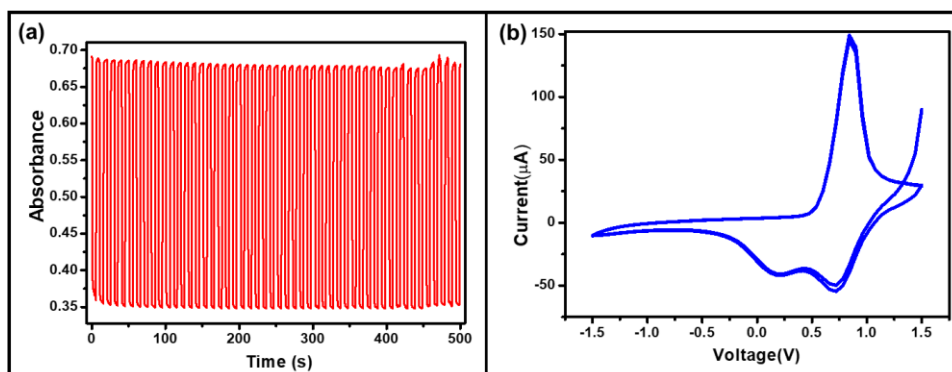


Figure 3.16: (a) Stability and (b) CV curve of pP3HTed device indicating good stability of the device.

❖ **ITO/PANI/EV/ITO**

In order to validate PANI's p-type nature, an ECD was fabricated by choosing an n-type EV as the complimentary EC material. In a similar fashion, using the device combination of ITO/PANI/EV/ITO, a pEVed ECD has been fabricated and characterized for all the above discussed parameters in a very similar fashion. Interestingly this device was found to possess a few excellent characteristics like multiwavelength switching, IR switching and also compatibility in flexible substrates. The next chapter deals exclusively with this device combination at length with a wholesome discussion on all the characteristics.

3.5 Conclusion

Overall, the above discussion very clearly establishes that PANI, due to its ambipolar nature, can be used as a generic electrochromic active layer to fabricate a solid-state electrochromic device where application-oriented constraints of choosing a counter ion is present. Furthermore, it not only allows one to choose any electrochromic active or passive counter ion but also allows one to fabricate a solid-state electrochromic device without compromising the overall electrochromic performance which can further be improved through various engineering methodologies. In other words, electrochromic performance substantiates the fact that PANI holds the ability to work as both n-type and p-type active electrochromic active material. Furthermore, various other combinations of both electrochromic active and passive n-type and p-type materials can be used alongside PANI to obtain excellent electrochromic properties and also other applications, which has been achieved in the next chapters. The device performance can further be improved by appropriate engineering the device design or choosing more appropriate layers in the device.

Chapter 4

Polyaniline/ethyl viologen based all-organic multi-wavelength switching ECD

A polyaniline-ethyl viologen (PANI-EV) based solid state electrochromic device has been fabricated and discussed in this chapter*. Individual behavior of the EV has first been understood well before the device fabrication, to check its compatibility with PANI electrode, which has been thoroughly studied in the previous chapter. In-situ kinematics were performed on the complete solid-state device and electrochromic performance was measured. An excellent electrochromic performance could be observed as evident from the color switching time of less than a second while switching with a color contrast of ~75% and good cycle life. The device displays switching in visible, as well as IR & NIR regions with an applied bias of as low as 1.5V. In addition to the multiple wavelengths switching, a device has also been fabricated on a plastic electrode to demonstrate all-organic flexible liquid electrolyte solid state versatile electrochromic device.

* Ghosh. T. et. al., Adv. Electron.Mater.2023, 9, 2201042

4.1 An all-organic flexible ECD

It is established that the bi-layered ECD combination works best in terms of performance parameter. In that, getting both the EC materials to be organic adds more advantages of its own like ease of processability, flexibility of design, lower voltage requirement to drive an ECD etc. Plenty of examples are available in literature which suggest that all-organic ECDs displays highly efficient parameters pertaining to applications mostly in optical industry[106–110].

Additionally, identifying a complimentary pair of organic materials for example a p-type PANI and an n-type EV, is expected to provide further superior results. Prior to fabricating a complete ECD, the constituents, PANI and EV should be separately checked for compatibility. The previous chapter dealt extensively with characterization of PANI film and thus we report the EC properties of EV as reported below.

4.2 Ethyl viologen di perchlorate as electrochromic active layer

One of the most widely reported organic compounds from the family of bipyridinium salts (Viologens), EV holds the status of being an excellent EC active counter electrode besides demonstrating other applications like sensing, liquid electrolyte for batteries etc.[111–114]. The typical structure of a viologen molecule is shown in Figure 4.1 wherein suitable substituents to the R_1 , R_2 and X^- legends give rise to various combinations of viologen molecule.

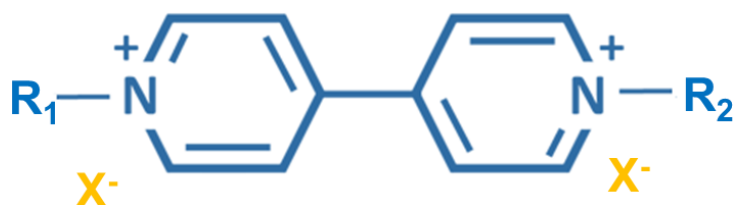


Figure 4.1: Schematic showing molecular structure of Viologen.

Here $R_1=R_2= \text{CH}_3$ and $X = \text{ClO}_4$ makes it an EVClO_4 molecule which is the compound used in our study. Among EVs, we chose the salt with perchlorate owing to the fact that ClO_4^- ion is highly mobile thus providing us with an added advantage of working as an electrolyte[115–118]. This means, EV works both as the EC material as well as the electrolyte when used in combination with a complimentary pair.

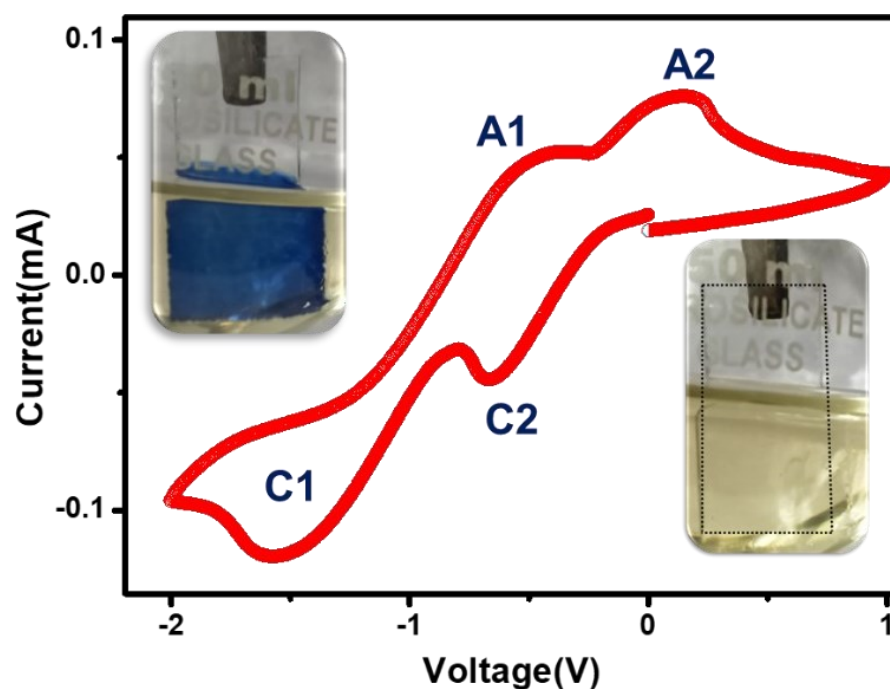


Figure 4.2: CV curve recorded from EVClO_4 solution in ACN, recorded at 50mV/s scan rate, showing actual color change of material over an ITO glass slide as inset images.

Figure 4.2 shows the CV curves of EV solution (in acetonitrile) at a scan rate of 50mV/s with a blank ITO being the working electrode. Different redox states can be observed during a scan from -2V to 1V and is shown along with the inset images showing the corresponding color change of the actual electrode at respective biases. The cathodic peaks C1 and C2 indicates the reduction process i.e., EV^{2+} to $\text{EV}^{\bullet+}$ and subsequently $\text{EV}^{\bullet+}$ to EV respectively[119,120].

The anodic peaks A1 and A2, on the other hand indicates the reversed oxidation process of EV changing to $\text{EV}^{\bullet+}$ and $\text{EV}^{\bullet+}$ back to EV^{2+} respectively. Originally transparent in color, the EV solution (which is

in contact with the ITO electrode) changes to blue when reduced and comes back to its original transparent state during the oxidation process, indicating a reversible n-type behavior. Subsequently, utilizing this property two solid state ECDs has been fabricated with EV, first a mono-layered and then a bi-layered ECD as discussed below.

4.2.1 Linear EV solid state device

A monolayer EC device has been fabricated in a one-step method, wherein 5wt% of EVCIO_4 in ACN was mixed in equal proportion with PEO gel and 10 μl of this solution was drop casted in between two ITOs (as explained in section 2.3.2). In-situ absorbance spectra of the device was then recorded by feeding it a bias of 2V. The black curve (Figure 4.3a) shows the initial spectra of the device, recorded in a 0V bias condition. Since EV has no color of its own, originally the device is transparent in nature, as also evident from the completely flat absorbance curve. When applied with +2V, the device turns blue, and the red curve denotes the absorbance spectra with a prominent peak at $\sim 400\text{nm}$ which typically belongs to reduced state of EV. On reversing the bias to -2V, we observed that the overall color of the device remained blue with almost no change in absorbance, meaning zero reversibility.

The reason for this observation lies in the fact that since the EV molecule is evenly sandwiched between two ITO electrodes, it behaves like a linear device[121]. Therefore, even upon reversing the bias, either layer of the EV molecule is constantly supplied with a negative bias which results in the device being bluish in color and thus affects the reversibility of the material, an observation which is consistent with the behavior of a linear PANI device as was established in the last chapter.

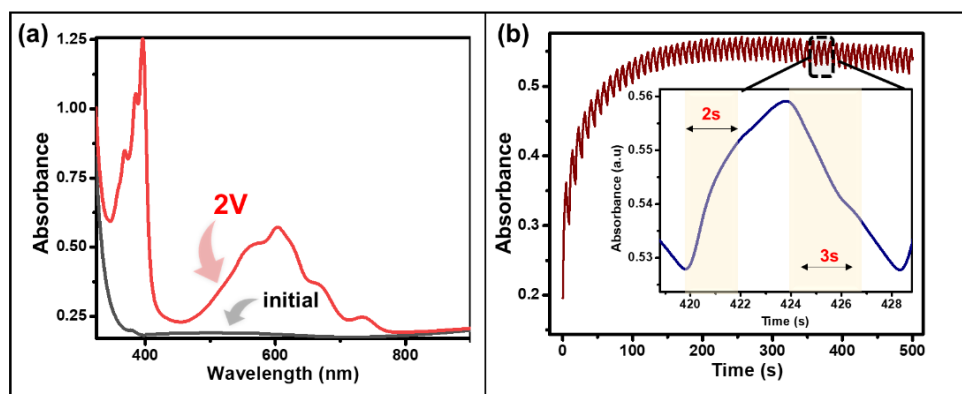


Figure 4.3: In-situ absorbance spectra (a) and device kinematics (b) of a mono layer EV device.

The same is confirmed (Figure 4.3b) wherein the absorbance of the device was recorded by applying a pulse of 5s at $\pm 2V$. From the figure it is quite visible that the device doesn't return back to its original transparent state even on reversing the bias. However, as already established this drawback can be easily addressed by adding a pair of complimentary EC electrode. Here, PANI was used as the complimentary electrode with EV and a complete all-organic device was fabricated as discussed below.

4.3 An ITO/PANI/EV/ITO solid-state device

As discussed above, detailed performance of PANI/EV all-organic ECD has been studied. On account of oxidation taking place at the PANI electrode and the consequent reduction of the EV molecule results in them being excellent complementary pairs for fabrication of an ECD.

4.3.1 Solid state device fabrication

The PANI film has been used to fabricate an electrochromic device with EV added in gel matrix through a flip chip technique as explained below. the fabricated device can be represented schematically as shown in Figure 4.4.

- An ITO coated glass substrates used as electrodes were first properly cleaned and sonicated with a 1:1:1 solution of acetone, IPA, and Ethanol for 30 minutes under ultrasonication process.
- Onto one ITO, a layer of PANI was coated electrochemically following the recipe explained in section 3.2.
- Next, a 4 wt% solution of Ethyl Viologen Diperchlorate (EVCIO₄) in Acetonitrile was added to PEO gel matrix (5 wt%) and was drop casted on the next ITO glass slide which was pre patterned with a double-sided tape.
- The two ITO glass slides were then sandwiched following the flip-chip method to obtain the final pEVed device.

The fabricated solid state ECD appears green in color owing to the EM state of PANI electrode and the neutral state of EV electrode (EV²⁺) which is transparent in color thus giving an overall appearance of green color to the device (Figure 4.4a). When the device is applied with +1.5V bias (with respect to PANI) i.e., in the ON state, the color of the device changes to dark blue as can be seen from the actual photograph of the device in Figure 4.4b (inset).

Upon reversing the bias, i.e., at -1.5V (OFF state) the color of the device switches to yellow (Figure 4.4c), because the EV electrode reverses back to its transparent state due to redox reversal and the PANI electrode turns yellow due to the formation of LM state under this bias.

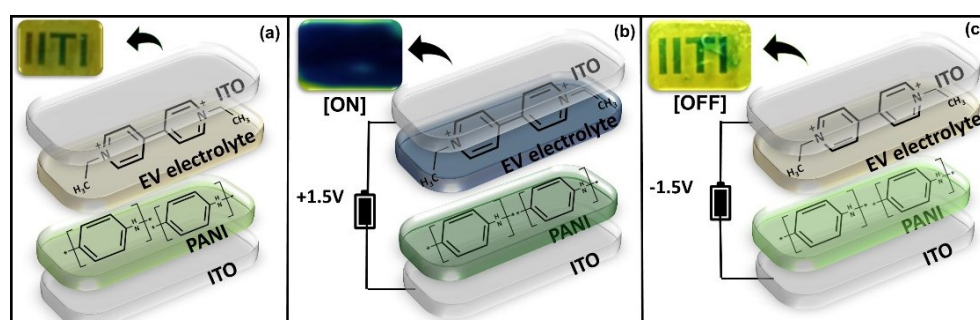


Figure 4.4: Schematic showing the as-fabricated pEVed device (a), and subsequent color modulation in the original device in ON (b), and OFF (c) states.

4.3.2 Solid state device performance

The electrochromic performance of the fabricated device has been studied in detail to check its appropriateness for application. The ECD has been characterized by applying a bias of 1.5V and noting its response.

4.3.2.1 In-situ absorbance spectra

The in-situ bias dependent UV-Vis spectra (shown in Figure 4.5) indicates that in the initial condition (green) the entire absorbance is taking place solely due to the PANI layer, as the electrolytic EV layer is completely transparent in color. A small broad hump $\sim 400\text{nm}$ (black curve) take place due to the π -polaron transition and a hump at around 750 nm corresponds to the π^* -polaron transition, much similar to what can be seen in case of spectroelectrochemistry of the individual PANI electrode (Figure 3.7, chapter 3)[122,123].

The red curve (Figure 4.5) shows the absorbance spectrum recorded at a bias of 1.5V with absorption maxima around $\sim 400\text{nm}$ and $\sim 600\text{nm}$ belonging to that of the reduced state of $\text{EV}^{\bullet+}$ and the one $\sim 700\text{nm}$ appears due to the $\pi - \pi^*$ transition happening in case of PANI. The broad absorption spectra with the maximum absorbance occurring near red wavelength lets the blue light transmit the most hence the device looked dark blueish in color as can be seen in the optical inset image (Figure 4.5).

Furthermore, on reversing the bias polarity, i.e., at -1.5V (OFF State), oxidation takes place at the EV electrode; reinstalling the EV^{2+} state which is transparent. At the PANI electrode however, the PG state is reduced to LM which is yellowish in color thus giving out an overall appearance of yellowish tint to the device. A maximum excellent contrast of 75% has been observed corresponding to 600nm wavelength.

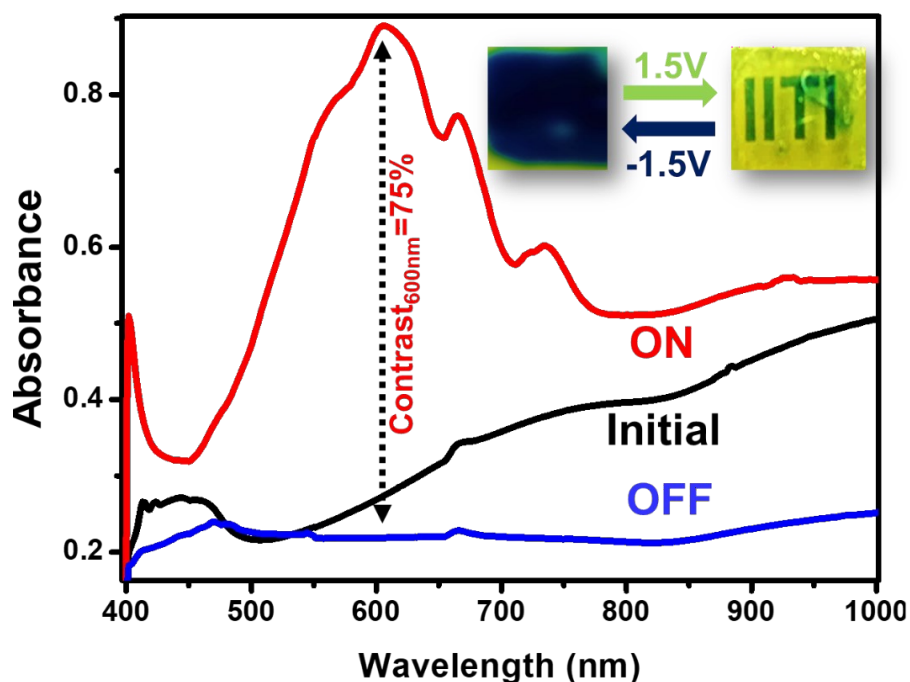


Figure 4.5: Bias dependent in-situ absorbance spectra of pEVED device with inset showing images of actual device.

The same can be verified by looking at the absorbance spectra (blue curve) which appears to absorb almost no light i.e., a nearly transparent nature is seen as expected from the color of the device. A clear distinguishable bias induced absorbance response indicates that the device switches between the two-colored states with good contrast values throughout the visible spectrum as has been discussed later on.

4.3.2.2 In-situ raman spectra

As mentioned above, bias induced redox change is the most likely mechanism for the color change as evident in the UV-Vis spectra. This has been validated using bias dependent in-situ Raman spectroscopy recorded on a working device by feeding with $\pm 1.5V$ bias. The Raman peaks between 1150 cm^{-1} to 1600 cm^{-1} corresponds to the stretching mode, with the prominent one at 1350 cm^{-1} belonging to the polaronic vibration (Figure 4.6). The polaronic Raman peak appears to be present in all the three bias states of the device much similar to the bipolaronic peak which appears at 1510 cm^{-1} . Interestingly the peaks appearing at 1580 cm^{-1} and 1630 cm^{-1} are present when the device is in Initial/OFF

state whereas and disappears from the ON device. In the latter state, an additional peak at 1603cm^{-1} appears[124].

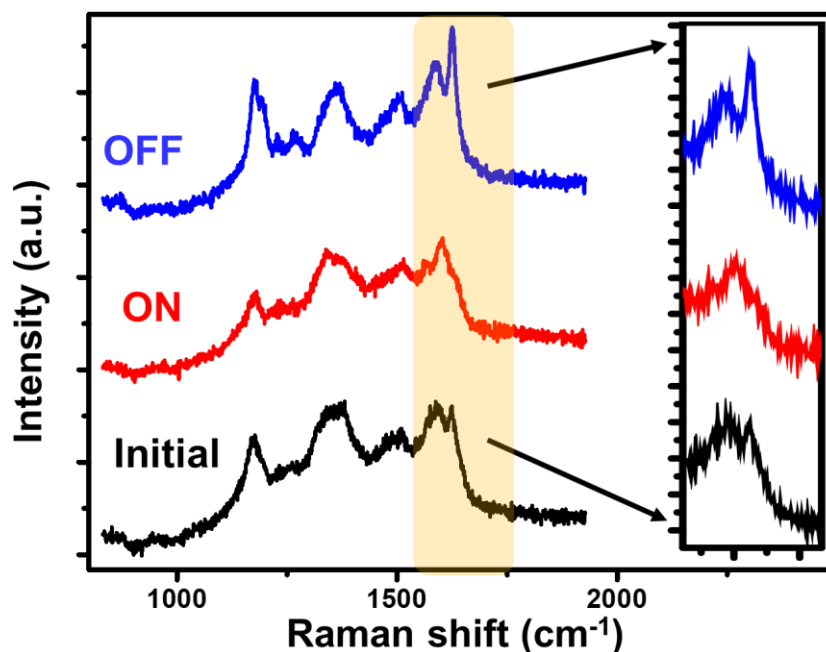


Figure 4.6: Bias dependent in-situ Raman spectra of pEVed with inset showing zoomed part the spectrum.

This new peak at 1630cm^{-1} is a shoulder peak of the one at 1580cm^{-1} which belongs to C=C vibration. In the ON state, as it appears, the shoulder peak merges with the one at 1580cm^{-1} which appears due to quinoid stretching vibration, the probable reason of which is that the bias distorts the C=C bond. Overall, the missing peak in case of ON state of the device is most likely the oxidation responsive polymeric peak of PANI suggesting bias dependent changes occurring in the fabricated ECD as validated from the in-situ Raman spectrum. The consistent spectral behavior of bias dependent Raman and UV-Vis spectra confirms that the bias induced color change from the solid-state device is due to redox induced dynamic doping process.

4.3.2.3 CIE color chart

The pEVed solid state ECD shows color switching between green, blue, and yellow which can be mapped on a CIE chromaticity chart (Figure

4.7) using the Osram Sylvania calculator software to identify the color co-ordinates of the ECD at three different states. The u' , v' co-ordinates of the fabricated ECD has been found to shift from (0.05,0.51) for Initial to (0.25,0.11) for ON and then to (0.25,0.51) for the OFF state.

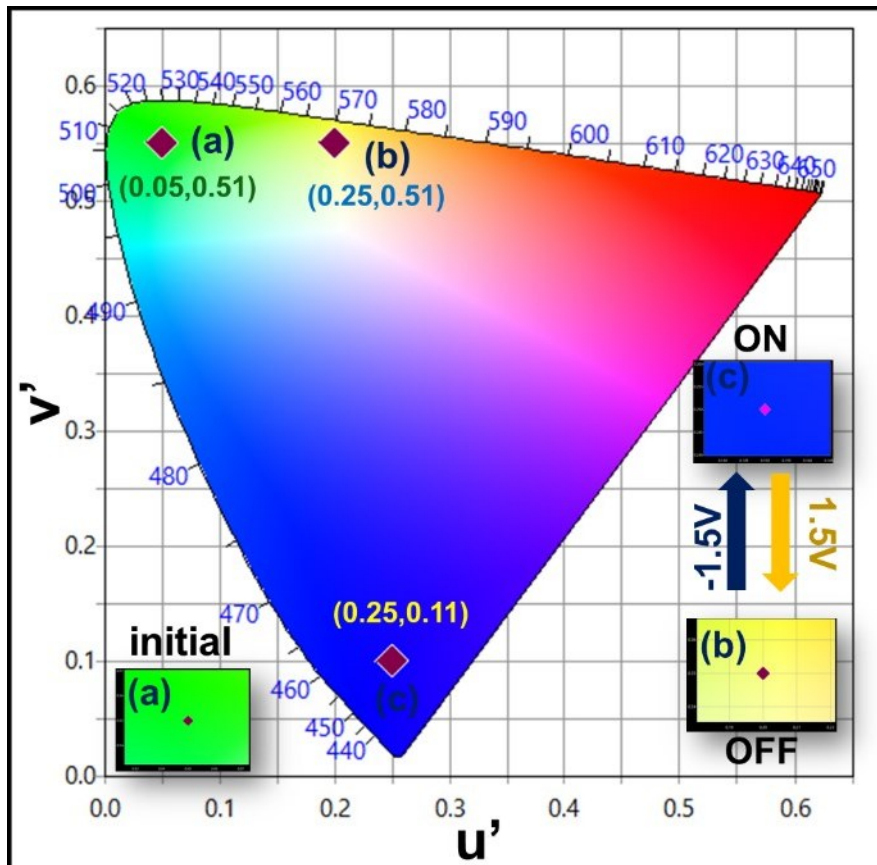


Figure 4.7: A CIE chart indicating color co-ordinates of the device.

4.3.2.4 Device performance kinematics

It is evident from above discussion that the device has sufficiently good contrast ratio (Figure 4.5) over the entire region of the visible light with a maximum value of $\sim 75\%$ obtained at around 600nm (red region). However, in addition to this wavelength, the device also appears to possess a decent contrast value corresponding to higher wavelengths in near infrared (NIR) i.e., at $\sim 800\text{nm}$ and infrared (IR) at $\sim 1000\text{ nm}$ regions as well. Thus, these wavelengths have been chosen for measuring in-situ kinematics to understand the devices' electrochromic properties in a holistic manner.

❖ Performance at 600nm wavelength

To begin with, a square pulse train of $\pm 1.5V$ each with 5s duration was fed to the ECD for an estimated time interval of 1500s to check its stability. In situ color modulation was monitored during the course of this applied consequent pulse train when tested for 600nm. The absorbance v/s time graph (Figure 4.8a) shows that the device possesses a very good repeatability for at least 300 pulses with little loss in contrast value. By taking a closer look at one of the cycles, switching time has been calculated. The time required by the device to change color from green to blue during $+1.5V$ is the coloration time represented by τ_c .

Similarly, time taken to switch from blue to yellow during $-1.5V$ is called bleaching time (τ_b). As indicated in Figure 4.8b, the τ_c and τ_b values to reach 77% and 67% of the maximum absorbance value was obtained to be 0.4s and 0.7s (however τ_c and τ_b values for 90% absorbance change is 0.7s and 1.2s respectively). It means that the device takes less than a second to switch between two colored states making it the fastest device in the family of PANI/EV devices as can be concluded from the comparison table 4.1.

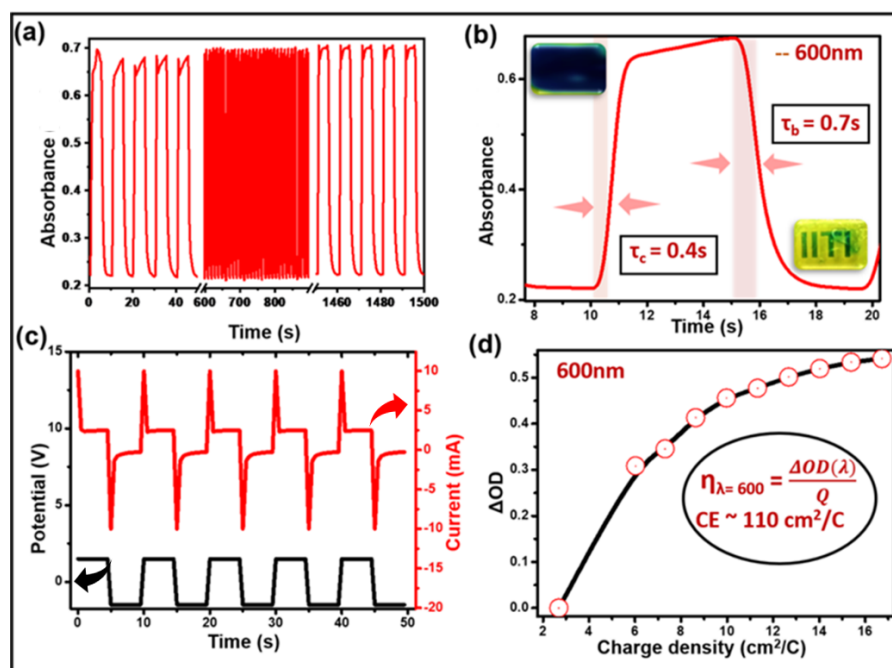


Figure 4.8: In-situ device kinematics recorded at 600nm wavelength

When device is under the influence of pulse train, certain charge is supplied for necessary redox process to take place that can be known from the corresponding current v/s time graph (Figure 4.8c) where it can be seen that along with other parameters; the ECD also possesses a good stability in the current value. The high current range as observed from the figure ($\pm 10\text{mA}$) is mostly because of the highly conducting nature of the EM state of PANI. To evaluate the power consumption involved during color switching, coloration efficiency (η), is calculated using Eq.1.2 (chapter 1). The η value thus obtained for 600nm is found to be $110\text{ cm}^2/\text{C}$, a moderate value in the family of PANI based devices, as can be seen below.

Table 4.1: Table showing comparison between various combinations of PANI and EV ECDs.

SI no.	Device structure	Switching Time	CE (cm^2/C)	References
1.	ITO/PANI/EV/ITO	0.7s/0.4s	110	This work
2.	ITO/PANI/ITO	1.4s/1.4s	49	[125]
3.	ITO/PANI/Graphene/ITO	0.6s/0.6s	50	[125]
4.	ITO/PANI/ WO_3 /PANI	2.2s/3.4s	86	[126]
s5.	ITO/PANI/NiO/ITO	0.75s/0.75s	<u>145</u>	[127]
6.	ITO/Heptyl Viologen/TMPD/ITO	1s/1s	<u>120</u>	[128]
7.	ITO/EV based/electrolyte/ITO	$\sim 1\text{s}$	~ 100	[129]

❖ Performance at 800nm and 1000nm wavelength

Similar in-situ kinematics measurements have been performed for two other wavelengths in the NIR and IR wavelengths i.e., 800nm and 1000nm respectively (Figure 4.9). Like in the visible region color modulation, the device shows good repeatability for these wavelengths when toggled between $\pm 1.5V$ for a 5s square pulse for around 50 cycles (Figures 4.9a & 4.9b). The coloration and bleaching times have also been calculated here yielding a τ_c values of 0.3s (for both the wavelengths) and τ_b values of 0.4s and 0.3s respectively for 800nm and 1000nm wavelength.

The switching time values of less than half a second in the longer wavelength region are better than those at 600nm, however the contrast value is a tad bit lower which is $\sim 50\%$ for 800nm and $\sim 45\%$ for 1000nm respectively. The stability of current value of the ECD (Figures 4.9e & 4.9f) remains the same indicating a very good ECD performance in terms of stability. A lower color contrast is also reflected in the coloration efficiencies as well which are estimated to be $75\text{cm}^2/C$ and $95\text{cm}^2/C$ for 800nm and 1000nm switching respectively.

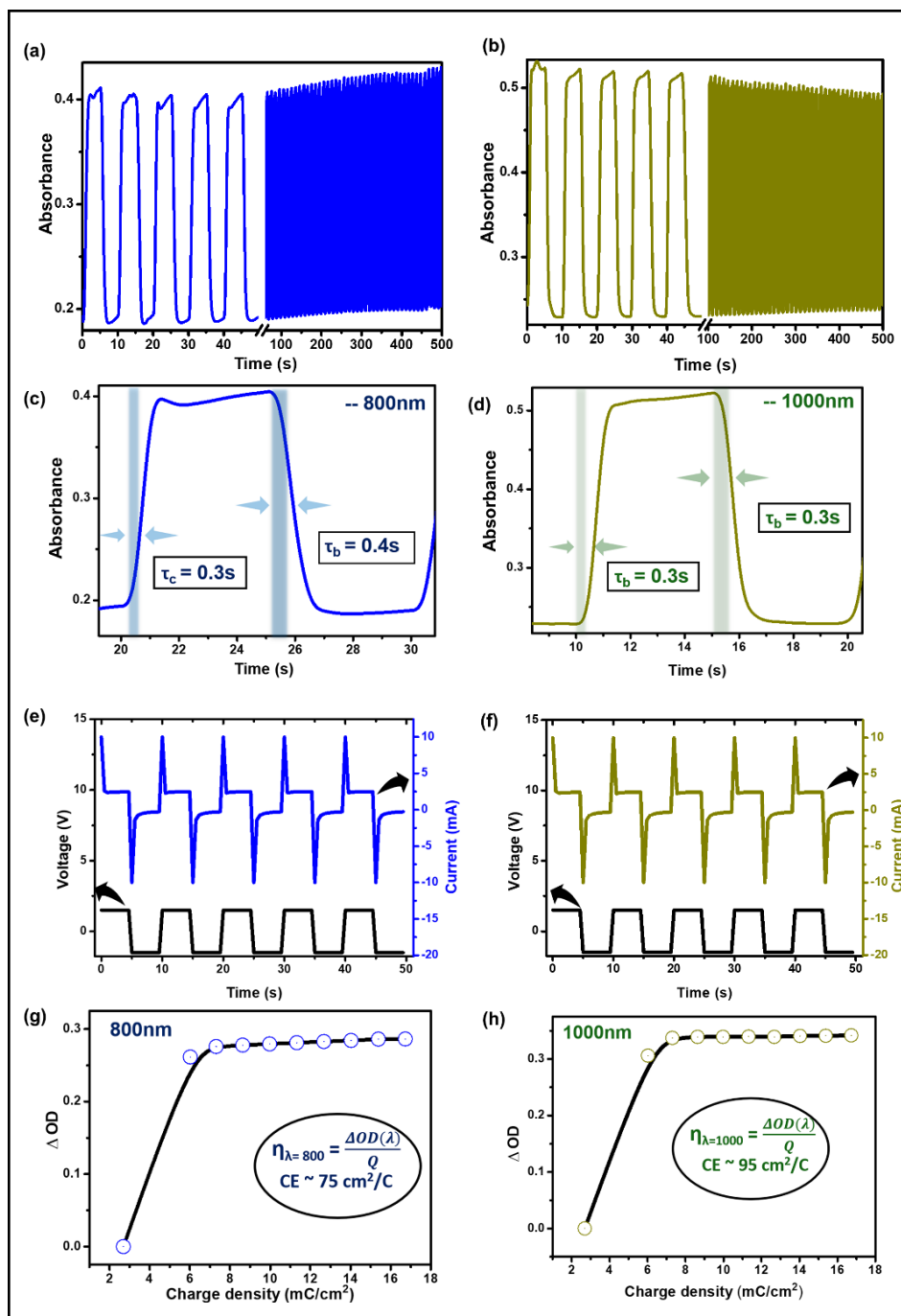


Figure 4.9: In-situ device kinematics recorded at 800nm and 1000nm wavelengths.

The fact that devices from the PANI family has lower efficiency values as compared to other polymers can be explained from the extremely high current values that the device allows to flow during color switching. After successfully establishing the pEVED combination to be superior in the family of contemporaries, we have next tried to fabricate

and characterize a flexible device using the same methodologies as the components are compatible.

4.4 Flexible all-organic ITO/PANI/EV/ITO device

As mentioned earlier, one of the aims to choose PANI in combination with EV was their “organic” nature making them processible on a flexible substrate unlike inorganic materials[130,131]. Since the ECD on rigid substrates possess decent switching speeds and contrast in the visible as well as NIR/IR region therefore it will be interesting to see whether the device can maintain this performance even on flexible substrate for versatile application as all-organic flexible ECD.

Electrodeposition of PANI layer on an ITO coated flexible PET substrate was used with the EV film on another ITO/PET substrate to fabricate a flexible device. The schematic in Figure 4.10 shows the layered arrangement of the device and fabrication process. By following the steps given in section 4.3.1 the flexible device was fabricated with the only difference being the substrate which in this case was ITO coated plastic, instead of glass. The inset image shows the actual photograph of the finished flexible device in a bent condition under ON state, i.e., when applied with +1.5V and the same appears to be blue which is well expected.

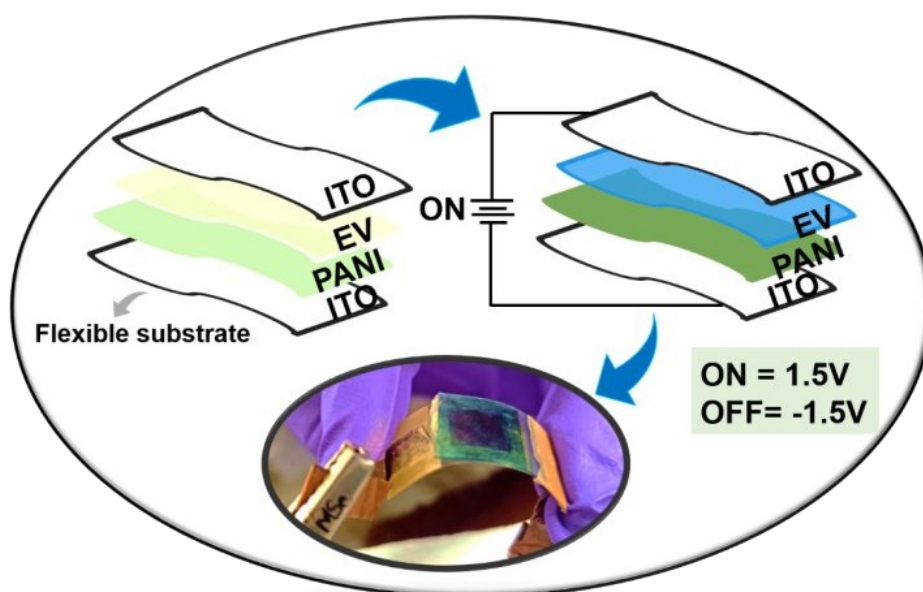


Figure 4.10: Schematic showing device fabrication steps using flexible PET substrates and inset image showing photo of actual device

Flexible device's performance parameters have been estimated using similar measurements as for the device fabricated on a rigid substrate as described above. Bias dependent in-situ kinematics carried out on the prepared flexible device are shown in Figure 4.11. The transmittance spectra (Figure 4.11a), recorded at three different biases shows that a good contrast value of $\sim 41\%$ between $+1.5\text{V}(\text{ON})$ and $-1.5\text{V}(\text{OFF})$ was obtained at a wavelength of 800nm . The inset image (Figure 4.11) shows the photographs of the actual flexible device in the ON and OFF states achieved under appropriate biases. Sequential voltage pulses of $\pm 1.5\text{V}$ of 5 s each were applied to study the color switching dynamics (Figure 4.11b) showing the stability of the device at the end of 100 bias transitions. The contrast of the device appears to have reduced by a very little amount of $\sim 10\%$ at the end of the 500 s signifying a good repeatability. The coloration and bleaching times calculated at the same wavelength of 800nm tells a fast response with $\tau_c = 0.5\text{s}$ and $\tau_b = 0.8\text{s}$ at 77% and 67% of maximum absorbance values respectively (Figure 4.11c).

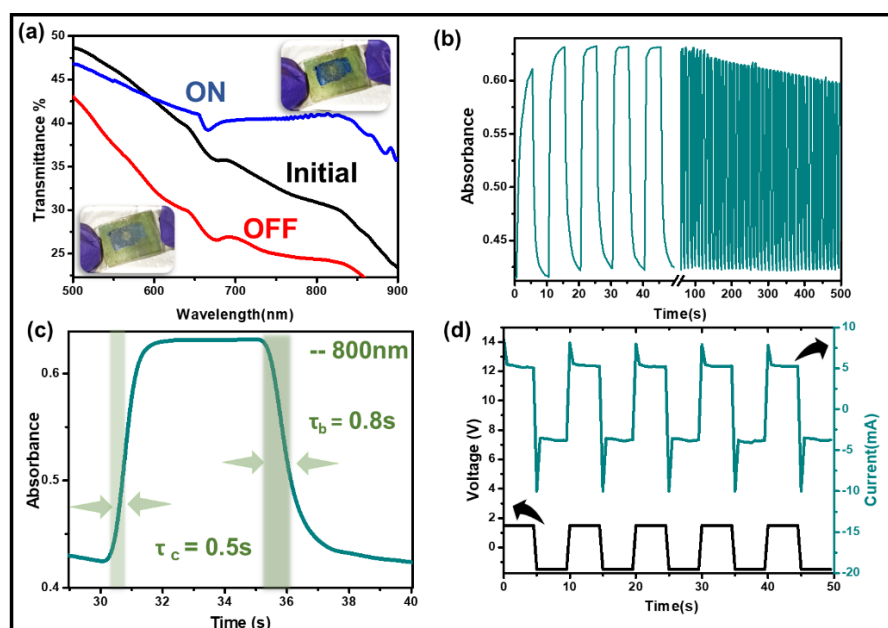


Figure 4.11: Kinematics recorded from the flexible pEved device showing (a) in-situ absorbance spectra (b) stability (c) switching times and (d) current and potential v/s time graphs.

It is worth mentioning here that a switching time of less than one second is really a sign of fast device especially from a flexible device. The current flowing through the device during color switching in response to applied bias has been shown in the Current and Voltage v/s time graph in Figure 4.11d showing a great current stability meaning that the device remains undamaged even when it is bent.

These results establish that the fabricated ECD shows excellent electrochromic behavior in terms of switching speed, contrast and also efficiency; that too at multiple wavelengths and on rigid as well as a flexible substrate. These performances are associated with the complementary redox nature of PANI and EV with respect to each other. In other words, PANI and EV makes a good complementary redox pair which on combining together yields a better performing liquid-electrolyte less solid-state device as compared to not only their individual devices but also as compared to its contemporaries.

4.5 Conclusions

In a nutshell, the electrodeposited PANI film-Viologen pair based electrochromic device proves to be the most versatile solid state liquid electrolyte less ECD which is evident from the following facts. First, it shows color switching in visible, NIR and IR regions of the electromagnetic spectrum. Secondly, it shows holistic improved electrochromic switching performance with high color contrast of as high as 75%, a very fast switching with switching time of as low as 0.3 s and great stability of more than 600 color modulation cycles consistently in all the three wavelengths mentioned above.

In addition, the PANI-EV based exhibits a moderate power efficiency of more than $110 \text{ cm}^2/\text{C}$ in the visible region and nearly $100 \text{ cm}^2/\text{C}$ in the IR/NIR region. Thirdly, the PANI-EV can be appropriately

designed to fabricate an all-organic flexible device without compromising the electrochromic performance in terms of switching speed, power efficiency, stability, and color contrast. Furthermore, the multi wavelength switching ECD, making it a more versatile device, paves a way into serving the purpose of a flexible all-organic electrochromic window in a better and more efficient manner. After analyzing the working of an all-organic ECD we can next move on to hybrid ECDs to understand if they serve better.

Chapter 5

Organic-inorganic hybrid electrochromic device using polyaniline/WO₃

After successfully establishing the advantages of an all-organic ECD, in this chapter we attempt an organic-inorganic hybrid. For this, electrochemically deposited tungsten oxide (WO₃) film through chronoamperometry has been studied here for application as electrochromic auxiliary electrode*. Thoroughly characterized film using electron microscopy, X-ray diffraction and Raman spectroscopy has been used for electrochromic measurement. Bias dependent in-situ spectroelectrochemistry measurements have been performed which show excellent results in terms of reversibility, cyclability, color contrast, appreciable switching time and good current stability at low working potential. This electrode has then been used alongside an already discussed PANI electrode to look into their EC properties as a hybrid ECD. Excellent device parameters established that the hybrid combination of ECD works well in terms of switching speed, color contrast and efficiency.

* Ghosh. T. et. al., J. Phys. D: Appl. Phys. 2022, 55, 5103

5.1 Advantages of a hybrid ECD

Replacing one of the organic EC layers in case of the aforementioned ECD combination with an inorganic layer makes the device a hybrid one. As discussed earlier, inorganic ECMs has their unique advantages like robustness, longer stability etc[132–134]. Coupling an organic and an in-organic EC layer, while fabricating a solid-state device leads to a unique structurization incorporating advantages of both the classes. Based on literature survey, these kinds of devices are found to more efficient, highly stable and runs longer than the all-organic kind[48,135–137]. Tungsten oxide was thus chosen owing to its n-type EC nature, as it would be interesting to fabricate a hybrid ECD.

5.2 Tungsten oxide

Among various inorganic EC active materials, tungsten oxide (WO_3) holds the reputation of being one of the oldest materials to be studied in this aspect of because of its structural properties and optical transparency[138]. Its ability to switch between blue and transparent states reversibly while applied with a small negative bias makes it an excellent n-type EC material. The schematic below shows the molecular structure of WO_3 wherein W has an oxidation state of +6 often written as W(VI)[139,140].

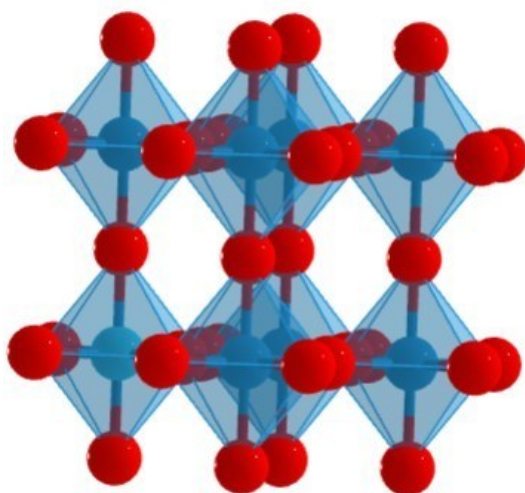


Figure 5.1: Schematic showing molecular structure of tungsten oxide[141].

Upon reduction, W(VI) gains an electron to transition into W(V) which results in an alteration of its electronic band structure ultimately resulting in a change of color. Electrochromic properties of WO_3 depends very much on the method of deposition of the film. Among the various techniques available for an electrochromic film deposition, hydrothermal and solvothermal method has been substantially used and reported but the major drawback of these techniques lies in the fact that the control over the film deposition is very less thus leading to a poor film quality which lacks uniformity[63,142–144]. In this work we have used chronoamperometry to deposit uniform thin films of WO_3 onto an ITO substrate[145].

5.2.1 Deposition of WO_3 film

Chronoamperometry method of electrodeposition using a constant voltage, and a three-electrode cell setup, is an established better method because it uses current to control the atom deposition thus yielding better films.

Steps for electrodeposition of WO_3 electrode:

- To prepare the percussor for electrodeposition 0.015M H_2O_2 was added to a solution of 0.0125M $\text{Na}_2\text{WO}_4 \cdot 2\text{H}_2\text{O}$ under constant stirring.
- The pH level of this colorless solution was adjusted by adding 0.48M HNO_3 dropwise.
- Slides of ITO glass of size 2cmX1cm were then thoroughly cleaned with a 1:1:1 solution of acetone, IPA, and ethanol for 30 minutes under ultrasonication process before using them.
- A constant voltage of -0.47V was then applied to an ITO coated glass substrate for a time period of 200s to deposit the film.
- The electrochemically deposited WO_3 electrode was then rinsed with distilled water and kept at 80°C for an hour to be used for further characterization.

5.2.2 Characterization of the WO₃ electrode

Prior to be used in a device configuration, the as deposited thin films of WO₃ has been thoroughly characterized using optical and electrochemical methods to understand its individual properties.

5.2.2.1 Scanning electron microscopy

The film deposited electrochemically via chronoamperometric technique appears to be uniform when seen using SEM (Figure 5.2). The film shows a better coverage on electrode as compared to the ones deposited through other methods like hydrothermal method. The SEM micrograph shows that the film (~4 μm thick) is evenly deposited over the ITO glass substrate where the speherical structures represents a few hundred nanometer sized flowers made of WO₃ as can be established using XRD and Raman measurements as discussed later on.

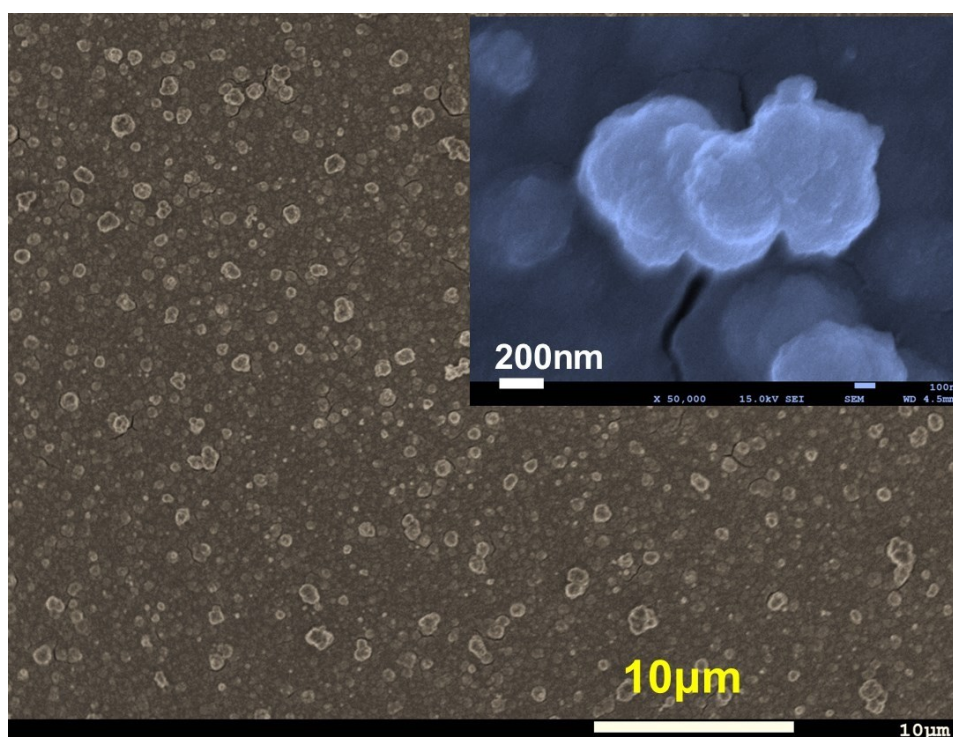


Figure 5.2: Electron micrographs from WO₃ film showing nano flower like structure

The deposited film appears to have a high surface area as can be seen in the zoomed portion (inset, Figure 5.2) of the nano flower. Such a

combined property of uniform thickness and high surface area is an essential requirement for active electrochromic electrodes..

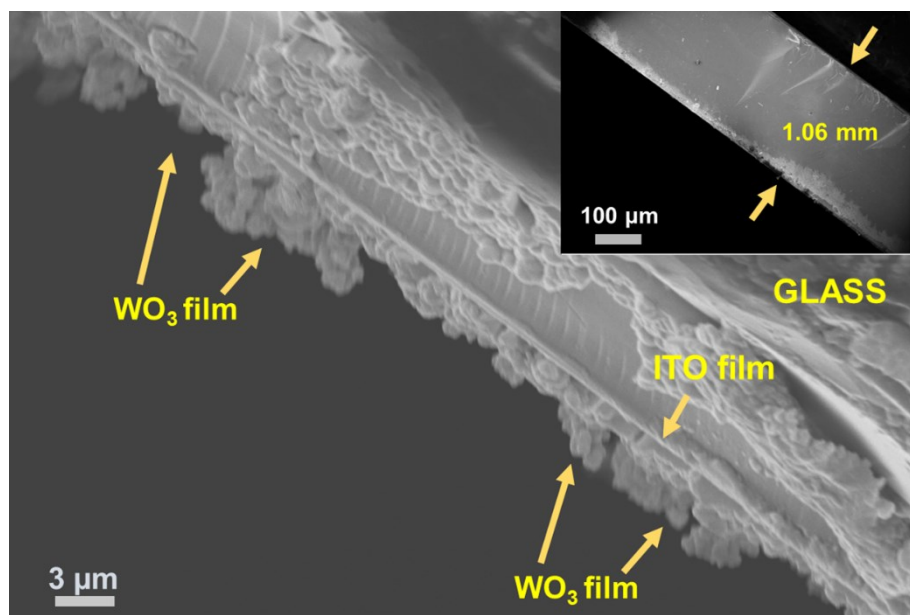


Figure 5.3: Cross sectional view of the WO_3 deposited ITO as seen using SEM micrograph in the zoomed portion and the overall picture (inset).

Next, cross-sectional SEM has been performed which shows (Figure 5.3) the three regions/layers i.e., the glass substrate, the ITO layer and the WO_3 film on top. The inset image shows the cross-sectional view of the ~1mm thick glass substrate and the white layer on the left side of which is the as-deposited film. The high magnification image shows an almost uniform thin film of WO_3 which is of the order of few micrometres, thus confirming successful deposition.

5.2.2.2 X-ray of electrodeposited WO_3 film

The XRD pattern (Figure 5.4) from electrodeposited film shows many distinct peaks. The peaks marked with ‘&’ represent the presence of WO_3 in accordance with the JCPDS data (file no. 01-072-1465) and has been identified to be present at 22° (001), 23.4° (110), 25° (101), 42° (220), 55° (202)[23]. The broad peak at 23.4° corresponds to

monoclinic phase of WO_3 . Additionally, the sharp peaks in the XRD pattern are appearing due to the underlying ITO film on the glass substrate onto which the WO_3 film has been deposited[146–148]. The presence of clear diffraction peaks ('&' marked) implies the presence of intended WO_3 phase in the film which has been further confirmed using Raman spectroscopy.

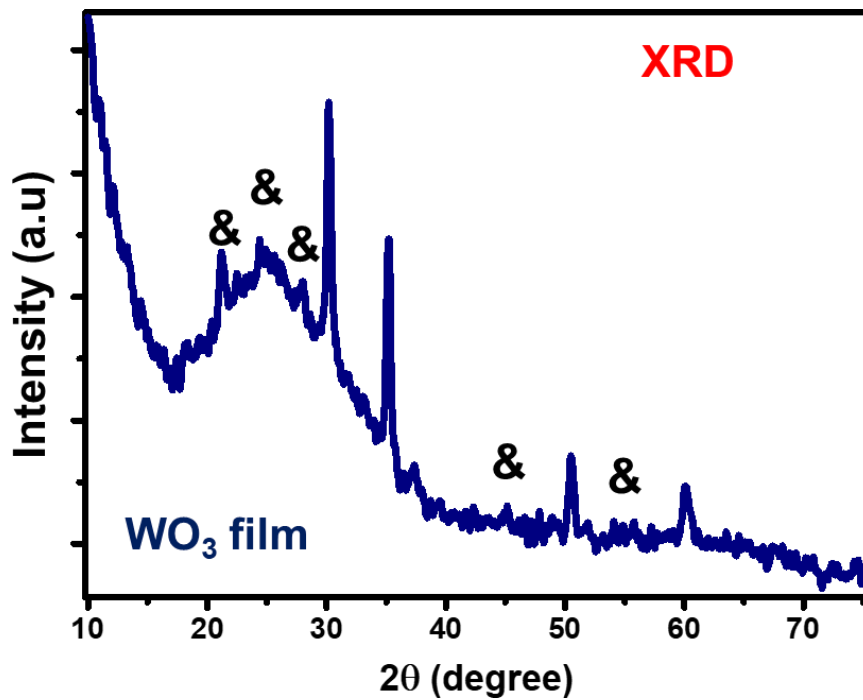


Figure 5.4: The XRD pattern of the WO_3 film.

5.2.2.3 Raman spectroscopy

The broad Raman peaks (Figure 5.5) marked '\$' around $\sim 758\text{cm}^{-1}$ corresponds to O-W-O stretching mode and the one at 1010cm^{-1} is a shoulder peak for the same[25,149,150]. Whereas the peak at 217cm^{-1} corresponds to bending vibration of the same bond, thus confirming the monoclinic phase of WO_3 . The basic characterization techniques, SEM, XRD and Raman, thus reveal that a continuous film of crystalline WO_3 has been deposited, as intended.

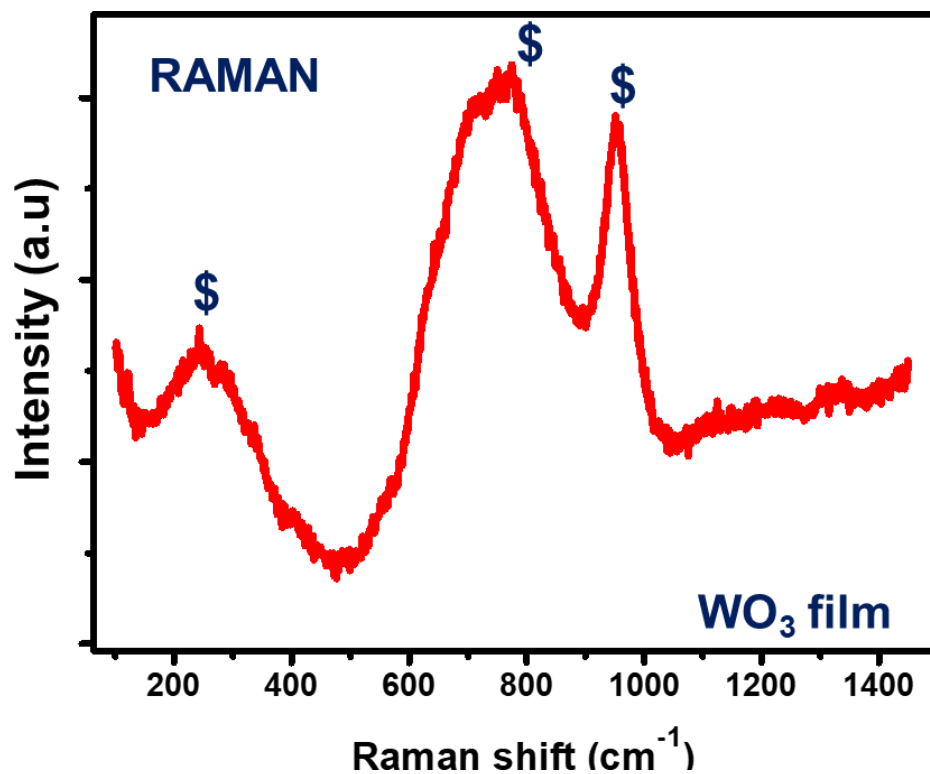


Figure 5.5: Raman spectrum of WO₃ film.

5.2.2.4 Cyclic voltammetry

A three-electrode cell set up with the above prepared WO₃ film electrode used as working electrode (WE), a Pt-wire as counter electrode (CE) and Ag/AgCl as the reference electrode (RE) has been used to carry out electrochemical studies in an electrolytic solution containing 0.5M H₂SO₄. The CV curve (Figure 5.6a) has been obtained by sweeping the voltage in the potential range -0.3V to 0.5V between the WE and RE at a scan rate of 100mV/s and the corresponding current was obtained between the WE and CE.

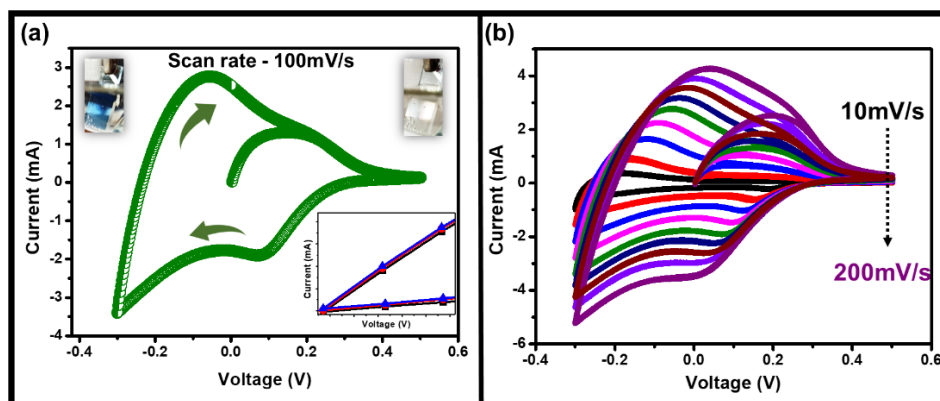


Figure 5.6: Cyclic voltammograms recorded from WO₃ films at (a) 100mV/s with inset images showing actual photo of electrode and (b) showing scan rate dependent CV curves.

Two characteristic redox peaks at 0.1V and -0.1V can be seen due to the reversible intercalation and deintercalation of H⁺ ions in and out the WO₃ electrode. The reaction governing the H⁺ insertion due to charging and H⁺ extraction during the discharge process is given by following redox reaction (Eq. 5.1)[151]:



During the cathodic scan (scanning from 0.5V to -0.3V), reduction takes place and the color of the WO₃ electrode changes from transparent to blue (left inset, Figure 5.6a). Since this reduction is reversible, the blue electrode regains its transparent state during the anodic scan which oxidizes the (blue) electrode (right inset, Figure 5.6a). This process is known as the bleaching process typically used in the context of redox induced electrochromic color modulation.

The Figure 5.6b shows the scan rate dependent CV wherein an interesting observation is the shifting of the anodic/cathodic peaks to higher/lower potential with increasing scan rate. Overall, the scan rate dependent redox peak position and maximum current value implies an excellent electrochemical behavior of the electrode.

5.2.2.5 In-situ absorbance spectroscopy

In-situ spectro electrochemical measurement of the WO₃ electrode has then been performed in a two-electrode setup with the WO₃ and a Pt wire as the two electrodes kept inside the quartz cuvette placed in the sample holder of the spectrophotometer. The figure below (Figure 5.7) shows the transmission spectra (%T) under different bias conditions where the voltage written on the graph shows the potential applied on the WO₃ electrode with respect to the Pt wire.

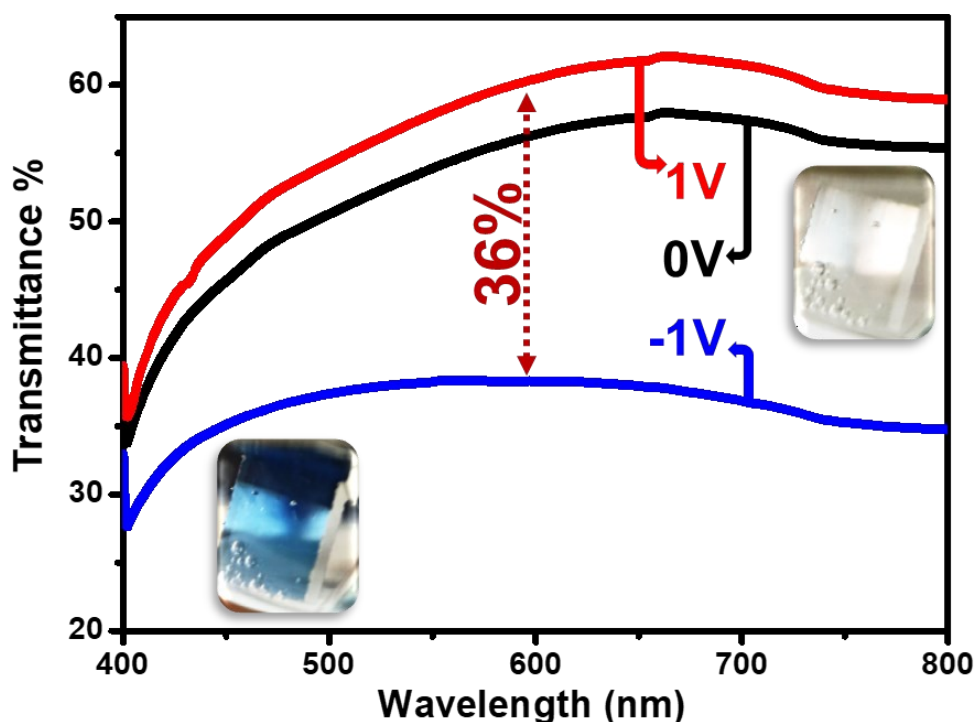


Figure 5.7: In-situ bias dependent absorbance spectra of WO_3 film

The transmission curves under different bias values of 0V (initial transparent state), 1V (bleached/oxidized state) and -1V (colored/reduced state) reveal that the electrode becomes less transparent, as compared to the initial state, when a bias of -1V is applied as the curve corresponding to the initial state is different from the colored (reduced) state. Corresponding optical image of the electrode (inset, Figure 5.7) shows that the color of the electrode changes back from blue to transparent when the bias of 1V is applied because under this bias condition the electrode gets oxidized back to its transparent state leading to the bleaching of the electrode color.

The transmission spectra corresponding to the initial (0V) and bleached (1V) states are almost similar showing a reversible nature of the coloration/bleaching process, a necessary requirement for application in electrochromic electrodes/devices. An appreciable color contrast of $\sim 36\%$ corresponding to 600nm wavelength was observed between the blue and transparent states and excellent kinematics were recorded, as shown below.

5.2.2.6 Electrode's color switching kinematics

To further study its potential application as an electrochromic active electrode, in-situ color switching kinetics has been recorded (Figure 5.8) to measure how long it takes to switch the color (switching time) of the electrode. A square pulse of $\pm 1V$ was applied for sufficiently long duration of 10s and corresponding change in %T value was monitored to estimate its colored-bleached switching time. Coloration time, the time taken to change from transparent to blue (90%) measured at 600nm, was found to be 2s. Similarly, the bleaching time, the time taken to switch from blue to transparent state, of $\sim 2.5s$ was also obtained (as shown in Figure 5.8a). Coloration cyclability, a measure of the electrode's stability, has been checked by applying multiple pulses of $\pm 1V$ (as discussed above) for 20cycles (i.e., 400s) and corresponding sequential %T modulation was measured (Figure 5.8b).

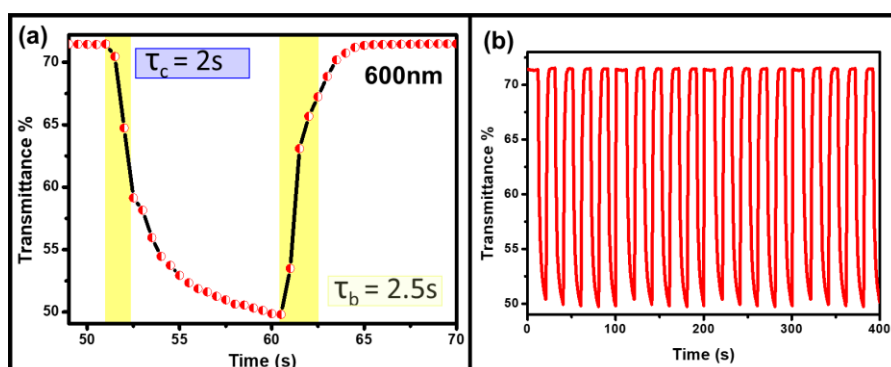


Figure 5.8: Electrode kinematics showing (a) switching times and (b) cyclic stability of the electrode.

It is quite clear from the stability curve (Figure 5.8b) that along with a good cyclability, the electrode shows good reversibility too as evident from the fact that %T values in the either state does not change even after multiple cycles which makes it a potential candidate for its application as an electrochromic active electrode. It is important here to highlight that abovementioned color modulations have been observed for an absolute bias of $\pm 1V$ which is in contrast with the existing reports where higher voltages are required for metal oxides belonging to the

same family when prepared using techniques other than the electrochemical methods (the present case).

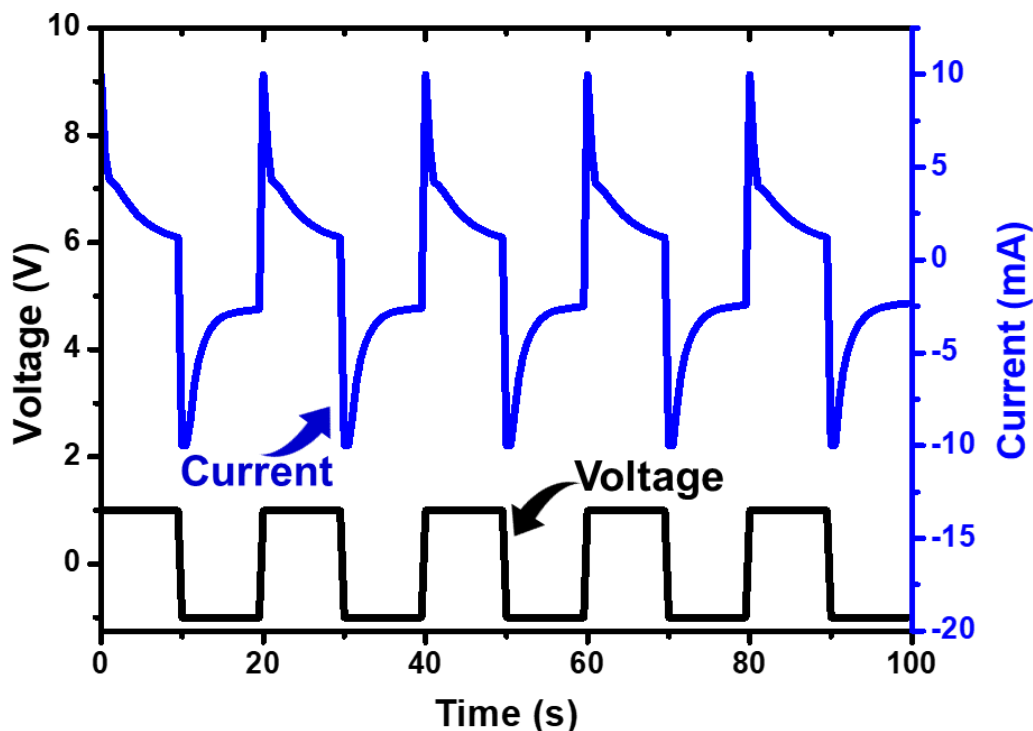


Figure 5.9: Graph showing current response for applied voltage pulse train as a function of time.

To further support the stability and robustness of the electrode (health of the electrode) the current flowing through the electrode while switching the color has been monitored when under $\pm 1V$ rectangular pulse train (Figure 5.9). The current value seems to remain stable even at 100th second, confirming the good stability of the electrode. The electrochemical and in-situ spectrochemical results discussed above show that even with a limited voltage the WO_3 electrode show good color modulation and cyclability/stability.

The above discussion about color change and cyclic stability suggests that electrodeposited WO_3 film can work as an excellent auxiliary electrochromic electrode and its performance can be further increased by adjusting a few parameters, like deposition time, precursor concentrations and applied bias. However, to obtain the best performance, it has to be coupled with another complimentary EC

electrode made into an ECD which has been done and discussed in the next section.

5.3 A hybrid solid state PANI/WO₃ electrochromic device

As gathered from the ongoing discussion, WO₃ being an n-type EC material and thus changing color in the negative bias would work as an excellent complimentary electrode with PANI thus a PANI/WO₃ hybrid device can be fabricated.

5.3.1 Fabrication of the solid-state device

The individual electrodes being electrodeposited onto ITO substrates as mentioned in detail in section 3.2 for PANI and section 5.2 for WO₃ have then been integrated together. For the gel electrolyte a 5 wt% LiClO₄ in ACN mixed with equal proportions of PEO gel was found to be suitable. Using the flip-chip technique (section 2.3.2), the final ECD was obtained. The same has been explained by the schematic shown (Figure 5.10) below.

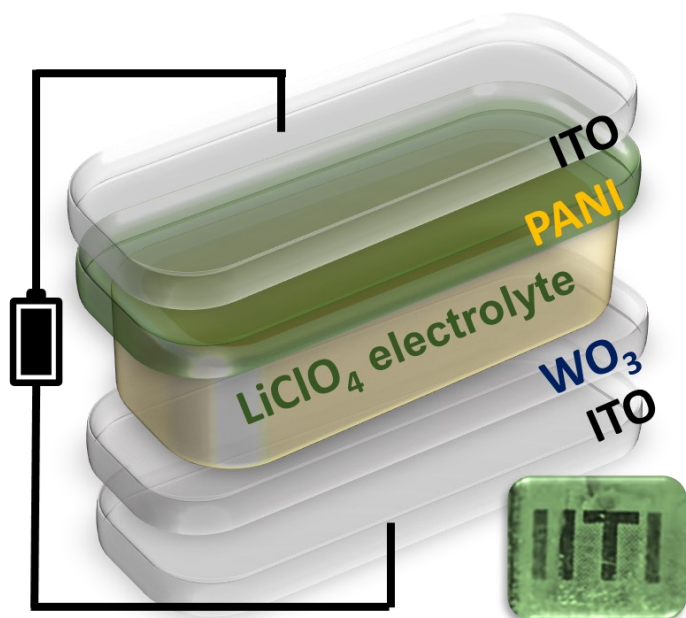


Figure 5.10: Schematic showing the PANI/WO₃ device structure along with the actual photograph of as-fabricated device (inset).

5.3.2 Performance characteristics of the finished device

The original device in an unbiased condition appears to be greenish in color owing to the transparent nature of WO_3 thin film and green colored PANI film (inset, Figure 5.10). To characterize the ECD, a nominal bias of $\pm 1.5\text{V}$ was used and its optical response was recorded as explained in detail below.

5.3.2.1 In-situ absorption spectroscopy

A positive bias of 1.5V (namely ON state) was fed to the device from the end of the PANI electrode such as to oxidize it to turn blue in color and simultaneously the WO_3 electrode receives -1.5V supply for it to get reduced and turn bluish. Therefore, a subsequent oxidation of PANI and reduction of WO_3 made the overall ECD appear blue in color. This is evident from the inset image (Figure 5.11), which shows the actual photo of the device in an ON state.

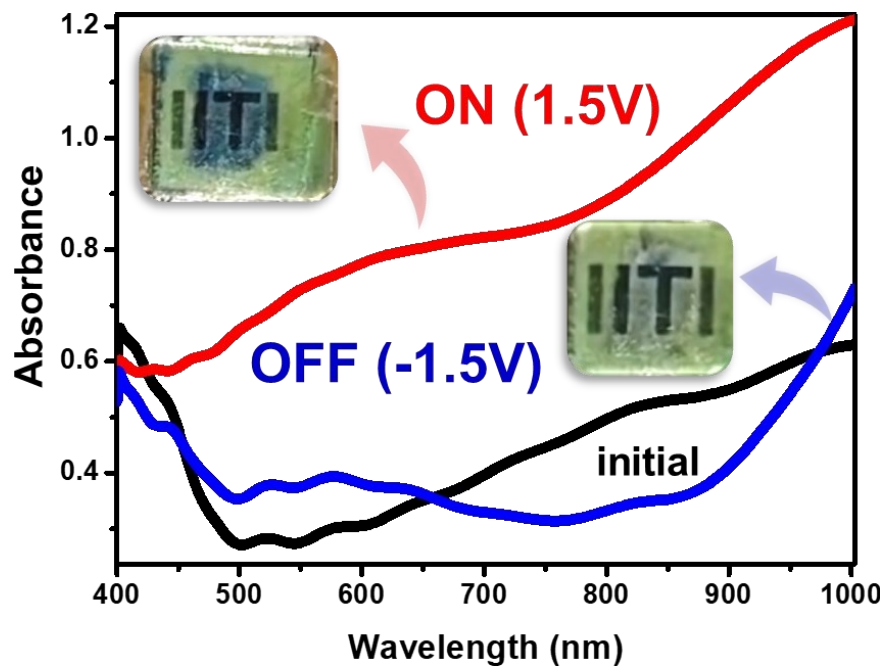


Figure 5.11: In-situ absorbance spectra of device with inset showing actual photos of device at indicated biases

On reversing the bias now, i.e., in OFF state, PANI is now reduced and turns light yellowish and WO_3 is oxidized back to its transparent state.

This leads the device to appear almost transparent which is evident from the actual photo of the device, shown in inset and also from the blue curve which seems not to absorb any visible wavelengths. Another interesting observation from the absorbance spectra indicates that the device in ON state absorbs NIR wavelength largely, a property which can be further explored for heat shield applications.

5.3.2.2 Device performance kinematics & coloration efficiency

As observed (Figure 5.11), the ECD appears to absorb almost all visible wavelengths starting from 500nm up to 1000nm in its ON state. Thus a few wavelengths were chosen (500nm, 700nm, 900nm) among them to study device kinematics. A voltage pulse of 5s width at $\pm 1.5V$ was then fed into the device for 10 cycles to establish the working of the ECD. Figure 5.12a shows the potential and current v/s time graph with a good stability for at least 100 s. The in-situ absorbance response of the device at 900nm, corresponding to the applied bias train (Figure 5.12b) confirms the stability and good cyclic repeatability of the device for 10 cycles. Choosing one cycle, switching time of the ECD was calculated at 77% (coloration) and 67% (bleaching) of the maximum wavelength. As indicated in Figure 5.12c, a coloration and bleaching time of 0.4s and 0.9s was obtained which is considered to be a quick response. In addition, a very good contrast ratio of $\sim 65\%$ was obtained at 900nm.

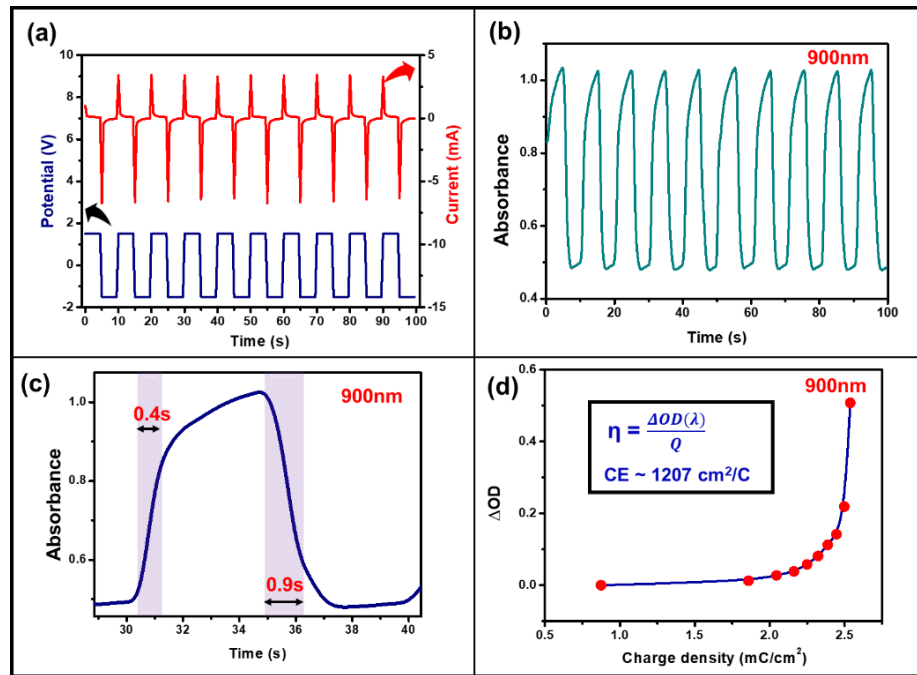


Figure 5.12: Device kinematics showing (a) voltage pulse and simultaneous current response (b) absorbance response to applied pulse (c) switching times (d) coloration efficiency.

Further, using equation 1.2, (chapter 1) the power consumption of the device was calculated in the form of coloration efficiency (Figure 5.12c). Thus, at 900nm, using the slope of change in absorbance to charge intercalated, a very good CE value of $\sim 1207 \text{ cm}^2/\text{C}$ was obtained. This value is one of the highest CE values in the individual family of WO_3 and PANI. Moreover, the entire observation establishes that the ECD works excellently well in the NIR region of the spectrum with a very good contrast value and thus can be utilized as a heat filter device.

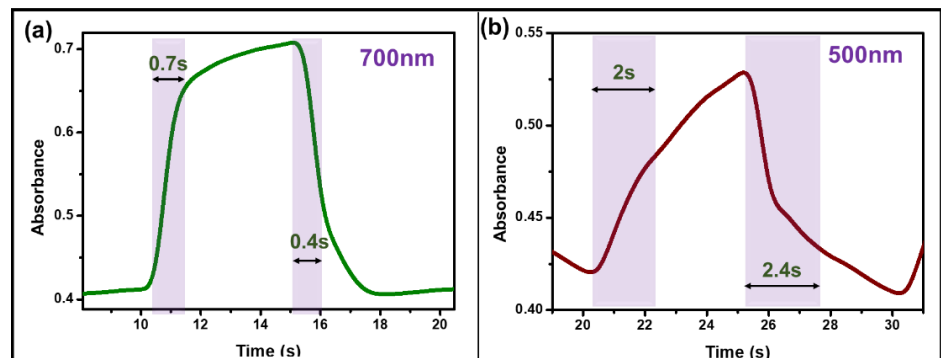


Figure 5.13: Switching times reported at (a) 700 nm and (b) 500nm wavelength.

Furthermore, the same process was repeated for two more (visible) wavelengths i.e., 700nm and 500nm and the results were summarized in Figure 5.13a and b respectively. At 700nm, the ECD showed a somewhat reduced contrast ration of 48% and a very good switching time of 0.7s (coloration) and 0.4s (bleaching), implying the ECD works well at a visible wavelength of 700nm. However, the ECD tends to show very sluggish behavior at 500nm wavelength with a switching time of over 2s for both coloration and bleaching. The contrast ratio too dropped up to only ~20% at this wavelength.

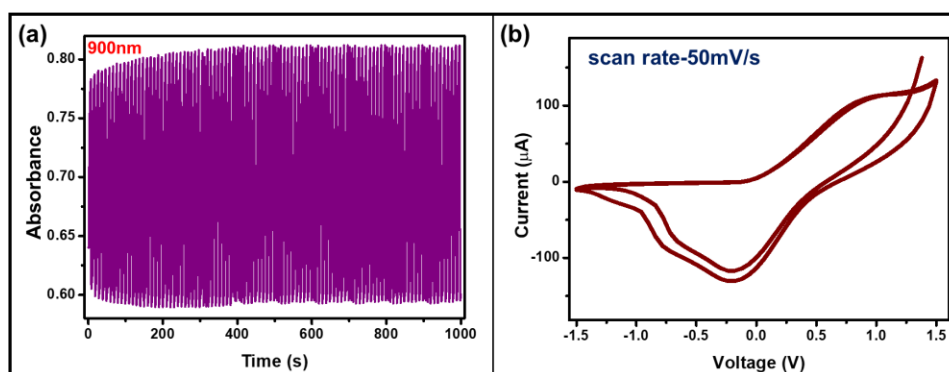


Figure 5.14: (a) Devices' stability and (b) CV curve

The device was next tested for cyclic stability by applying a voltage pulse of ± 1.5 V for 1000s, and the response has been recorded at 900nm wavelength. Figure 5.14 a shows a very good stability of the device for at least 100 cycles with almost no change in the absorbance. Simultaneously after running the device for 1000s, a CV curve was recorded at a scan rate of 50mV/s, to finally validate the stability of the device (Figure 5.14b). Overall, the excellent results obtained by analyzing the electrochromic parameters suggests that the combination of PANI and WO_3 as a hybrid complimentary redox pair is an utterly successful one.

5.4 Conclusion

To summarize the entire discussion, chronoamperometric method used to deposit WO_3 results in device grade thin films with well-maintained uniformity which were nano-flowered in shape. This WO_3 film, which was analyzed to be monoclinic in nature has been thoroughly studied using electrochemical methodologies to establish it as an n-type auxiliary electrode which would change color between transparent and blue state. Taking this hint, it was then paired with a PANI film to fabricate a hybrid ECD.

The hybrid PANI/ WO_3 solid state electrochromic device, which changes color between transparent and blue states, absorbs a range of wavelengths from visible up to NIR. Thorough characterization of the device implied its excellent electrochromic abilities such as faster switching time, good contrast, very high efficiency, and stability. Additionally, the ability of the device to switch well in the NIR region can be further utilized to fabricate a heat shielding hybrid ECD.

Chapter 6

Hybrid electrochromic PANI@WO₃ core-shell for multifunctional energy application

In this chapter, polyaniline and tungsten oxide have been amalgamated using chronoamperometry to obtain a core-shell structure and its energy generation and storage application has been reported*. Electrodepositing WO₃ and PANI onto highly conducting substrates one on top of other, results in formation of PANI@WO₃ electrode which displays multifunctional applications. Morphological studies suggest that the deposited electrode possesses a highly uniform fibrous surface structure thus promising an enhanced charge trapping property. Electrochemistry performed using the conventional three electrode step up suggests a very good charge storage capacity, stability and mostly indicating a pseudo capacitive behavior. Besides very good values of areal capacitance, power density and energy density establishes its supercapacitive performance. Next, its behavior as an electrocatalyst was also observed through polarization curves and their corresponding Tafel plots. Finally, its electrochromic behavior was confirmed by characterizing the electrode for in-situ absorption properties and analyzing all the conventional parameters.

* Ghosh. T. et. al., Under Review

6.1 Hybrid core-shell

In broad terms, core-shells refer to combination of two (or more) materials layered upon one another i.e., compounds which have inner (core) and outer (shell) layers made of different components[152,153]. They can be synthesized using both chemical and physical methods, even both the layers can be fabricated using different techniques. For example, the inner core can be deposited using hydrothermal method and on top of that the outer core can be electrically deposited. Core-shell structure enjoys the benefit of both the materials and enables multifunctional applications with proper manipulation of the no. of layers, thickness of layers and composition[154–157]. The choice of materials depends on targeted application(s), however here we have chosen PANI and WO_3 owing to their individualistic properties and therefore to obtain multifunctional electrode. Besides being hybrid in nature, it proves to be sturdier and more resistant than most of its all-organic or all-inorganic contemporaries[53,157].

6.2 Fabricating the PANI@ WO_3 core-shell

For this study we have made use of electrodeposition method to generate the PANI@ WO_3 core-shell structure. The schematic below explains the step-by-step method of fabrication.

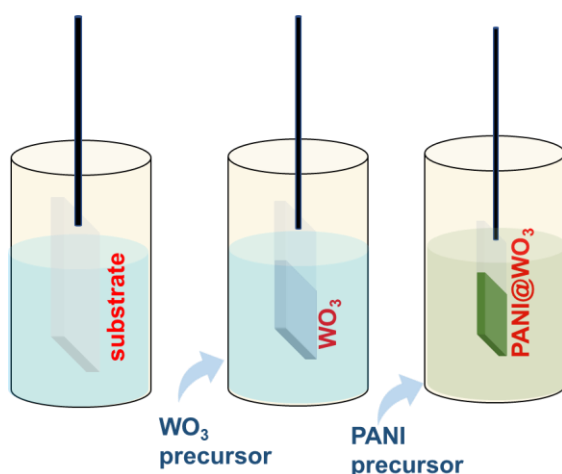


Figure 6.1: Schematic showing core-shell electrodeposition process.

We have used two types of substrates, carbon cloth and FTO for this particular study used for energy and electrochromic applications respectively. The deposition was carried out by adopting the following recipe:

- First the substrates were properly cleaned and sonicated.
- Next using the preparation recipe explained in section 5.2.1, WO_3 has been deposited onto the substrate and left to dry.
- On top of the WO_3 layer, PANI has been deposited following the same recipe explained in section 3.2 with WO_3 coated substrate being used as the WE in this case.
- The as-deposited PANI@ WO_3 electrodes has then been dried by heating them at 80°C for an hour prior to use.

Besides the core-shell, individual WO_3 and PANI films were deposited onto CC substrates (as control experiment) to study and compare all the properties.

6.3 Characterizing the core-shell

The prepared electrode(s) have then been characterized using different morphological methods to confirm and understand the core-shell behavior. The data obtained from the individual electrodes too have been shown to draw a comparison.

6.3.1 Surface morphology study using SEM

The SEM images from individual WO_3 and PANI films and PANI@ WO_3 electrodes deposited on CC substrate (Figure 6.2) shows a crystalline flower like morphology for individual WO_3 film showing evenly distributed film over the surface of the carbon strands (Figure 6.2a). On the other hand, the individual PANI film possess a fiber like structure also uniformly coating the entire area (Figure 6.2b). It is important here to mention that WO_3 film on ITO substrate has been studied at length in chapter 5 (section 5.2).

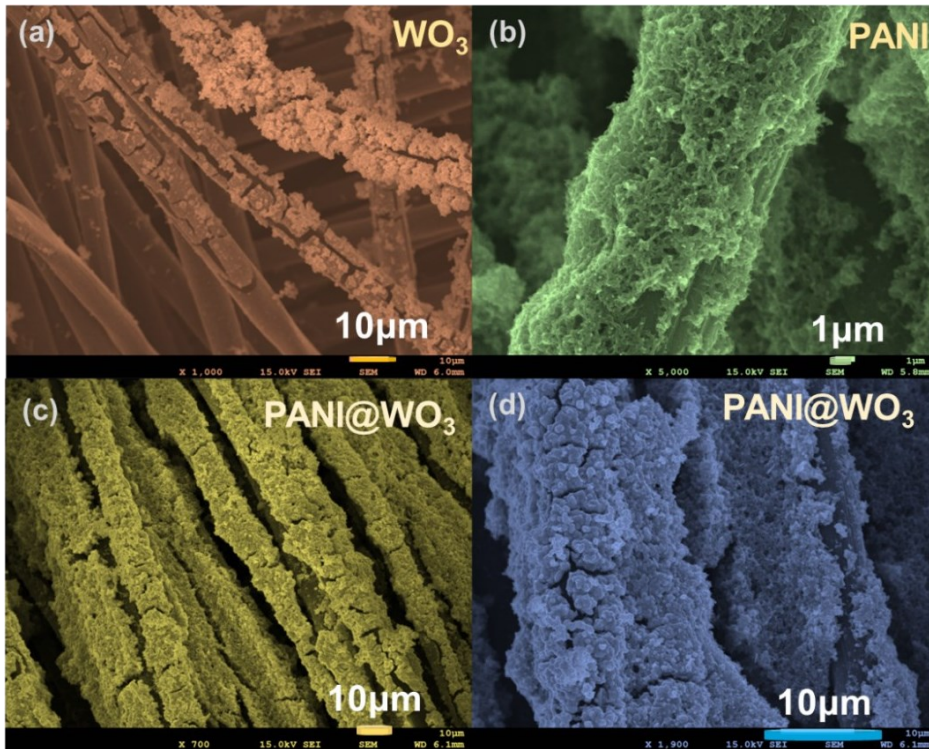


Figure 6.2: Images showing SEM micrographs recorded from individual (a) PANI, (b) WO₃ electrode and PANI@WO₃ core-shell at different magnification (c,d).

The PANI@WO₃ core-shell however tends to portray a highly uniform fibrous network like structure (Figure 6.2c). The zoomed image (Figure 6.2d) clearly shows the growth of both the flower shaped WO₃ film and the fiber like PANI film. This confirms the core-shell structure indicating a successful fabrication. Besides, uniform morphology promises a large surface area of interaction and higher charge storage capabilities that will be established in the subsequent sections.

6.3.2 Raman spectroscopy

Raman spectra from the PANI@WO₃ core-shell (Figure 6.3a) structured electrode along with the individual films (Figures 6.3b, 6.3c) are shown in Figure 6.3 where the latter has already been discussed in section 5.2.2 and 3.3.1 respectively.

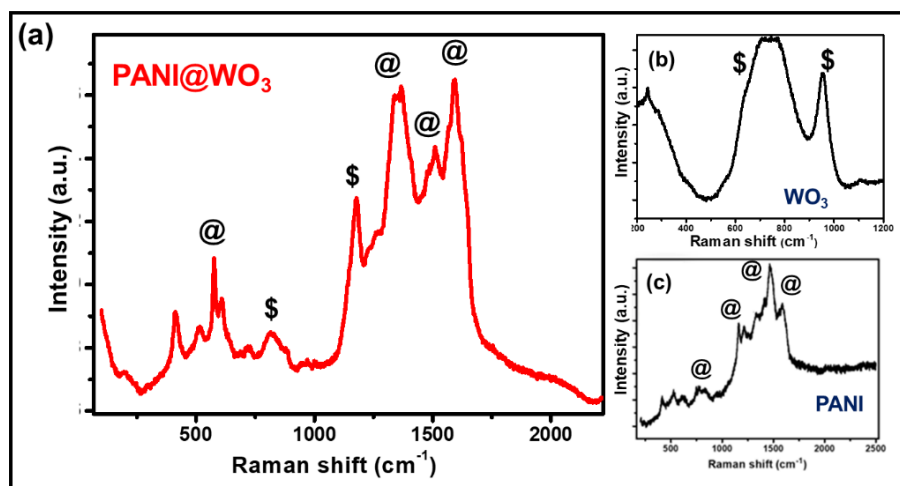


Figure 6.3: Raman spectrum from (a) PANI@WO₃ core-shell, (b) WO₃ and (c) PANI electrode.

The peaks identified as '\$' belong to WO₃ and those identified as '@' belong to PANI film. Analyzing the Raman peaks of the PANI@WO₃ electrode it is evident that the Raman spectra contains all the individual peaks from both the material showing no signs of new chemical binds or any phase change etc. Thus, the Raman spectra too confirms the successful formation of the core-shell structure.

6.3.3 X-ray diffraction

To fully confirm that the core-shell structure consists of no new chemical bond or phase information, XRD studies of the as-deposited electrode has been performed and compared with the already available data of WO₃ electrode, as discussed in section 5.2.2. The figure shows the XRD pattern of the PANI@WO₃ electrode with the inset showing the same for the individual WO₃ electrode.

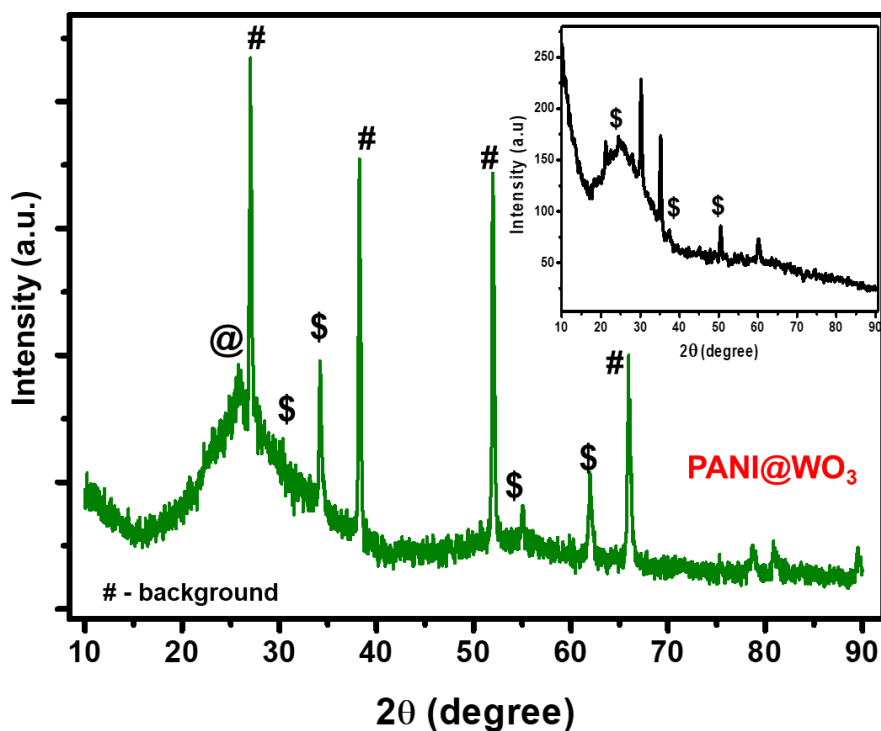


Figure 6.4: X-ray pattern of PANI@WO₃ core-shell electrode along with the XRD pattern for individual WO₃ film (inset).

The peaks marked '@' are that of PANI film, as identified from the JCPDS database, and the sharp peaks marked '#' belongs to the background. All the other peaks have been matched thoroughly with the WO₃ film and found that no new peaks, other than individual PANI or WO₃ has been observed. This confirms the assumption that no new phase formation took place besides validating the fact that PANI@WO₃ core-shell structure has been successfully obtained.

6.3.4 Fourier transform infrared spectroscopy

Finally, an FTIR spectrum has been recorded from the PANI@WO₃ electrode, whose peaks have been analyzed using the available literature. Various chemical bond information, as marked below, has been obtained belonging to both PANI and WO₃ and peaks at around 500-1600cm⁻¹ belonging to strong PANI bonds. All the characterizations performed thus hinted towards the successful fabrication of the as deposited PANI@WO₃ core-shell for it to be studied later for various application.

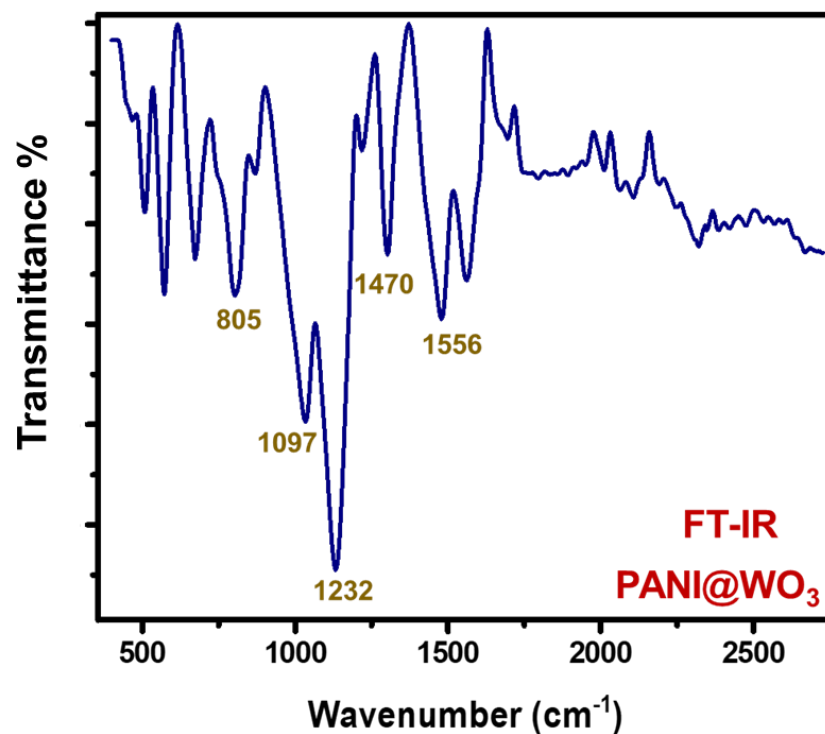


Figure 6.5: Fourier transform spectrum of PANI@WO₃ electrode.

6.4 Multifunctional application of the core-shell electrode

Following the thorough characterizations of the electrode, it is believed to display multifunctional behavior. To establish the same, the PANI@WO₃ electrode has been tested for energy related smart window applications as explained below.

6.4.1 Supercapacitive energy storage properties

Both PANI and WO₃ are known to possess charge storage properties, which is believed to be enhanced for the core-shell structure[139,158]. Using a 0.5M H₂SO₄ electrolytic solution and PANI@WO₃ as the WE, CV curves were recorded in the range of 1.2V to -0.5V and at three scan rates (Figure 6.6a). The dipped electrode area accounted for 1.1 cm² giving out a maximum current density of 180mA/cm² at a scan rate of 50mV/s. A very high value of current density along with a good area under the CV curve demonstrates excellent charge storage capacity.

Besides the non-rectangular shape of the curve with distinct redox peak indicates pseudo-capacitive nature. Further, CV curves were recorded

at multiple scan rates (from 10mV/s up to 100mV/s) and the square root of scan rates (\sqrt{v}) were plotted against respective anodic and cathodic peak currents (I_p). A very well expected linear relationship between the two validates the electrodes' reversibility (Figure 6.6b).

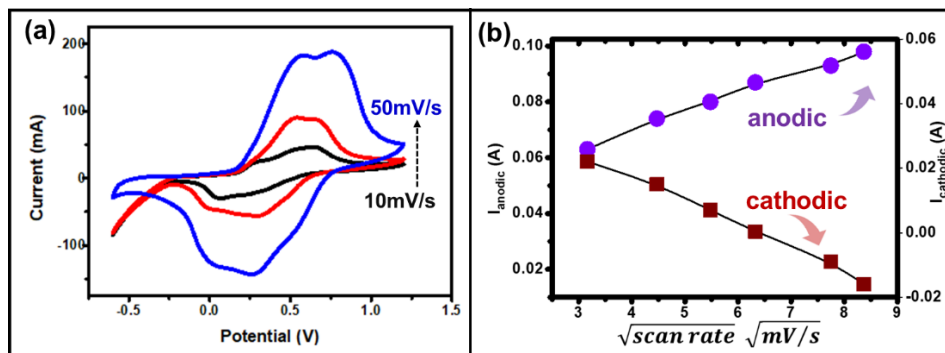


Figure 6.6: (a) Cyclic voltammograms recorded at three different scan rates and (b) peak current v/s square root of scan rate graph.

To further establish stability, CV curves were recorded for 50 cycles at 20mV/s scan rate (Figure 6.7a). It was observed that the current value dropped by a very small amount coupled with no significant change in the shape of the curve indicated a very good reversibility too. To further understand the nature of the electrode, Nyquist plots were recorded in the range of 0.1 Hz to 1 MHz by applying an alternating current of 5mV amplitude (Figure 6.7b).

A semi-circular pattern at high frequency (Figure 6.7b) arises from electrolytic resistance and solution charge transfer. However, the inset image shows an incomplete semi-circle at lower frequencies which arises due to redox mechanism and therefore justifies the pseudo capacitive nature of the electrode. This means that charge transfer mechanism is not governed by double layer formation at the electrode-electrolyte interface as observed in case of supercapacitors, rather intercalation and deintercalation of ions taking place at the interface, thus confirming the pseudo-capacitive behavior of the PANI@WO₃ electrode.

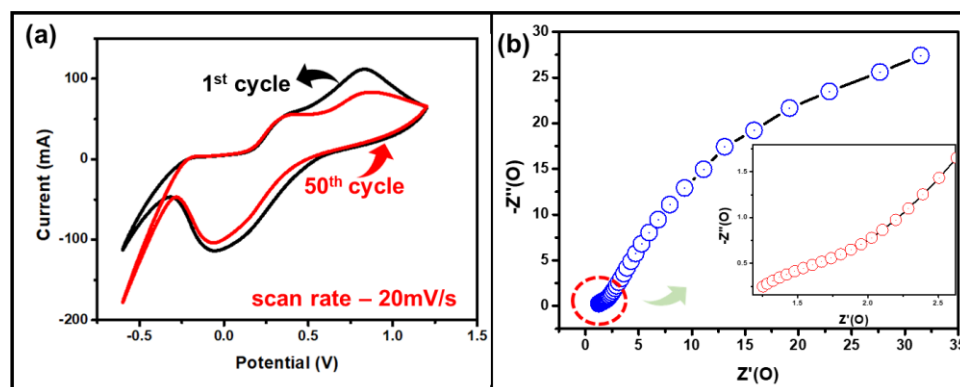


Figure 6.7: (a) Cyclic voltammograms showing electrodes' stability at 1st and 50th cycle and (b) Nyquist plot recorded in the frequency range 0.1 Hz to 1MHz along with a zoomed portion (inset).

After establishing the capacitive nature, it is essential to record the charging and discharging pattern. Figure 6.8a reports the charging and discharging graphs of the electrode recorded in a wide potential range of -0.5V to +1V at increasing current densities. The decrease of charging/discharging times with an increase in current density indicates faster ion transport and with it, a simultaneous decrease in capacitance value.

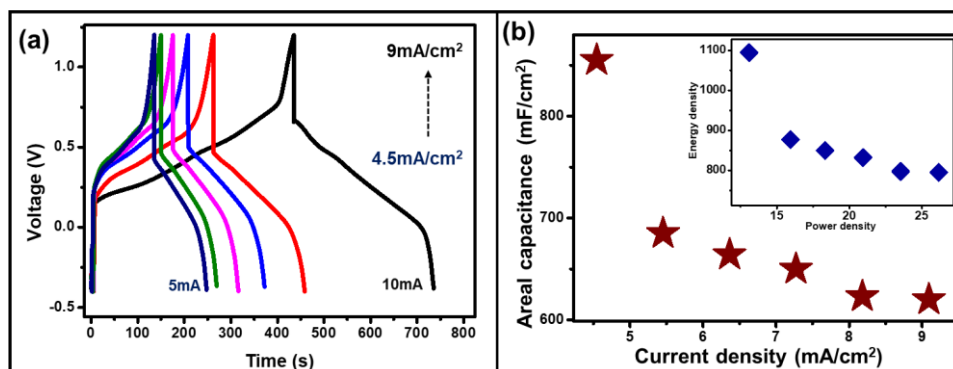


Figure 6.8: (a) Charge-discharge curves under varying current densities and (b) corresponding current densities v/s areal capacitance with Ragone plot (inset).

Besides the symmetrical charging and discharging pattern refer to the good reversibility of the electrode. The sudden IR drop occurring at the beginning of the discharge cycle arises from the resistance added by the supercapacitor. A good discharging time of 380s was recorded at a

current density of 4.5mA/cm². Areal capacitance, a measure of charge stored into the electrode per unit applied potential per unit area is represented by the following Eq. 6.1[159]:

$$C_a = \frac{I \times \Delta t}{A \times \Delta V}, \quad (6.1)$$

where C_a refers to areal capacitance which is expressed in mF/cm², Δt is the discharging time recorded against a particular applied current, A refers to active area of the electrode and ΔV refers to the applied potential window. For this study, the value of ΔV was kept constant at 1.6V and the active area of electrode, A was 1.1cm².

Varying the value of I , different values of Δt were obtained and consequently different values of C_a was obtained. A very good value of C_a i.e., 855mF/cm² was obtained at a current density of 4.5mA/cm². Figure 6.8b shows a plot of areal capacitance values obtained against different values of current densities. It is evident from the figure that the values of areal capacitance decrease with increasing current density and the lowest value of 653 mF/cm² was recorded at a maximum current density of 9mA/cm².

The Ragone plot (inset, Figure 6.8b) shows a variation of power density plotted against a variation of its energy density (measured in units of per unit area)[160]. The formulas to calculate both energy density (E_d) and power density (P_d) is given by Eq. 6.2 and 6.3 respectively:

$$E_d = \frac{1}{2} \times C_a \times (\Delta V)^2 \quad (6.2)$$

$$P_d = 3600 \times E_d / \Delta t, \quad (6.3)$$

where E_d and P_d are expressed in Wh/cm² and W/cm² respectively. Both E_d and P_d were calculated for varying values of current densities and were plotted against each other. The exponential curve obtained is known as the Ragone plot which shows a maximum E_d of 1.09 kWh/cm² and P_d of 6.5kW/cm² was obtained against the optimized current density of 4.5mA/cm². These values are considered to be very

high in the family of PANI@WO₃ core-shell structure as can be confirmed from table 6.2.

Table 6.2: Comparison of charge storing abilities, energy, and power densities among various material compositions.

Sl no.	Materials	Areal capacitance (mF/cm ²)	Energy density (Wh/cm ²)	Power density (W/cm ²)	References
1.	WO _{3-x} /MoO _{3-x}	216	0.0019	0.73	[53]
2.	PANI/WO ₃ composite	215	-	-	[161]
3.	WO ₃ ·H ₂ O nanosheets	43.3	-	-	[8]
4.	PANI@MnO ₂	-	8.49	163	[158]
5.	WO ₃ /WS ₂	55	0.0105	1.4	[162]
6.	WO ₃ /graphene/PANI	11.26	-	-	[146]
7.	WO ₃ /PANI composite	120	-	-	[163]
8.	<i>PANI@WO₃</i>	<u>855</u>	<u>1040</u>	<u>1600</u>	<i>This work</i>

To further check for the electrochemical stability, the electrode's charge-discharge ability has been tested for 500 cycles at a current density of 45.5 mA/cm². Inset (Figure 6.9a) shows excellent stability with almost no loss in the discharging time. Capacitive retention is

another parameter which justifies the retention of charge storage abilities after the electrode was run for a few hundred cycles.

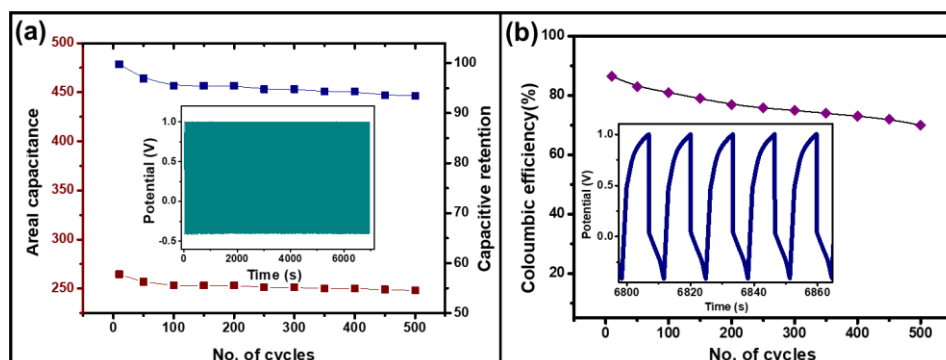


Figure 6.9: (a) Capacitive retention and areal capacitance v/s no. of cycles with stability shown in inset and (b) coulombic efficiency calculation.

Figure 6.9a shows the areal capacitance and capacitive retention plotted against number of cycles. It is clear from the figure that the values plotted for 10 cycles represent an almost linear behavior indicating a very good charge retention capability of the electrode. Finally, to consolidate the discussion another important parameter namely coulombic efficiency has been measured using the following Eq. 6.4:

$$C_e = \Delta t / \Delta t' \times 100\%, \quad (6.4)$$

where, C_e represents coulombic efficiency (expressed in %), Δt and $\Delta t'$ represents the discharging and charging times respectively. Figure 6.9b shows a linearly varying pattern of C_e , from a maximum efficiency of 86% recorded at the 1st cycle, slowly decreasing up to 65% for the 500th cycle. All of these results establishes the excellent charge storage capacity and stability of the core-shell electrode.

6.4.2 Electrocatalytic activity

The above discussion very well established the pseudo capacitive capabilities of the PANI@WO₃ electrode. However, in addition to this, the core-shell structure is also investigated to explore its catalytic activities. Interestingly while recording CV (Figure 6.6a), bubble

formation was observed (inset, Figure 6.10) at the WE, with an overshoot of current both in positive and negative scan directions indicating possible hydrogen and oxygen evolution taking place at the surface of PANI@WO₃ electrode[164,165].

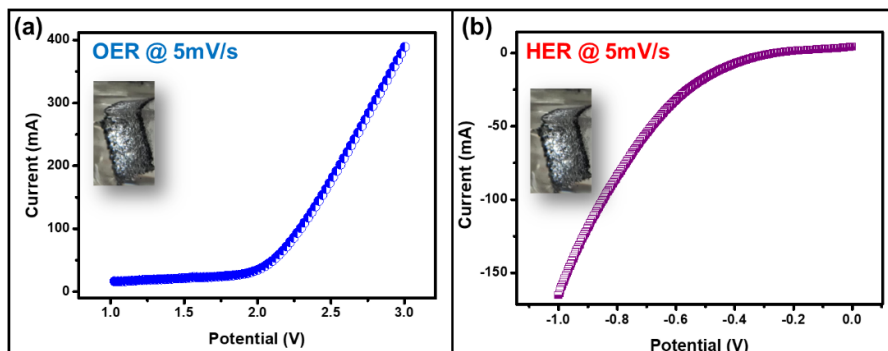


Figure 6.10: Linear sweep curves recorded from the PANI@WO₃ electrode at a scan rate of 5mV/s showing (a) HER and (b) OER reactions with inset showing actual bubble formation.

To establish this property, LSV curves were recorded at a very low scan rate of 5mV/s in two potential ranges (v/s reversible hydrogen electrode or RHE), i.e., from 1V to 3V for observing OER and from 0V to -1V to observe HER reactions. The LSV curves have been measured in a 0.5M H₂SO₄ electrolytic solution, having a pH of 1.3 and at room temperature, considering the thermodynamic potential of Ag/AgCl electrode to be 0.221V. Figure 6.10a and b shows the anodic and cathodic polarization curves recorded at a scan rate of 5mV/s, and their inset images shows the observed bubble formation around the electrode.

The value of overpotential calculated for OER reaction as against an Ag/AgCl electrode was found to be ~930mV which is a considerably high value in comparison to ideal data available, although the electrode clearly exhibited OER catalytic activity[166]. However, the overpotential value for HER was obtained to be around ~310mV which is a decent value as compared to its contemporaries. Tafel plots representing observed overpotential values plotted against log of current density (Figure 6.11) shows the expected linear behavior.

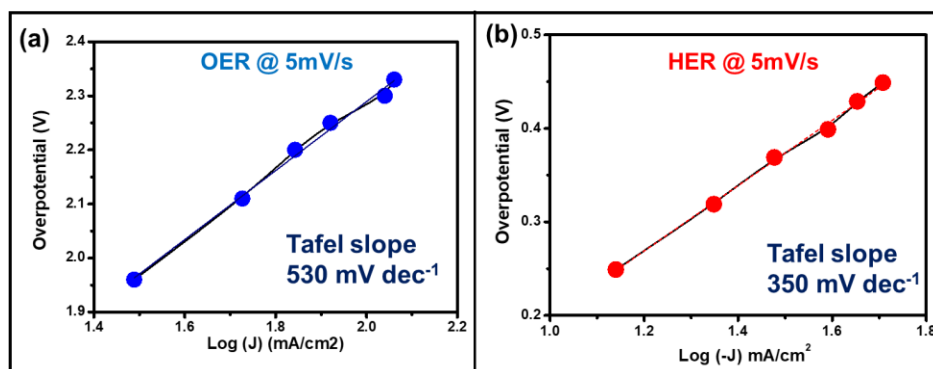


Figure 6.11: Tafel plot for (a) OER and (b) HER reactions measured from the PANI/WO₃ core-shell electrode on CC substrate.

The Tafel slope of $\sim 530 \text{ mV dec}^{-1}$ indicates sluggish OER activity of the electrode. A Tafel slope value of 350 mV dec^{-1} indicates good kinetics of electrocatalytic HER activity[167]. Severe bubble formation at the surface of the electrode visually confirms the catalytic activity and interestingly this is the first report of electrocatalysis from a PANI@WO₃ core-shell. It can be thus concluded that the PANI@WO₃ electrode works as a good electrocatalyst for both HER and OER reactions, however the values of overpotential can be further improved by testing the electrode in different electrolytes.

6.4.3 Electrochromic property of PANI@WO₃ (FTO) electrode

Additionally, since both WO₃ and PANI are very well-established chromophores, the PANI@WO₃ has finally been tested from electrochromic properties. For this purpose, the substrate has been changed to an FTO coated glass substrate and following the same recipe (section 6.2), the core-shell has been fabricated. Figure 6.12a shows the CV curve recorded at a scan rate of 50mV/s with distinguished cathodic and anodic peaks appearing at +0.55V and -0.2V respectively. The inset images show the actual color change of the electrode recorded at the indicated biases. It is observed that the electrode changes color from blue at the negative bias to greenish at around 0.5V and to dark greenish at higher positive bias.

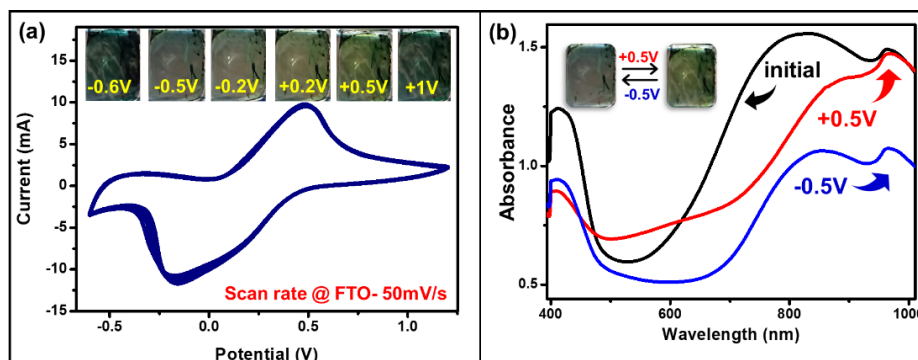


Figure 6.12: (a) Electrochromic properties of PANI@WO₃ electrode on an FTO substrate showing CV curve (50mV/s) along with actual photographs of the electrode (inset) and (b) in-situ bias dependent absorbance spectra recorded at $\pm 0.5V$.

In an unbiased state, WO₃ being transparent, the electrode appears green owing to the color of PANI. At 0.5V, the PANI electrode is in the EM state thus giving out a green appearance. With the increase in bias up to 1V, the EM state of PANI changes to PG state, which is dark greenish in color and since WO₃ is still transparent the overall electrode appears dark greenish. However, when a negative bias of -0.5V is applied, the PANI film turn to its LM state which is light yellowish in color. At this bias however, WO₃ changes to bluish color, thus giving the electrode an overall hue of blue color. This color changes happen in a gradual manner passing through a transparent state at around -0.2V.

To record in-situ absorbance spectra, the electrode was placed in a cuvette inside the UV-Vis spectrometer and was fed with an external bias. The black curve (Figure 6.12b) represents the initial unbiased state of the electrode with peak at ~400nm and a hump at ~750nm representing the π -polaron and π^* -polaron transition of the EM state of PANI. The electrode is then switched between +0.5V (red curve) and -0.5V (blue curve) with maximum contrast observed over the visible and NIR region. Here the maximum value of CR recorded at 600nm and 1000nm turns out to be ~40% and 55% respectively.

A small pulsating voltage of $\pm 0.5V$ for 10s was applied (Figure 6.13 a) and the corresponding response was recorded. Further, choosing 600nm

wavelength, switching times has been calculated (Figure 6.13b). Generally defined as the time taken to switch to 90% of the maximum absorbance value, the coloration and bleaching times obtained in this study are approximately 2.1s and 0.4s respectively. Besides, the same drill has been repeated with 1000nm wavelength (Figure 6.13c) which reports good values of coloration (1.4s) and bleaching times (2.1s).

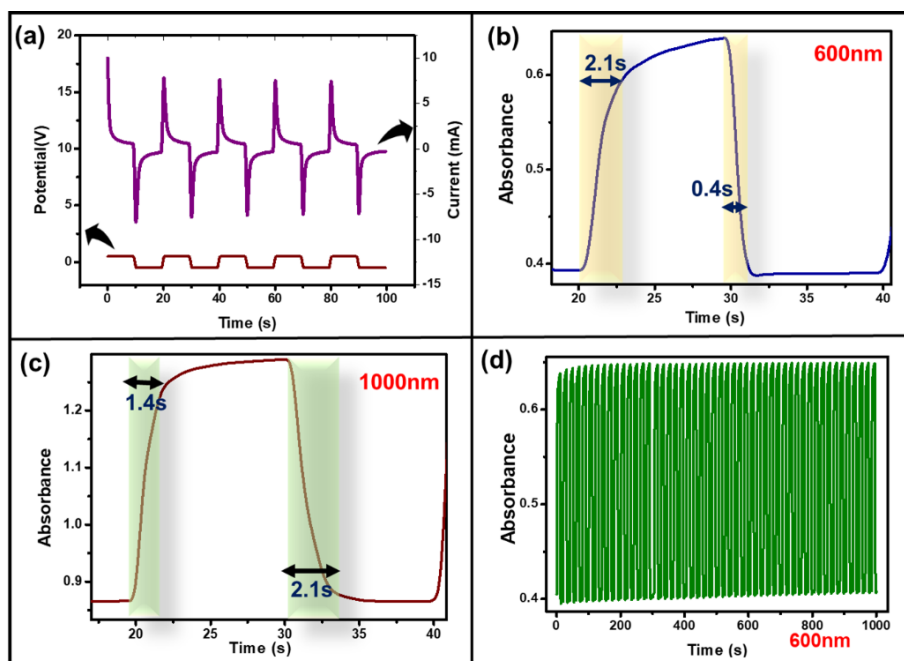


Figure 6.13: Electrode kinematics showing (a) current response against bias of $\pm 0.5V$, switching times calculated at (b) 600nm and (c) 1000nm and (d) stability recorded for 1000s.

Finally, to check for electrochromic stability, the voltage pulse was applied for a longer time interval of 1000s and the corresponding response was recorded at 600nm wavelength (Figure 6.13 d). A negligible loss in contrast value even at the end of 100 cycles establishes the excellent electrochromic stability of the electrode. High stability, good reversibility, and smaller switching times (fast switching) corresponding to a very small amount of bias establishes that the core-shell PANI@WO₃ electrode is a very good choice for electrochromic applications that also shows energy related applications. To encapsulate the overall discussion, PANI@WO₃ electrode has been established as an excellent charge storage electrode. Besides, the electrode is found to

display excellent electrochromic properties. However, although physically visible, the electrocatalytic activity were observed to be a little sluggish which can be improvised upon by calibrating the thickness of each layer or reciprocating the entire experiment in alkaline medium, however that falls beyond the scope of this study.

6.5 Conclusion

A two-step chronoamperometric method of electrodeposition enables the successful fabrication of PANI@WO₃ core-shell electrode which exhibits multifunctional application. Well characterized film deposited on carbon cloth substrate shows excellent charge storing capacity, along with high current density and good retention value hinted towards the pseudo capacitive nature of the electrode which was also verified by plotting Nyquist plot. A high value of areal capacitance 855 mF/cm²), energy density (1.09kWh/cm²) and power density (6.5kW/cm²) confirms the electrodes' energy storing nature.

Further, a physical observation of bubble formation seen during voltametric scan indicated that hydrogen/oxygen evolution reaction must be taking place. The same was confirmed by recording polarization curves and calculating overpotential values which indicate moderately high performance of the core-shell electrode as an electrocatalyst. Additionally, the PANI@WO₃ electrode also shows power efficient electrochromic behavior that displays color switching between green, blue, yellow, and transparent states with application of a voltage of as low as 0.5V. Additionally it shows fast switching (~0.4s), high stability (> 200 pulses) and good contrast values (> 50%). The core-shell electrode shows electrochromic performance in the visible as well as IR region. Overall, the PANI@WO₃ core-shell deposited using a simple electrochemical deposition technique proves to be a highly efficient electrode which has the ability to store charge, act as an electrocatalyst and exhibit color switching properties.

Chapter 7

Conclusions and future scope

7.1 Important conclusions

In a nutshell, the important results from work done throughout the thesis can be summarized from the following points:

1. Chronoamperometry method proves to be the most efficient technique to successfully deposit thin films of both organic (PANI) inorganic (WO_3) and hybrid (PANI@ WO_3) types.
2. PANI, due to its ambipolar nature, can be used as a generic electrochromic active layer to fabricate a solid-state electrochromic device where application-oriented constraints of choosing a counter ion is present.
3. An all-organic ECD consisting of a p-type PANI and an n-type viologen layer exhibits superior electrochromic performance as compared to their family of devices with versatile properties like multi wavelength switching, highly fast and efficient device also suitability for incorporation into flexible ECDs.
4. A hybrid ECD fabricated using PANI and WO_3 combination exhibits its own versatile advantages like higher stability, fast switching in NIR region also good contrast values, also suggesting its further utilization in heat filtering devices.
5. A hybrid PANI@ WO_3 core-shell arrangement fabricated using the chronoamperometry method results in good uniform film which was further found to exhibit multifunctional applications like charge storage, electrochromism and electrocatalysis.
6. Besides, the hybrid core-shell electrode tends to portray excellent pseudo-capacitive properties with high capacitance, energy density and power density values, alongside proving to

be a very good electrochromic electrode with high contrast and fast switching speeds.

7.2 New findings reported in the thesis

1. Chronoamperometry deposition method is relatively better to coat electrochromic materials as compared to other conventional ones like hydrothermal, solvothermal or spin coating etc.
2. A thin film of PANI changes in color both in positive and negative bias making it an ambipolar electrochromic material.
3. Ambipolar device can be designed using PANI that can be switched at any bias polarity.
4. Multiwavelength switching throughout the visible region of wavelengths can be obtained from a PANI/EV all-organic ECD.
5. Using a hybrid ECD combination of PANI/WO₃, we can fabricate a heat filtering device.
6. A single core-shell electrode obtained from a combination of PANI and WO₃ exhibits excellent multifunctional applications, with this work being the first report of the composite exhibiting electrocatalysis.

7.3 Possible future scope

After successfully studying and characterizing both all-organic and hybrid ECDs for various functionalities, a lot of new ideas can be pursued such as:

1. Figuring out more such ambipolar electrochromic materials, similar to PANI, because they are advantageous owing to the fact they provides extra flexibility to choose not only the counter ion layer of any charge carrier type but also to choose a layer which is either electrochromic active or passive.
2. Studying all-organic and all-inorganic core shell structures to explore their possibilities of incorporation into flexible devices for user friendly applications.

3. Exploring more such electrochromic materials which would display multifunctional properties like catalysis, sensing, memory storage etc., all in one electrode/device combination.
4. Studying the effect of various 2D materials like MXenes, COFs etc. in the core-shell structure and in the electrochromic domain.

7.4 Societal impact of the work

Following are a few important aspects of the thesis work which can be expected to provide societal aid if developed in a proper direction.

1. In a developing nation like India, conservation and preserving natural resources is highly essential, and ECDs can play a major role in this sector by reducing the energy demand in the form of heat regulators in building, aircrafts etc. Upgrading the present-of-the art of ECDs in the material domain can lead to better and more efficient devices than the existing ones.
2. Multiple functionalities of a particular device has a huge role to play by increasing convenience, cutting costs, and also reduced energy demands, to name a few.
3. Lastly, fabricating and developing industry ready ECDs can help boost the technology as well as economic sector of the society which ultimately can lead to further overall development.

Appendices

Appendix A1. Herbal electronic resistive memory

A raw Aloe Vera flower extract has been studied to reveal memristive behavior. The extract solution extracted in methanol using a simple one step method shows two distinct conductivities in its as-prepared and chemically reduced states. The amount of current flowing through the extract solution can be increased by means of a phenomenon similar to dynamic doping and can also be switched between the two memory like states for multiple cycles. An impressive on/off ratio value and cyclability can be achieved, which may pave the way for designing a solid-state herbal memristor using the active molecule(s) present in the Aloe Vera flower to take more advantage of this natural gift.

[Ghosh. T. et. al., ACS Appl. Electron. Mater. 2021, 3, 4, 1556–1559]

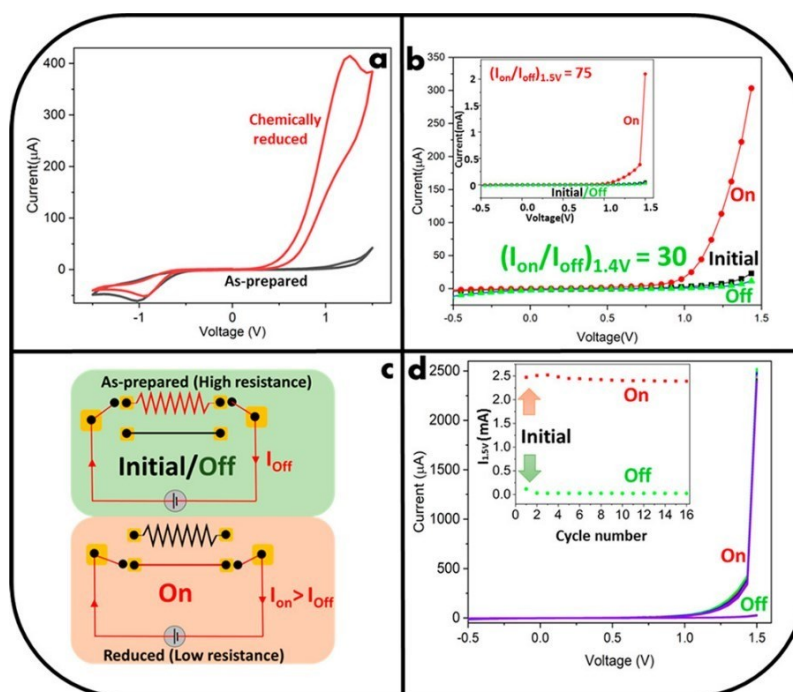


Figure A1: (a) Comparison of CV curves obtained from as-prepared and chemically reduced (doped) Aloe Vera flower extracts and (b)

solution-state I–V curves under different memory states. (c) Schematic showing switching between two different resistance states using a resistive circuit. (d) I–V curves for 16 consecutive cycles showing on/off switching between two distinct resistive states (inset).

Appendix A2. Atypical emission from Giloy and Cassia herbs

Optical and electrochemical properties from Cassia and Giloy leaves' raw extract have been studied, and they show similar properties as UV absorber but different emission properties, under UV excitation, even though they appear the same in natural light. Giloy and Cassia extracts show red and green luminescence, respectively, under UV excitation. Like the appearance, their redox properties are also similar, which shows that both can act as antioxidants. Raman spectroscopy and excitation wavelength dependent photoluminescence data have been compared. The difference in relative emission intensities have been explained based on the presence of corresponding color centers in different ratios in the two leaves.

[Ghosh. T. et. al., ACS Appl. Bio Mater. 2021, 4, 8, 5981–5986]

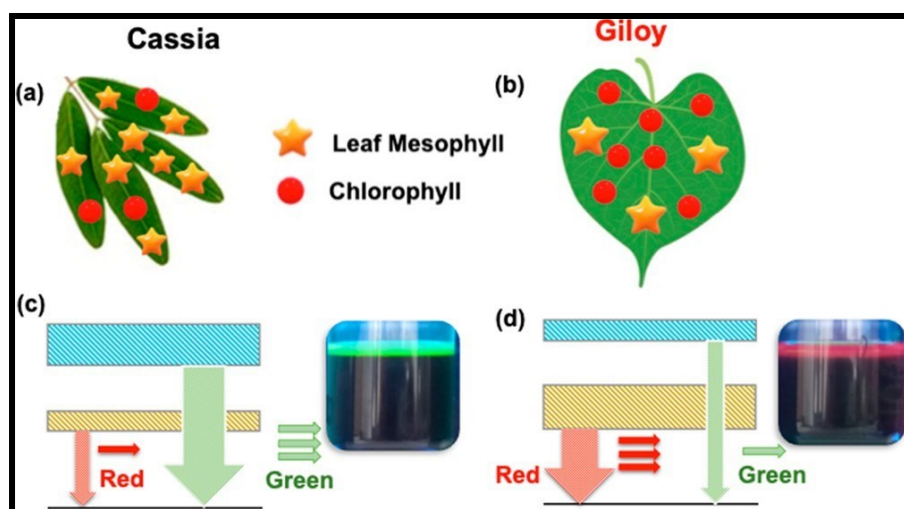


Figure A2: Schematic showing the presence of abundant compounds in Cassia and Giloy leaves (a, b) and possible green and red emission process in Cassia and Giloy leaves (c, d), respectively.

Appendix A3. Carbon dots from cigarette buds

Used cigarette filters were used as raw material to study the nature of condensed tobacco smoke (tar) using microscopy, optical, IR, photoluminescence, and Raman spectroscopy, as well as X-ray diffraction and electron and fluorescence microscopy. The tar present in the cigarette filter bud was used to synthesize luminescent low dimensional carbon using a simple methanol extraction technique. The collected material shows light blue emission under UV excitation with emission peak energy depending strongly on the excitation wavelength. The presence of amorphous phase carbon was established using Raman spectroscopy, and a quantum yield of more than 9% was estimated, which was moderately high in comparison with the one shown by carbon dots prepared by using other sources and can be used for bioimaging applications.

[Ghosh. T. et. al., *Can. J. Chem.* (2022) 100 (7): 545-551]

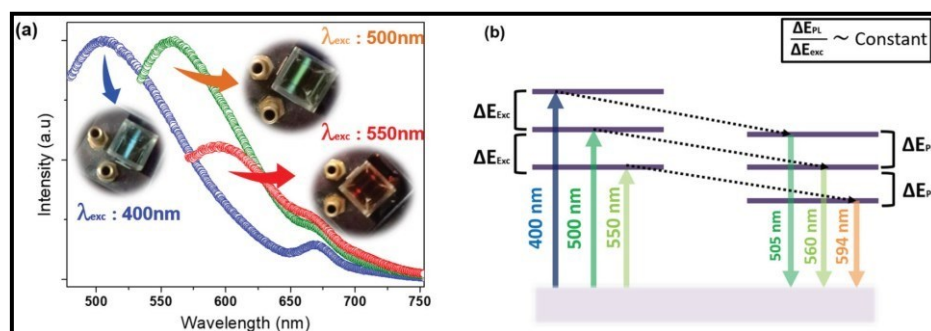


Figure A3: (a) Excitation wavelength dependent PL recorded at 400, 500, and 550 nm excitation sources. (b) Schematic showing relative red shift in PL emission due to a shift in excitation wavelength, a signature of the giant red-edge effect.

References

- [1] C. Toumey, Plenty of room, plenty of history, *Nature Nanotech.* 4 (2009) 783–784. <https://doi.org/10.1038/nnano.2009.357>.
- [2] W.C.W. Chan, A. Khademhosseini, W. Parak, P.S. Weiss, Cancer: Nanoscience and Nanotechnology Approaches, *ACS Nano.* 11 (2017) 4375–4376. <https://doi.org/10.1021/acs.nano.7b03308>.
- [3] H. Chen, P. Timashev, Y. Zhang, X. Xue, X.-J. Liang, Nanotechnology-based combinatorial phototherapy for enhanced cancer treatment, *RSC Adv.* 12 (2022) 9725–9737. <https://doi.org/10.1039/D1RA09067D>.
- [4] G. Whitesides, Nanoscience, Nanotechnology, and Chemistry, *Small.* 1 (2005) 172–179. <https://doi.org/10.1002/smll.200400130>.
- [5] S. Zhu, H. Meng, Z. Gu, Y. Zhao, Research trend of nanoscience and nanotechnology – A bibliometric analysis of Nano Today, *Nano Today.* 39 (2021) 101233. <https://doi.org/10.1016/j.nantod.2021.101233>.
- [6] M.F. El-Kady, Y. Shao, R.B. Kaner, Graphene for batteries, supercapacitors and beyond, *Nat Rev Mater.* 1 (2016) 16033. <https://doi.org/10.1038/natrevmats.2016.33>.
- [7] D. Wei, M.R.J. Scherer, C. Bower, P. Andrew, T. Ryhänen, U. Steiner, A Nanostructured Electrochromic Supercapacitor, *Nano Lett.* 12 (2012) 1857–1862. <https://doi.org/10.1021/nl2042112>.
- [8] Z. Bi, X. Li, X. He, Y. Chen, X. Xu, X. Gao, Integrated electrochromism and energy storage applications based on tungsten trioxide monohydrate nanosheets by novel one-step low temperature synthesis, *Solar Energy Materials and Solar Cells.* 183 (2018) 59–65. <https://doi.org/10.1016/j.solmat.2018.04.001>.
- [9] A. Agrawal, C. Susut, G. Stafford, U. Bertocci, B. McMorran, H.J. Lezec, A.A. Talin, An Integrated Electrochromic Nanoplasmonic Optical Switch, *Nano Lett.* 11 (2011) 2774–2778. <https://doi.org/10.1021/nl201064x>.
- [10] S. Kandpal, T. Ghosh, C. Rani, A. Chaudhary, J. Park, P.S. Lee, R. Kumar, Multifunctional Electrochromic Devices for Energy Applications, *ACS Energy Lett.* (2023) 1870–1886. <https://doi.org/10.1021/acsenerylett.3c00159>.
- [11] R.J. Mortimer, Organic electrochromic materials, *Electrochimica Acta.* 44 (1999) 2971–2981. [https://doi.org/10.1016/S0013-4686\(99\)00046-8](https://doi.org/10.1016/S0013-4686(99)00046-8).

- [12] S.K. Deb, Opportunities and challenges in science and technology of WO₃ for electrochromic and related applications, *Solar Energy Materials and Solar Cells*. 92 (2008) 245–258.
<https://doi.org/10.1016/j.solmat.2007.01.026>.
- [13] S.K. Deb, Optical and photoelectric properties and colour centres in thin films of tungsten oxide, *Philosophical Magazine*. 27 (1973) 801–822.
<https://doi.org/10.1080/14786437308227562>.
- [14] R.J. Mortimer, Electrochromic Materials, *Annu. Rev. Mater. Res.* 41 (2011) 241–268. <https://doi.org/10.1146/annurev-matsci-062910-100344>.
- [15] R. Kumar, D.K. Pathak, A. Chaudhary, Current status of some electrochromic materials and devices: a brief review, *J. Phys. D: Appl. Phys.* 54 (2021) 503002. <https://doi.org/10.1088/1361-6463/ac10d6>.
- [16] C.J. Barile, D.J. Slotcavage, M.D. McGehee, Polymer–Nanoparticle Electrochromic Materials that Selectively Modulate Visible and Near-Infrared Light, *Chem. Mater.* 28 (2016) 1439–1445.
<https://doi.org/10.1021/acs.chemmater.5b04811>.
- [17] S.-L. Li, M. Han, Y. Zhang, G.-P. Li, M. Li, G. He, X.-M. Zhang, X-ray and UV Dual Photochromism, Thermochromism, Electrochromism, and Amine-Selective Chemochromism in an Anderson-like Zn₇ Cluster-Based 7-Fold Interpenetrated Framework, *J. Am. Chem. Soc.* 141 (2019) 12663–12672. <https://doi.org/10.1021/jacs.9b04930>.
- [18] T. Ghosh, S. Kandpal, C. Rani, A. Chaudhary, R. Kumar, Recipe for Fabricating Optimized Solid-State Electrochromic Devices and Its Know-How: Challenges and Future, *Advanced Optical Materials*. (2023) 2203126.
<https://doi.org/10.1002/adom.202203126>.
- [19] R. Kumar, R.G. Pillai, N. Pekas, Y. Wu, R.L. McCreery, Spatially Resolved Raman Spectroelectrochemistry of Solid-State Polythiophene/Viologen Memory Devices, *J. Am. Chem. Soc.* 134 (2012) 14869–14876. <https://doi.org/10.1021/ja304458s>.
- [20] T. Ghosh, S. Kandpal, C. Rani, L. Bansal, R. Kumar, Electrochromic Strategies for Modulation between Primary Colors: Covering the Visible Spectrum, *ACS Appl. Opt. Mater.* (2023) acsaom.3c00052.
<https://doi.org/10.1021/acsaom.3c00052>.
- [21] A. Chaudhary, D.K. Pathak, S. Mishra, P. Yogi, P.R. Sagdeo, R. Kumar, Polythiophene -viologen bilayer for electro-trichromic device, *Solar Energy Materials and Solar Cells*. 188 (2018) 249–254.
<https://doi.org/10.1016/j.solmat.2018.08.029>.

- [22] D.K. Pathak, H.C. Moon, Recent progress in electrochromic energy storage materials and devices: a minireview, *Mater. Horiz.* 9 (2022) 2949–2975. <https://doi.org/10.1039/D2MH00845A>.
- [23] A.C. Anithaa, K. Asokan, C. Sekar, Highly sensitive and selective serotonin sensor based on gamma ray irradiated tungsten trioxide nanoparticles, *Sensors and Actuators B: Chemical*. 238 (2017) 667–675. <https://doi.org/10.1016/j.snb.2016.07.098>.
- [24] Y. Yang, Y. Qi, W. Zhai, J. Tan, S. Feng, J. Zhang, M. Shen, L. Wang, X. Yu, X. Qu, Enhanced Electrochromic Performance of Film Based on Preyssler-Type Polyoxometalate and Tungsten Oxide, *Electron. Mater. Lett.* 16 (2020) 424–432. <https://doi.org/10.1007/s13391-020-00228-x>.
- [25] A.K. Nayak, M. Verma, Y. Sohn, P.A. Deshpande, D. Pradhan, Highly Active Tungsten Oxide Nanoplate Electrocatalysts for the Hydrogen Evolution Reaction in Acidic and Near Neutral Electrolytes, *ACS Omega*. 2 (2017) 7039–7047. <https://doi.org/10.1021/acsomega.7b01151>.
- [26] E. Ozkan, S.-H. Lee, C.E. Tracy, J.R. Pitts, S.K. Deb, Comparison of electrochromic amorphous and crystalline tungsten oxide films, *Solar Energy Materials and Solar Cells*. 79 (2003) 439–448. [https://doi.org/10.1016/S0927-0248\(03\)00019-9](https://doi.org/10.1016/S0927-0248(03)00019-9).
- [27] T. Fukuda, H. Takezoe, K. Ishikawa, A. Fukuda, H.S. Woo, S.K. Jeong, E.J. Oh, J.S. Suh, Ir and Raman studies in three polyanilines with different oxidation level, *Synthetic Metals*. 69 (1995) 175–176. [https://doi.org/10.1016/0379-6779\(94\)02409-R](https://doi.org/10.1016/0379-6779(94)02409-R).
- [28] S. Takagi, S. Makuta, A. Veamatahau, Y. Otsuka, Y. Tachibana, Organic/inorganic hybrid electrochromic devices based on photoelectrochemically formed polypyrrole/TiO₂ nanohybrid films, *J. Mater. Chem.* (2012) 10.1039.c2jm33135g. <https://doi.org/10.1039/c2jm33135g>.
- [29] M. Lahav, M.E. van der Boom, Polypyridyl Metallo-Organic Assemblies for Electrochromic Applications, *Adv. Mater.* 30 (2018) 1706641. <https://doi.org/10.1002/adma.201706641>.
- [30] M. Nicho, Synthesis of derivatives of polythiophene and their application in an electrochromic device, *Solar Energy Materials and Solar Cells*. 82 (2004) 105–118. <https://doi.org/10.1016/j.solmat.2004.01.009>.
- [31] B. Zhang, J. Luo, Z. Chen, S. Liu, Y. Tian, Color combination of polythiophene films doped with three dye molecules for electrochromism, *Optical Materials*. 127 (2022) 112292. <https://doi.org/10.1016/j.optmat.2022.112292>.

- [32] T.J. Konno, R. Sinclair, Crystallization of amorphous carbon in carbon—cobalt layered thin films, *Acta Metallurgica et Materialia*. 43 (1995) 471–484. [https://doi.org/10.1016/0956-7151\(94\)00289-T](https://doi.org/10.1016/0956-7151(94)00289-T).
- [33] J.B. Arockiam, H. Son, S.H. Han, G. Balamurugan, Y.-H. Kim, J.S. Park, Iron Phthalocyanine Incorporated Metallo-Supramolecular Polymer for Superior Electrochromic Performance with High Coloration Efficiency and Switching Stability, *ACS Appl. Energy Mater.* 2 (2019) 8416–8424. <https://doi.org/10.1021/acsaem.9b01022>.
- [34] M.P. Browne, J.M. Vasconcelos, J. Coelho, M. O’Brien, A.A. Rovetta, E.K. McCarthy, H. Nolan, G.S. Duesberg, V. Nicolosi, P.E. Colavita, M.E.G. Lyons, Improving the performance of porous nickel foam for water oxidation using hydrothermally prepared Ni and Fe metal oxides, *Sustainable Energy Fuels*. 1 (2017) 207–216. <https://doi.org/10.1039/C6SE00032K>.
- [35] X. Guo, J. Chen, A.L.-S. Eh, W.C. Poh, F. Jiang, F. Jiang, J. Chen, P.S. Lee, Heat-Insulating Black Electrochromic Device Enabled by Reversible Nickel–Copper Electrodeposition, *ACS Appl. Mater. Interfaces*. 14 (2022) 20237–20246. <https://doi.org/10.1021/acsaami.2c02626>.
- [36] A. Paoella, C. Faure, V. Timoshevskii, S. Marras, G. Bertoni, A. Guerfi, A. Vijh, M. Armand, K. Zaghib, A review on hexacyanoferrate-based materials for energy storage and smart windows: challenges and perspectives, *J. Mater. Chem. A*. 5 (2017) 18919–18932. <https://doi.org/10.1039/C7TA05121B>.
- [37] M.K. Bera, C. Chakraborty, U. Rana, M. Higuchi, Electrochromic Os(II)-Based Metallo-Supramolecular Polymers, *Macromol. Rapid Commun.* 39 (2018) 1800415. <https://doi.org/10.1002/marc.201800415>.
- [38] C. Chakraborty, R.K. Pandey, U. Rana, M. Kanao, S. Moriyama, M. Higuchi, Geometrically isomeric Pt(II)/Fe(II)-based heterometallo-supramolecular polymers with organometallic ligands for electrochromism and the electrochemical switching of Raman scattering, *J. Mater. Chem. C*. 4 (2016) 9428–9437. <https://doi.org/10.1039/C6TC02929A>.
- [39] N. Eloom Dov, S. Shankar, D. Cohen, T. Bendikov, K. Rechav, L.J.W. Shimon, M. Lahav, M.E. van der Boom, Electrochromic Metallo-Organic Nanoscale Films: Fabrication, Color Range, and Devices, *J. Am. Chem. Soc.* 139 (2017) 11471–11481. <https://doi.org/10.1021/jacs.7b04217>.
- [40] H.-C. Lu, L.-Y. Hsiao, S.-Y. Kao, Y. Seino, D.C. Santra, K.-C. Ho, M. Higuchi, Durable Electrochromic Devices Driven at 0.8 V by Complementary Chromic Combination of Metallo-Supramolecular Polymer and Prussian Blue Analogues for Smart Windows with Low-Energy Consumption, *ACS*

Appl. Electron. Mater. 3 (2021) 2123–2135.
<https://doi.org/10.1021/acsaelm.1c00132>.

[41] N. Malik, M. Lahav, M.E. Boom, Electrochromic Metallo–Organic Nanoscale Films: A Molecular Mix and Match Approach to Thermally Robust and Multistate Solid-State Devices, *Adv. Electron. Mater.* 6 (2020) 2000407. <https://doi.org/10.1002/aelm.202000407>.

[42] S. Roy, C. Chakraborty, Nanostructured metallo-supramolecular polymer-based gel-type electrochromic devices with ultrafast switching time and high colouration efficiency, *J. Mater. Chem. C* 7 (2019) 2871–2879. <https://doi.org/10.1039/C8TC06138F>.

[43] Q. Hao, Z.-J. Li, C. Lu, B. Sun, Y.-W. Zhong, L.-J. Wan, D. Wang, Oriented Two-Dimensional Covalent Organic Framework Films for Near-Infrared Electrochromic Application, *J. Am. Chem. Soc.* 141 (2019) 19831–19838. <https://doi.org/10.1021/jacs.9b09956>.

[44] P. Salles, D. Pinto, K. Hantanasirisakul, K. Maleski, C.E. Shuck, Y. Gogotsi, Electrochromic Effect in Titanium Carbide MXene Thin Films Produced by Dip-Coating, *Adv. Funct. Mater.* 29 (2019) 1809223. <https://doi.org/10.1002/adfm.201809223>.

[45] R.R. Salunkhe, Y.V. Kaneti, Y. Yamauchi, Metal–Organic Framework-Derived Nanoporous Metal Oxides toward Supercapacitor Applications: Progress and Prospects, *ACS Nano*. 11 (2017) 5293–5308. <https://doi.org/10.1021/acsnano.7b02796>.

[46] A.M. Österholm, D.E. Shen, J.A. Kerszulis, R.H. Bulloch, M. Kuepfert, A.L. Dyer, J.R. Reynolds, Four Shades of Brown: Tuning of Electrochromic Polymer Blends Toward High-Contrast Eyewear, *ACS Appl. Mater. Interfaces*. 7 (2015) 1413–1421. <https://doi.org/10.1021/am507063d>.

[47] L. Yin, M. Cao, K.N. Kim, M. Lin, J.-M. Moon, J.R. Sempionatto, J. Yu, R. Liu, C. Wicker, A. Trifonov, F. Zhang, H. Hu, J.R. Moreto, J. Go, S. Xu, J. Wang, A stretchable epidermal sweat sensing platform with an integrated printed battery and electrochromic display, *Nat Electron*. 5 (2022) 694–705. <https://doi.org/10.1038/s41928-022-00843-6>.

[48] M. Zhu, Y. Huang, Y. Huang, W. Meng, Q. Gong, G. Li, C. Zhi, An electrochromic supercapacitor and its hybrid derivatives: quantifiably determining their electrical energy storage by an optical measurement, *J. Mater. Chem. A* 3 (2015) 21321–21327. <https://doi.org/10.1039/C5TA06237C>.

[49] T.G. Yun, M. Park, D.-H. Kim, D. Kim, J.Y. Cheong, J.G. Bae, S.M. Han, I.-D. Kim, All-Transparent Stretchable Electrochromic Supercapacitor

Wearable Patch Device, *ACS Nano*. 13 (2019) 3141–3150.
<https://doi.org/10.1021/acsnano.8b08560>.

[50] J. Chen, Z. Wang, Z. Chen, S. Cong, Z. Zhao, Fabry–Perot Cavity-Type Electrochromic Supercapacitors with Exceptionally Versatile Color Tunability, *Nano Lett.* 20 (2020) 1915–1922.
<https://doi.org/10.1021/acs.nanolett.9b05152>.

[51] R.R. Salunkhe, Y.V. Kaneti, Y. Yamauchi, Metal–Organic Framework-Derived Nanoporous Metal Oxides toward Supercapacitor Applications: Progress and Prospects, *ACS Nano*. 11 (2017) 5293–5308.
<https://doi.org/10.1021/acsnano.7b02796>.

[52] X. Tang, J. Chen, Z. Wang, Z. Hu, G. Song, S. Zhang, Z. Chen, Q. Wu, M. Liu, S. Cong, Z. Zhao, Vibrant Color Palettes of Electrochromic Manganese Oxide Electrodes for Colorful Zn-Ion Battery, *Advanced Optical Materials*. 9 (2021) 2100637. <https://doi.org/10.1002/adom.202100637>.

[53] X. Xiao, T. Ding, L. Yuan, Y. Shen, Q. Zhong, X. Zhang, Y. Cao, B. Hu, T. Zhai, L. Gong, J. Chen, Y. Tong, J. Zhou, Z.L. Wang, $\text{WO}_{3-x}/\text{MoO}_{3-x}$ Core/Shell Nanowires on Carbon Fabric as an Anode for All-Solid-State Asymmetric Supercapacitors, *Adv. Energy Mater.* 2 (2012) 1328–1332.
<https://doi.org/10.1002/aenm.201200380>.

[54] H. Huang, J. Yao, L. Li, F. Zhu, Z. Liu, X. Zeng, X. Yu, Z. Huang, Reinforced polyaniline/polyvinyl alcohol conducting hydrogel from a freezing–thawing method as self-supported electrode for supercapacitors, *J Mater Sci*. 51 (2016) 8728–8736. <https://doi.org/10.1007/s10853-016-0137-8>.

[55] S. Niu, S. Li, Y. Du, X. Han, P. Xu, How to Reliably Report the Overpotential of an Electrocatalyst, *ACS Energy Lett.* 5 (2020) 1083–1087.
<https://doi.org/10.1021/acsenerylett.0c00321>.

[56] P. Trogadas, M.-O. Coppens, Nature-inspired electrocatalysts and devices for energy conversion, *Chemical Society Reviews*. 49 (2020) 3107–3141. <https://doi.org/10.1039/C8CS00797G>.

[57] M.F. Iqbal, Y. Yang, M.U. Hassan, X. Zhang, G. Li, K.N. Hui, M. Esmat, M. Zhang, Polyaniline grafted mesoporous zinc sulfide nanoparticles for hydrogen evolution reaction, *International Journal of Hydrogen Energy*. 47 (2022) 6067–6077. <https://doi.org/10.1016/j.ijhydene.2021.11.255>.

[58] Y.-L. Liu, R. Liu, Y. Qin, Q.-F. Qiu, Z. Chen, S.-B. Cheng, W.-H. Huang, Flexible Electrochemical Urea Sensor Based on Surface Molecularly Imprinted Nanotubes for Detection of Human Sweat, *Anal. Chem.* 90 (2018) 13081–13087. <https://doi.org/10.1021/acs.analchem.8b04223>.

- [59] S. Noh, T.-H. Le, H. Jo, S. Kim, H. Yoon, Ternary Nanohybrids Comprising N-Doped Graphene and WSe_2-WO_3 Nanosheets Enable High-Mass-Loading Electrodes with Long-Term Stability for Hydrogen Evolution, *ACS Appl. Nano Mater.* 4 (2021) 14094–14104. <https://doi.org/10.1021/acsanm.1c03409>.
- [60] N. Sahu, B. Parija, S. Panigrahi, Fundamental understanding and modeling of spin coating process: A review, *Indian J Phys.* 83 (2009) 493–502. <https://doi.org/10.1007/s12648-009-0009-z>.
- [61] M. Yoshimura, K. Byrappa, Hydrothermal processing of materials: past, present and future, *J Mater Sci.* 43 (2008) 2085–2103. <https://doi.org/10.1007/s10853-007-1853-x>.
- [62] D. Sobha Jayakrishnan, Electrodeposition: the versatile technique for nanomaterials, in: *Corrosion Protection and Control Using Nanomaterials*, Elsevier, 2012: pp. 86–125. <https://doi.org/10.1533/9780857095800.1.86>.
- [63] Y. Kim, J. Jung, S. Kim, W.-S. Chae, Cyclic Voltammetric and Chronoamperometric Deposition of CdS, *Mater. Trans.* 54 (2013) 1467–1472. <https://doi.org/10.2320/matertrans.M2013125>.
- [64] J. Waelder, R. Vasquez, Y. Liu, S. Maldonado, A Description of the Faradaic Current in Cyclic Voltammetry of Adsorbed Redox Species on Semiconductor Electrodes, *J. Am. Chem. Soc.* 144 (2022) 6410–6419. <https://doi.org/10.1021/jacs.2c00782>.
- [65] S. Zaefferer, A critical review of orientation microscopy in SEM and TEM, *Cryst. Res. Technol.* 46 (2011) 607–628. <https://doi.org/10.1002/crat.201100125>.
- [66] M. Tanwar, L. Bansal, C. Rani, S. Rani, S. Kandpal, T. Ghosh, D.K. Pathak, I. Sameera, R. Bhatia, R. Kumar, Fano-Type Wavelength-Dependent Asymmetric Raman Line Shapes from MoS_2 Nanoflakes, *ACS Phys. Chem Au.* (2022) acsphyschemau.2c00021. <https://doi.org/10.1021/acspchemau.2c00021>.
- [67] C. Rani, M. Tanwar, S. Kandpal, T. Ghosh, L. Bansal, R. Kumar, Nonlinear Temperature-Dependent Phonon Decay in Heavily Doped Silicon: Predominant Interferon-Mediated Cold Phonon Annihilation, *J. Phys. Chem. Lett.* (2022) 5232–5239. <https://doi.org/10.1021/acs.jpcllett.2c01248>.
- [68] N. Salvadó, S. Butí, M.J. Tobin, E. Pantos, A.J.N.W. Prag, T. Pradell, Advantages of the Use of SR-FT-IR Microspectroscopy: Applications to Cultural Heritage, *Anal. Chem.* 77 (2005) 3444–3451. <https://doi.org/10.1021/ac050126k>.

- [69] J. Epp, X-ray diffraction (XRD) techniques for materials characterization, in: *Materials Characterization Using Nondestructive Evaluation (NDE) Methods*, Elsevier, 2016: pp. 81–124. <https://doi.org/10.1016/B978-0-08-100040-3.00004-3>.
- [70] N.A. Baka, A. Abu-Siada, S. Islam, M.F. El-Naggar, A new technique to measure interfacial tension of transformer oil using UV-Vis spectroscopy, *IEEE Trans. Dielect. Electr. Insul.* 22 (2015) 1275–1282. <https://doi.org/10.1109/TDEI.2015.7076831>.
- [71] H. Harada, *In vitro* organ culture of *Actinidia chinensis* PL as a technique for vegetative multiplication, *Journal of Horticultural Science*. 50 (1975) 81–83. <https://doi.org/10.1080/00221589.1975.11514606>.
- [72] A.D. Broadbent, A critical review of the development of the CIE1931 RGB color-matching functions, *Color Res. Appl.* 29 (2004) 267–272. <https://doi.org/10.1002/col.20020>.
- [73] R.H. Bulloch, J.A. Kerszulis, A.L. Dyer, J.R. Reynolds, Mapping the Broad CMY Subtractive Primary Color Gamut Using a Dual-Active Electrochromic Device, *ACS Appl. Mater. Interfaces*. 6 (2014) 6623–6630. <https://doi.org/10.1021/am500290d>.
- [74] F.R. Clapper, R.G. Gendron, S.A. Brownstein, Color gamuts of additive and subtractive color-reproduction systems, *J. Opt. Soc. Am.* 63 (1973) 625. <https://doi.org/10.1364/JOSA.63.000625>.
- [75] K.M. Coakley, M.D. McGehee, Conjugated Polymer Photovoltaic Cells, *Chem. Mater.* 16 (2004) 4533–4542. <https://doi.org/10.1021/cm049654n>.
- [76] B. He, W.T. Neo, T.L. Chen, L.M. Klivansky, H. Wang, T. Tan, S.J. Teat, J. Xu, Y. Liu, Low Bandgap Conjugated Polymers Based on a Nature-Inspired Bay-Annulated Indigo (BAI) Acceptor as Stable Electrochromic Materials, *ACS Sustainable Chem. Eng.* 4 (2016) 2797–2805. <https://doi.org/10.1021/acssuschemeng.6b00303>.
- [77] L.R. Savagian, A.M. Österholm, D.E. Shen, D.T. Christiansen, M. Kuepfert, J.R. Reynolds, Conjugated Polymer Blends for High Contrast Black-to-Transmissive Electrochromism, *Advanced Optical Materials*. 6 (2018) 1800594. <https://doi.org/10.1002/adom.201800594>.
- [78] A. Chaudhary, D.K. Pathak, M. Tanwar, J. Koch, H. Pfnür, R. Kumar, Polythiophene-nanoWO₃ bilayer as an electrochromic infrared filter: a transparent heat shield, *J. Mater. Chem. C*. 8 (2020) 1773–1780. <https://doi.org/10.1039/C9TC05523A>.

- [79] S. Kandpal, T. Ghosh, C. Rani, M. Tanwar, M. Sharma, S. Rani, D.K. Pathak, R. Bhatia, I. Sameera, J. Jayabalan, R. Kumar, Bifunctional Application of Viologen-MoS₂-CNT/Polythiophene Device as Electrochromic Diode and Half-Wave Rectifier, *ACS Mater. Au.* 2 (2022) 293–300. <https://doi.org/10.1021/acsmaterialsau.1c00064>.
- [80] M.J.L. Santos, A.G. Brolo, E.M. Girotto, Study of polaron and bipolaron states in polypyrrole by in situ Raman spectroelectrochemistry, *Electrochimica Acta.* 52 (2007) 6141–6145. <https://doi.org/10.1016/j.electacta.2007.03.070>.
- [81] Q. Guo, X. Zhao, Z. Li, D. Wang, G. Nie, A novel solid-state electrochromic supercapacitor with high energy storage capacity and cycle stability based on poly(5-formylindole)/WO₃ honeycombed porous nanocomposites, *Chemical Engineering Journal.* 384 (2020) 123370. <https://doi.org/10.1016/j.cej.2019.123370>.
- [82] T. Ghosh, S. Kandpal, C. Rani, L. Bansal, M. Tanwar, R. Kumar, Multiwavelength Color Switching from Polyaniline-Viologen Bilayer: Inching toward Versatile All-Organic Flexible Electrochromic Device, *Adv Elect Materials.* 9 (2023) 2201042. <https://doi.org/10.1002/aelm.202201042>.
- [83] J.E. Albuquerque, L.H.C. Mattoso, D.T. Balogh, R.M. Faria, J.G. Masters, A.G. MacDiarmid, A simple method to estimate the oxidation state of polyanilines, *Synthetic Metals.* 113 (2000) 19–22. [https://doi.org/10.1016/S0379-6779\(99\)00299-4](https://doi.org/10.1016/S0379-6779(99)00299-4).
- [84] J.G. Masters, Y. Sun, A.G. MacDiarmid, A.J. Epstein, Polyaniline: Allowed oxidation states, *Synthetic Metals.* 41 (1991) 715–718. [https://doi.org/10.1016/0379-6779\(91\)91166-8](https://doi.org/10.1016/0379-6779(91)91166-8).
- [85] Y.E. Firat, A. Peksoz, Electrochemical synthesis of polyaniline/inorganic salt binary nanofiber thin films for electrochromic applications, *J Mater Sci: Mater Electron.* 28 (2017) 3515–3522. <https://doi.org/10.1007/s10854-016-5951-x>.
- [86] T. Ghosh, L. Bansal, S. Kandpal, C. Rani, M. Tanwar, R. Kumar, Ambipolar All-Organic Solid-State Electrochromic Device Using Electrodeposited Polyaniline: Improving Performance by Design, *ACS Appl. Opt. Mater.* (2022) acsaom.2c00115. <https://doi.org/10.1021/acsaom.2c00115>.
- [87] S. Chao, M.S. Wrighton, Characterization of a solid-state polyaniline-based transistor: water vapor dependent characteristics of a device employing a poly(vinyl alcohol)/phosphoric acid solid-state electrolyte, *J. Am. Chem. Soc.* 109 (1987) 6627–6631. <https://doi.org/10.1021/ja00256a011>.

- [88] S.K. Manohar, C. Fafadia, N. Saran, R. Rao, Faradaic effects in all-organic transistors, *Journal of Applied Physics*. 103 (2008) 094501. <https://doi.org/10.1063/1.2903565>.
- [89] A. Saheb, M. Josowicz, J. Janata, Chemically Sensitive Field-Effect Transistor with Polyaniline–Ionic Liquid Composite Gate, *Anal. Chem.* 80 (2008) 4214–4219. <https://doi.org/10.1021/ac800340q>.
- [90] M.J. Panzer, C.D. Frisbie, Polymer Electrolyte-Gated Organic Field-Effect Transistors: Low-Voltage, High-Current Switches for Organic Electronics and Testbeds for Probing Electrical Transport at High Charge Carrier Density, *J. Am. Chem. Soc.* 129 (2007) 6599–6607. <https://doi.org/10.1021/ja0708767>.
- [91] B.-X. Zou, Y. Liang, X.-X. Liu, D. Diamond, K.-T. Lau, Electrodeposition and pseudocapacitive properties of tungsten oxide/polyaniline composite, *Journal of Power Sources*. 196 (2011) 4842–4848. <https://doi.org/10.1016/j.jpowsour.2011.01.073>.
- [92] T. Takei, Y. Kobayashi, H. Hata, Y. Yonesaki, N. Kumada, N. Kinomura, T.E. Mallouk, Anodic Electrodeposition of Highly Oriented Zirconium Phosphate and Polyaniline-Intercalated Zirconium Phosphate Films, *J. Am. Chem. Soc.* 128 (2006) 16634–16640. <https://doi.org/10.1021/ja065677m>.
- [93] D.K. Pathak, A. Chaudhary, M. Tanwar, U.K. Goutam, H. Pfnür, R. Kumar, Chronopotentiometric Deposition of Nanocobalt Oxide for Electrochromic Auxiliary Active Electrode Application, *Phys. Status Solidi A*. 217 (2020) 2000173. <https://doi.org/10.1002/pssa.202000173>.
- [94] A. Chaudhary, G. Sivakumar, D.K. Pathak, M. Tanwar, R. Misra, R. Kumar, Pentafluorophenyl substituted fulleropyrrolidine: a molecule enabling the most efficient flexible electrochromic device with fast switching, *J. Mater. Chem. C*. 9 (2021) 3462–3469. <https://doi.org/10.1039/D0TC04991C>.
- [95] S. Mishra, P. Yogi, P.R. Sagdeo, R. Kumar, $\text{TiO}_2\text{-Co}_3\text{O}_4$ Core–Shell Nanorods: Bifunctional Role in Better Energy Storage and Electrochromism, *ACS Appl. Energy Mater.* 1 (2018) 790–798. <https://doi.org/10.1021/acsaem.7b00254>.
- [96] M.-C. Bernard, A. Hugot-Le Goff, Raman spectroscopy for the study of polyaniline, *Synthetic Metals*. 85 (1997) 1145–1146. [https://doi.org/10.1016/S0379-6779\(97\)80187-7](https://doi.org/10.1016/S0379-6779(97)80187-7).
- [97] J. Tokarský, M. Maixner, P. Peikertová, L. Kulhánková, J.V. Burda, The IR and Raman spectra of polyaniline adsorbed on the glass surface; comparison of experimental, empirical force field, and quantum chemical

results, *European Polymer Journal*. 57 (2014) 47–57.
<https://doi.org/10.1016/j.eurpolymj.2014.04.023>.

[98] M. Trchová, Z. Morávková, M. Bláha, J. Stejskal, Raman spectroscopy of polyaniline and oligoaniline thin films, *Electrochimica Acta*. 122 (2014) 28–38. <https://doi.org/10.1016/j.electacta.2013.10.133>.

[99] E.T. Kang, K.G. Neoh, K.L. Tan, Polyaniline with high intrinsic oxidation state, *Surf. Interface Anal.* 20 (1993) 833–840.
<https://doi.org/10.1002/sia.740201006>.

[100] S. Mu, J. Kan, J. Lu, L. Zhuang, Interconversion of polarons and bipolarons of polyaniline during the electrochemical polymerization of aniline, *Journal of Electroanalytical Chemistry*. 446 (1998) 107–112.
[https://doi.org/10.1016/S0022-0728\(97\)00529-9](https://doi.org/10.1016/S0022-0728(97)00529-9).

[101] Y.M. Kim, X. Li, K.-W. Kim, S.H. Kim, H.C. Moon, Tetrathiafulvalene: effective organic anodic materials for WO₃-based electrochromic devices, *RSC Adv.* 9 (2019) 19450–19456. <https://doi.org/10.1039/C9RA02840D>.

[102] A. Chaudhary, D.K. Pathak, M. Tanwar, P. Yogi, P.R. Sagdeo, R. Kumar, Polythiophene–PCBM-Based All-Organic Electrochromic Device: Fast and Flexible, *ACS Appl. Electron. Mater.* 1 (2019) 58–63.
<https://doi.org/10.1021/acsaelm.8b00012>.

[103] S. Alkan, C.A. Cutler, J.R. Reynolds, High-Quality Electrochromic Polythiophenes via BF₃-Et₂O Electropolymerization, *Adv. Funct. Mater.* 13 (2003) 331–336. <https://doi.org/10.1002/adfm.200304307>.

[104] S. Kandpal, T. Ghosh, M. Sharma, D.K. Pathak, M. Tanwar, C. Rani, R. Bhatia, I. Sameera, A. Chaudhary, R. Kumar, Multi-walled carbon nanotubes doping for fast and efficient hybrid solid state electrochromic device, *Appl. Phys. Lett.* 118 (2021) 153301. <https://doi.org/10.1063/5.0046669>.

[105] S. Kandpal, T. Ghosh, C. Rani, S. Rani, D.K. Pathak, M. Tanwar, R. Bhatia, I. Sameera, R. Kumar, MoS₂ nano-flower incorporation for improving organic-organic solid state electrochromic device performance, *Solar Energy Materials and Solar Cells*. 236 (2022) 111502.
<https://doi.org/10.1016/j.solmat.2021.111502>.

[106] A. Chaudhary, D.K. Pathak, T. Ghosh, S. Kandpal, M. Tanwar, C. Rani, R. Kumar, Prussian Blue-Cobalt Oxide Double Layer for Efficient All-Inorganic Multicolor Electrochromic Device, *ACS Appl. Electron. Mater.* 2 (2020) 1768–1773. <https://doi.org/10.1021/acsaelm.0c00342>.

[107] A. Chaudhary, D.K. Pathak, S. Mishra, P. Yogi, P.R. Sagdeo, R. Kumar, Enhancing Viologen's Electrochromism by Incorporating Thiophene: A Step

Toward All-Organic Flexible Device, *Phys. Status Solidi A*. (2018) 1800680.
<https://doi.org/10.1002/pssa.201800680>.

[108] V.H. Vinh Quy, K.-W. Kim, J. Yeo, X. Tang, Y.R. In, C. Jung, S.M. Oh, S.J. Kim, S.W. Lee, H.C. Moon, S.H. Kim, Tunable electrochromic behavior of biphenyl poly(viologen)-based ion gels in all-in-one devices, *Organic Electronics*. 100 (2022) 106395.
<https://doi.org/10.1016/j.orgel.2021.106395>.

[109] S. Halder, R.P. Behere, N. Gupta, B.K. Kuila, C. Chakraborty, Enhancement of the electrochemical performance of a cathodically coloured organic electrochromic material through the formation of hydrogen bonded supramolecular polymer assembly, *Solar Energy Materials and Solar Cells*. 245 (2022) 111858.
<https://doi.org/10.1016/j.solmat.2022.111858>.

[110] M. Jamdegni, A. Kaur, Review—Polymeric/Small Organic Molecules-Based Electrochromic Devices: How Far Toward Realization, *J. Electrochem. Soc.* 169 (2022) 030541. <https://doi.org/10.1149/1945-7111/ac5c04>.

[111] L.G. Kiefer, C.J. Robert, T.D. Sparks, Lifetime of electrochromic optical transition cycling of ethyl viologen diperchlorate-based electrochromic devices, *SN Appl. Sci.* 3 (2021) 554.
<https://doi.org/10.1007/s42452-021-04552-1>.

[112] D.K. Pathak, A. Chaudhary, M. Tanwar, U.K. Goutam, R. Kumar, Nano-cobalt oxide/viologen hybrid solid state device: Electrochromism beyond chemical cell, *Appl. Phys. Lett.* 116 (2020) 141901.
<https://doi.org/10.1063/1.5145079>.

[113] S. Zhao, W. Huang, Z. Guan, B. Jin, D. Xiao, A novel bis(dihydroxypropyl) viologen-based all-in-one electrochromic device with high cycling stability and coloration efficiency, *Electrochimica Acta*. 298 (2019) 533–540. <https://doi.org/10.1016/j.electacta.2018.12.135>.

[114] Y. Zhang, M. Guo, G. Li, X. Chen, Z. Liu, J. Shao, Y. Huang, G. He, Ultrastable Viologen Ionic Liquids-Based Ionogels for Visible Strain Sensor Integrated with Electrochromism, Electrofluorochromism, and Strain Sensing, *CCS Chem.* (2022) 1–14.
<https://doi.org/10.31635/ccschem.022.202202310>.

[115] A. Chaudhary, M. Poddar, D.K. Pathak, R. Misra, R. Kumar, Electron Donor Ferrocenyl Phenothiazine: Counter Ion for Improving All-Organic Electrochromism, *ACS Appl. Electron. Mater.* 2 (2020) 2994–3000.
<https://doi.org/10.1021/acsaelm.0c00606>.

[116] S. Mishra, S. Lambora, P. Yogi, P.R. Sagdeo, R. Kumar, Organic Nanostructures on Inorganic Ones: An Efficient Electrochromic Display by

Design, *ACS Appl. Nano Mater.* 1 (2018) 3715–3723.
<https://doi.org/10.1021/acsnm.8b00871>.

[117] S. Mishra, P. Yogi, A. Chaudhary, D.K. Pathak, S.K. Saxena, A.S. Krylov, P.R. Sagdeo, R. Kumar, Understanding perceived color through gradual spectroscopic variations in electrochromism, *Indian J Phys.* 93 (2019) 927–933. <https://doi.org/10.1007/s12648-018-1353-7>.

[118] S. Mishra, H. Pandey, P. Yogi, S.K. Saxena, S. Roy, P.R. Sagdeo, R. Kumar, Interfacial redox centers as origin of color switching in organic electrochromic device, *Optical Materials.* 66 (2017) 65–71.
<https://doi.org/10.1016/j.optmat.2017.01.030>.

[119] E. Hwang, S. Seo, S. Bak, H. Lee, M. Min, H. Lee, An Electrolyte-Free Flexible Electrochromic Device Using Electrostatically Strong Graphene Quantum Dot-Viologen Nanocomposites, *Adv. Mater.* 26 (2014) 5129–5136.
<https://doi.org/10.1002/adma.201401201>.

[120] S. Kandpal, T. Ghosh, C. Rani, S. Rani, L. Bansal, M. Tanwar, R. Bhatia, I. Sameera, R. Kumar, MoS₂ doping and concentration optimization for application-specific design of P3HT-viologen-based solid state electrochromic device, *J. Phys. D: Appl. Phys.* 55 (2022) 375101.
<https://doi.org/10.1088/1361-6463/ac7426>.

[121] J.T.S. Allan, S. Quaranta, I.I. Ebralidze, J.G. Egan, J. Poisson, N.O. Laschuk, F. Gaspari, E.B. Easton, O.V. Zenkina, Terpyridine-Based Monolayer Electrochromic Materials, *ACS Appl. Mater. Interfaces.* 9 (2017) 40438–40445. <https://doi.org/10.1021/acsmi.7b11848>.

[122] J.E. de Albuquerque, L.H.C. Mattoso, R.M. Faria, J.G. Masters, A.G. MacDiarmid, Study of the interconversion of polyaniline oxidation states by optical absorption spectroscopy, *Synthetic Metals.* 146 (2004) 1–10.
<https://doi.org/10.1016/j.synthmet.2004.05.019>.

[123] A.A. Nekrasov, V.F. Ivanov, A.V. Vannikov, Analysis of the structure of polyaniline absorption spectra based on spectroelectrochemical data, *Journal of Electroanalytical Chemistry.* 482 (2000) 11–17.
[https://doi.org/10.1016/S0022-0728\(00\)00005-X](https://doi.org/10.1016/S0022-0728(00)00005-X).

[124] M.C. Bernard, A. Hugot-Le Goff, Quantitative characterization of polyaniline films using Raman spectroscopy, *Electrochimica Acta.* 52 (2006) 595–603. <https://doi.org/10.1016/j.electacta.2006.05.039>.

[125] L. Zhao, L. Zhao, Y. Xu, T. Qiu, L. Zhi, G. Shi, Polyaniline electrochromic devices with transparent graphene electrodes, *Electrochimica Acta.* 55 (2009) 491–497.
<https://doi.org/10.1016/j.electacta.2009.08.063>.

- [126] G.F. Cai, J.P. Tu, D. Zhou, J.H. Zhang, X.L. Wang, C.D. Gu, Dual electrochromic film based on WO₃/polyaniline core/shell nanowire array, *Solar Energy Materials and Solar Cells*. 122 (2014) 51–58. <https://doi.org/10.1016/j.solmat.2013.11.015>.
- [127] S. Mishra, S. Lambora, P. Yogi, P.R. Sagdeo, R. Kumar, Organic Nanostructures on Inorganic Ones: An Efficient Electrochromic Display by Design, *ACS Appl. Nano Mater.* 1 (2018) 3715–3723. <https://doi.org/10.1021/acsnm.8b00871>.
- [128] K. Madasamy, D. Velayutham, V. Suryanarayanan, M. Kathiresan, K.-C. Ho, Viologen-based electrochromic materials and devices, *J. Mater. Chem. C*. 7 (2019) 4622–4637. <https://doi.org/10.1039/C9TC00416E>.
- [129] S. Jin, X. Zhang, X. Guo, M. Zhu, P. Liu, The Flexible Electrochromic Device That Turns Blue Under Both Positive and Negative Application Voltages, *Front. Nanotechnol.* 4 (2022) 887442. <https://doi.org/10.3389/fnano.2022.887442>.
- [130] H.C. Moon, C.-H. Kim, T.P. Lodge, C.D. Frisbie, Multicolored, Low-Power, Flexible Electrochromic Devices Based on Ion Gels, *ACS Appl. Mater. Interfaces*. 8 (2016) 6252–6260. <https://doi.org/10.1021/acsnm.6b01307>.
- [131] Y. Liu, K. He, G. Chen, W.R. Leow, X. Chen, Nature-Inspired Structural Materials for Flexible Electronic Devices, *Chem. Rev.* 117 (2017) 12893–12941. <https://doi.org/10.1021/acs.chemrev.7b00291>.
- [132] A. Chaudhary, D.K. Pathak, M. Tanwar, S. Kandpal, T. Ghosh, C. Rani, R. Kumar, Improved ionic solid/viologen hybrid electrochromic device using pre-bleached Prussian-blue electrode, *IET Nanodielectrics*. 4 (2021) 193–200. <https://doi.org/10.1049/nde2.12015>.
- [133] M.A. Deshmukh, M. Gicevicius, A. Ramanaviciene, M.D. Shirsat, R. Viter, A. Ramanavicius, Hybrid electrochemical/electrochromic Cu(II) ion sensor prototype based on PANI/ITO-electrode, *Sensors and Actuators B: Chemical*. 248 (2017) 527–535. <https://doi.org/10.1016/j.snb.2017.03.167>.
- [134] S.M. Islam, T.S. Hernandez, M.D. McGehee, C.J. Barile, Hybrid dynamic windows using reversible metal electrodeposition and ion insertion, *Nat Energy*. 4 (2019) 223–229. <https://doi.org/10.1038/s41560-019-0332-3>.
- [135] L. Bansal, T. Ghosh, S. Kandpal, C. Rani, M. Tanwar, R. Kumar, Exploiting Charge Storage Capabilities of NiTiO₃/TiO₂ for Achieving the Most Efficient Hybrid Electrochromic Device, *ACS Appl. Eng. Mater.* (2022) acsaenm.2c00140. <https://doi.org/10.1021/acsaenm.2c00140>.

- [136] T.-H. Kim, H.J. Jeon, J.-W. Lee, Y.-C. Nah, Enhanced electrochromic properties of hybrid P3HT/WO₃ composites with multiple colorations, *Electrochemistry Communications*. 57 (2015) 65–69. <https://doi.org/10.1016/j.elecom.2015.05.008>.
- [137] V.K. Thakur, G. Ding, J. Ma, P.S. Lee, X. Lu, Hybrid Materials and Polymer Electrolytes for Electrochromic Device Applications, *Adv. Mater.* 24 (2012) 4071–4096. <https://doi.org/10.1002/adma.201200213>.
- [138] S.K. Deb, A Novel Electrophotographic System, *Appl. Opt.* 8 (1969) 192. <https://doi.org/10.1364/AO.8.S1.000192>.
- [139] A.I. Inamdar, J. Kim, Y. Jo, H. Woo, S. Cho, S.M. Pawar, S. Lee, J.L. Gunjekar, Y. Cho, B. Hou, S. Cha, J. Kwak, Y. Park, H. Kim, H. Im, Highly efficient electro-optically tunable smart-supercapacitors using an oxygen-excess nanograin tungsten oxide thin film, *Solar Energy Materials and Solar Cells*. 166 (2017) 78–85. <https://doi.org/10.1016/j.solmat.2017.03.006>.
- [140] X. He, X. Li, Z. Bi, Y. Chen, X. Xu, X. Gao, Dual-functional electrochromic and energy-storage electrodes based on tungsten trioxide nanostructures, *J Solid State Electrochem.* 22 (2018) 2579–2586. <https://doi.org/10.1007/s10008-018-3959-2>.
- [141] J.C. Murillo-Sierra, A. Hernández-Ramírez, L. Hinojosa-Reyes, J.L. Guzmán-Mar, A review on the development of visible light-responsive WO₃-based photocatalysts for environmental applications, *Chemical Engineering Journal Advances*. 5 (2021) 100070. <https://doi.org/10.1016/j.ceja.2020.100070>.
- [142] G. Inzelt, Chronoamperometry, Chronocoulometry, and Chronopotentiometry, in: G. Kreysa, K. Ota, R.F. Savinell (Eds.), *Encyclopedia of Applied Electrochemistry*, Springer New York, New York, NY, 2014: pp. 207–214. https://doi.org/10.1007/978-1-4419-6996-5_217.
- [143] A.K. Satpati, N. Arroyo-Currás, L. Ji, E.T. Yu, A.J. Bard, Electrochemical Monitoring of TiO₂ Atomic Layer Deposition by Chronoamperometry and Scanning Electrochemical Microscopy, *Chem. Mater.* 25 (2013) 4165–4172. <https://doi.org/10.1021/cm401635v>.
- [144] J.J. Garcá -Jareño, A. Sanmatias, J. Navarro-Laboulais, F. Vicente, Chronoamperometry of prussian blue films on ITO electrodes: ohmic drop and film thickness effect, *Electrochimica Acta*. 44 (1999) 4753–4762. [https://doi.org/10.1016/S0013-4686\(99\)00226-1](https://doi.org/10.1016/S0013-4686(99)00226-1).
- [145] T. Ghosh, C. Rani, S. Kandpal, M. Tanwar, L. Bansal, R. Kumar, Chronoamperometric deposition of transparent WO₃ film for application as power efficient electrochromic auxiliary electrode, *J. Phys. D: Appl. Phys.* 55 (2022) 365103. <https://doi.org/10.1088/1361-6463/ac76f5>.

- [146] H. Lyu, Triple Layer Tungsten Trioxide, Graphene, and Polyaniline Composite Films for Combined Energy Storage and Electrochromic Applications, *Polymers*. 12 (2019) 49. <https://doi.org/10.3390/polym12010049>.
- [147] M. M, G. V, P. P, S. R, S. C, Influence of Dopant Concentration on the Electrochromic Properties of Tungsten Oxide Thin Films, *Electrochimica Acta*. 174 (2015) 302–314. <https://doi.org/10.1016/j.electacta.2015.05.187>.
- [148] A. Chaudhary, D.K. Pathak, M. Tanwar, R. Dash, B. Joshi, T. Keerthivasan, S. Kandpal, T. Ghosh, C. Rani, R. Kumar, Hydrothermally grown nano-WO₃ electrochromic film: structural and Raman spectroscopic study, *Advances in Materials and Processing Technologies*. (2020) 1–7. <https://doi.org/10.1080/2374068X.2020.1835019>.
- [149] T.V. Nguyen, H.H. Do, T.Q. Trung, Q.V. Le, T.P. Nguyen, S.H. Hong, H.W. Jang, S.H. Ahn, S.Y. Kim, Stable and multicolored electrochromic device based on polyaniline-tungsten oxide hybrid thin film, *Journal of Alloys and Compounds*. 882 (2021) 160718. <https://doi.org/10.1016/j.jallcom.2021.160718>.
- [150] N. Wang, J. Zhu, X. Zheng, F. Xiong, B. Huang, J. Shi, C. Li, A facile two-step method for fabrication of plate-like WO₃ photoanode under mild conditions, *Faraday Discuss*. 176 (2014) 185–197. <https://doi.org/10.1039/C4FD00139G>.
- [151] H. Wang, G. Ma, Y. Tong, Z. Yang, Biomass carbon/polyaniline composite and WO₃ nanowire-based asymmetric supercapacitor with superior performance, *Ionics*. 24 (2018) 3123–3131. <https://doi.org/10.1007/s11581-017-2428-8>.
- [152] A. Sadollahkhani, A. Hatamie, O. Nur, M. Willander, B. Zargar, I. Kazeminezhad, Colorimetric Disposable Paper Coated with ZnO@ZnS Core–Shell Nanoparticles for Detection of Copper Ions in Aqueous Solutions, *ACS Appl. Mater. Interfaces*. 6 (2014) 17694–17701. <https://doi.org/10.1021/am505480y>.
- [153] A. Szczeszak, M. Skwierczyńska, D. Przybylska, M. Runowski, E. Śmiechowicz, A. Erdman, O. Ivashchenko, T. Grzyb, P. Kulpiński, K. Olejnik, Functionalization of cellulose fibers and paper with lanthanide-based luminescent core/shell nanoparticles providing 3-level protection for advanced anti-counterfeiting purposes, *Materials & Design*. 218 (2022) 110684. <https://doi.org/10.1016/j.matdes.2022.110684>.
- [154] T. Wang, D. Wu, Y. Wang, T. Huang, G. Histan, T. Wang, H. Zeng, One-step solvothermal fabrication of Cu@PANI core–shell nanospheres for hydrogen evolution, *Nanoscale*. 10 (2018) 22055–22064. <https://doi.org/10.1039/C8NR06245E>.

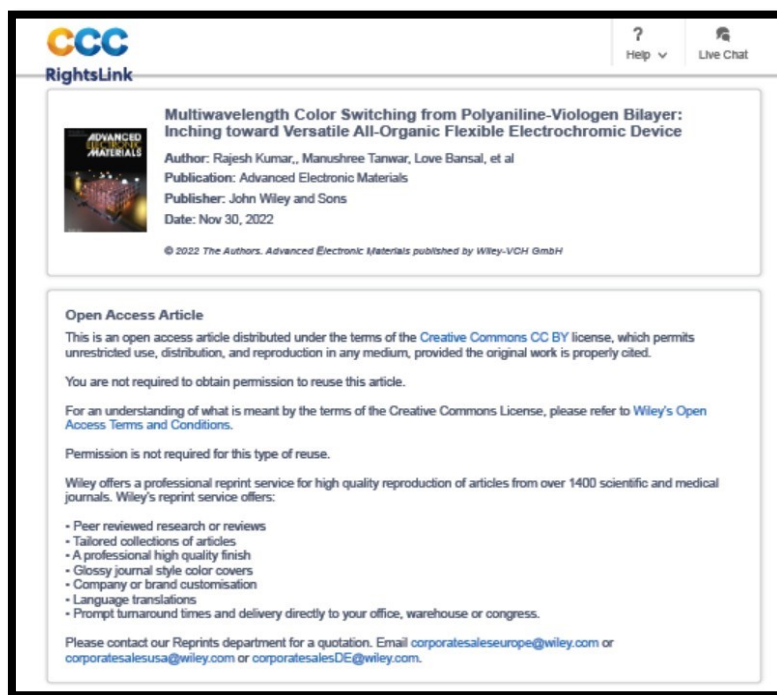
- [155] P. Vlazan, D.H. Ursu, C. Irina-Moiescu, I. Miron, P. Sfirloaga, E. Rusu, Structural and electrical properties of TiO₂/ZnO core-shell nanoparticles synthesized by hydrothermal method, *Materials Characterization*. 101 (2015) 153–158. <https://doi.org/10.1016/j.matchar.2015.01.017>.
- [156] M. Wang, X. Ren, G. Yuan, X. Niu, Q. Xu, W. Gao, S. Zhu, Q. Wang, Selective electroreduction of CO₂ to CO over co-electrodeposited dendritic core-shell indium-doped Cu@Cu₂O catalyst, *Journal of CO₂ Utilization*. 37 (2020) 204–212. <https://doi.org/10.1016/j.jcou.2019.12.013>.
- [157] R. Tena-Zaera, A. Katty, S. Bastide, C. Lévy-Clément, Annealing Effects on the Physical Properties of Electrodeposited ZnO/CdSe Core-Shell Nanowire Arrays, *Chem. Mater.* 19 (2007) 1626–1632. <https://doi.org/10.1021/cm062390f>.
- [158] M. Tian, X. Liu, X. Diao, X. Zhong, High performance PANI/MnO₂ coral-like nanocomposite anode for flexible and robust electrochromic energy storage device, *Solar Energy Materials and Solar Cells*. 253 (2023) 112239. <https://doi.org/10.1016/j.solmat.2023.112239>.
- [159] T.V. Pham, J. Kim, J.Y. Jung, J.H. Kim, H. Cho, T.H. Seo, H. Lee, N.D. Kim, M.J. Kim, High Areal Capacitance of N-Doped Graphene Synthesized by Arc Discharge, *Adv. Funct. Mater.* 29 (2019) 1905511. <https://doi.org/10.1002/adfm.201905511>.
- [160] J. Woods, A. Mahvi, A. Goyal, E. Kozubal, A. Odukomaiya, R. Jackson, Rate capability and Ragone plots for phase change thermal energy storage, *Nat Energy*. 6 (2021) 295–302. <https://doi.org/10.1038/s41560-021-00778-w>.
- [161] M. Szkoda, Z. Zarach, K. Trzciński, A.P. Nowak, An Aqueous Exfoliation of WO₃ as a Route for Counterions Fabrication—Improved Photocatalytic and Capacitive Properties of Polyaniline/WO₃ Composite, *Materials*. 13 (2020) 5781. <https://doi.org/10.3390/ma13245781>.
- [162] K.S. Kumar, N. Choudhary, D. Pandey, L. Hurtado, H.-S. Chung, L. Tetard, Y. Jung, J. Thomas, High-performance flexible asymmetric supercapacitor based on rGO anode and WO₃/WS₂ core/shell nanowire cathode, *Nanotechnology*. 31 (2020) 435405. <https://doi.org/10.1088/1361-6528/aba305>.
- [163] H. Wei, X. Yan, S. Wu, Z. Luo, S. Wei, Z. Guo, Electropolymerized Polyaniline Stabilized Tungsten Oxide Nanocomposite Films: Electrochromic Behavior and Electrochemical Energy Storage, *J. Phys. Chem. C*. 116 (2012) 25052–25064. <https://doi.org/10.1021/jp3090777>.

- [164] Z. Duan, K. Deng, C. Li, M. Zhang, Z. Wang, Y. Xu, X. Li, L. Wang, H. Wang, Polyaniline-coated mesoporous Rh films for nonacidic hydrogen evolution reaction, *Chemical Engineering Journal*. 428 (2022) 132646. <https://doi.org/10.1016/j.cej.2021.132646>.
- [165] J. Zhu, L. Hu, P. Zhao, L.Y.S. Lee, K.-Y. Wong, Recent Advances in Electrocatalytic Hydrogen Evolution Using Nanoparticles, *Chem. Rev.* 120 (2020) 851–918. <https://doi.org/10.1021/acs.chemrev.9b00248>.
- [166] E. Fabbri, T.J. Schmidt, Oxygen Evolution Reaction—The Enigma in Water Electrolysis, *ACS Catal.* 8 (2018) 9765–9774. <https://doi.org/10.1021/acscatal.8b02712>.
- [167] A. Damian, S. Omanovic, Ni and NiMo hydrogen evolution electrocatalysts electrodeposited in a polyaniline matrix, *Journal of Power Sources*. 158 (2006) 464–476. <https://doi.org/10.1016/j.jpowsour.2005.09.007>.

Annexures

Permission for reusing figures from published articles

1) T. Ghosh et al., Adv. Electron. Mater. 2023, 9, 2201042



The screenshot shows the RightsLink interface for the article "Multiwavelength Color Switching from Polyaniline-Viologen Bilayer: Inching toward Versatile All-Organic Flexible Electrochromic Device". The article is published in Advanced Electronic Materials by John Wiley and Sons on Nov 30, 2022. The interface includes a Creative Commons Attribution (CC BY) license notice, stating that the article is open access and can be reused without permission. It also provides information about Wiley's professional reprint service, which offers high-quality reproductions of articles from over 1400 scientific and medical journals. The service offers various options such as peer-reviewed research, tailored collections, professional finishes, glossy covers, company branding, language translations, and prompt delivery. Contact information for the Reprints department is provided at the bottom.

CCC RightsLink

Multiwavelength Color Switching from Polyaniline-Viologen Bilayer: Inching toward Versatile All-Organic Flexible Electrochromic Device

Author: Rajesh Kumar, Manushree Tanwar, Love Bansal, et al
Publication: Advanced Electronic Materials
Publisher: John Wiley and Sons
Date: Nov 30, 2022

© 2022 The Authors. Advanced Electronic Materials published by Wiley-VCH GmbH

Open Access Article

This is an open access article distributed under the terms of the [Creative Commons CC BY](#) license, which permits unrestricted use, distribution, and reproduction in any medium, provided the original work is properly cited.

You are not required to obtain permission to reuse this article.

For an understanding of what is meant by the terms of the Creative Commons License, please refer to [Wiley's Open Access Terms and Conditions](#).

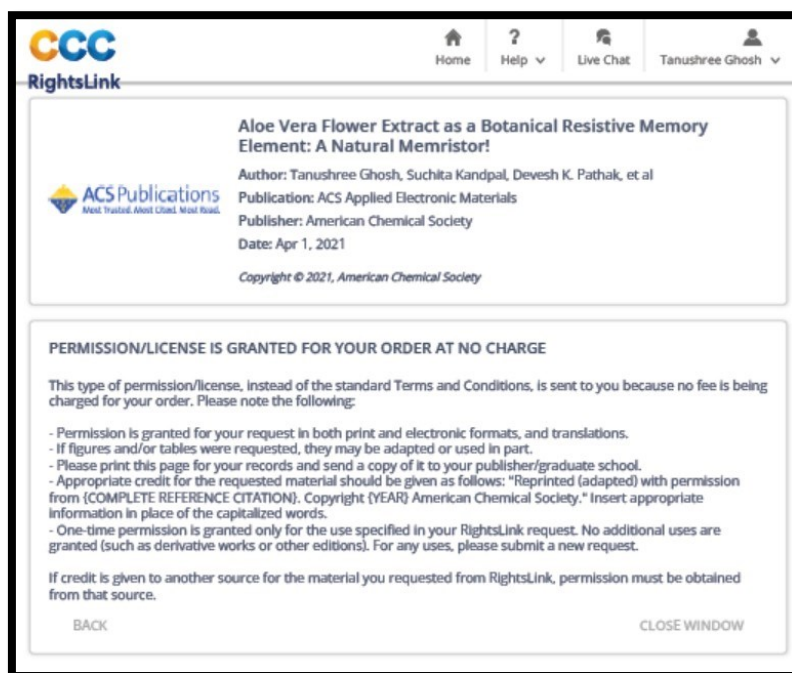
Permission is not required for this type of reuse.

Wiley offers a professional reprint service for high quality reproduction of articles from over 1400 scientific and medical journals. Wiley's reprint service offers:

- Peer reviewed research or reviews
- Tailored collections of articles
- A professional high quality finish
- Glossy journal style color covers
- Company or brand customisation
- Language translations
- Prompt turnaround times and delivery directly to your office, warehouse or congress.

Please contact our Reprints department for a quotation. Email corporatesaleseurope@wiley.com or corporatesalesusa@wiley.com or corporatesalesDE@wiley.com.

2) T. Ghosh et al., ACS Appl. Electron. Mater. 2021, 3, 1556–1559



The screenshot shows the RightsLink interface for the article "Aloe Vera Flower Extract as a Botanical Resistive Memory Element: A Natural Memristor". The article is published in ACS Applied Electronic Materials by American Chemical Society on Apr 1, 2021. The interface includes a Creative Commons Attribution (CC BY) license notice, stating that the article is open access and can be reused without charge. It provides detailed information about the permission granted, including that it applies to both print and electronic formats, and that figures and tables may be adapted or used in part. The user is instructed to print the page for records and send a copy to their publisher/graduate school. Appropriate credit for the requested material should be given as follows: "Reprinted (adapted) with permission from (COMPLETE REFERENCE CITATION). Copyright (YEAR) American Chemical Society." Insert appropriate information in place of the capitalized words. One-time permission is granted only for the use specified in your RightsLink request. No additional uses are granted (such as derivative works or other editions). For any uses, please submit a new request. If credit is given to another source for the material you requested from RightsLink, permission must be obtained from that source. The interface includes buttons for "BACK" and "CLOSE WINDOW".

CCC RightsLink

Aloe Vera Flower Extract as a Botanical Resistive Memory Element: A Natural Memristor!

Author: Tanushree Ghosh, Suchita Kandpal, Devesh K. Pathak, et al
Publication: ACS Applied Electronic Materials
Publisher: American Chemical Society
Date: Apr 1, 2021

Copyright © 2021, American Chemical Society

PERMISSION/LICENSE IS GRANTED FOR YOUR ORDER AT NO CHARGE

This type of permission/license, instead of the standard Terms and Conditions, is sent to you because no fee is being charged for your order. Please note the following:

- Permission is granted for your request in both print and electronic formats, and translations.
- If figures and/or tables were requested, they may be adapted or used in part.
- Please print this page for your records and send a copy of it to your publisher/graduate school.
- Appropriate credit for the requested material should be given as follows: "Reprinted (adapted) with permission from (COMPLETE REFERENCE CITATION). Copyright (YEAR) American Chemical Society." Insert appropriate information in place of the capitalized words.
- One-time permission is granted only for the use specified in your RightsLink request. No additional uses are granted (such as derivative works or other editions). For any uses, please submit a new request.

If credit is given to another source for the material you requested from RightsLink, permission must be obtained from that source.

BACK CLOSE WINDOW

3) T. Ghosh et al., ACS Appl. Bio Mater. 2021, 4, 5981–5986.

CCC RightsLink

Home ? Live Chat Sign In Create Account

Atypical Green Luminescence from Raw Cassia Siamea Extract: A Comparison with Red Emitting Tinospora Cordifolia

Author: Tanushree Ghosh, Suchita Kandpal, Chanchal Rani, et al
 Publication: ACS Applied Bio Materials
 Publisher: American Chemical Society
 Date: Aug 1, 2021
 Copyright © 2021, American Chemical Society

PERMISSION/LICENSE IS GRANTED FOR YOUR ORDER AT NO CHARGE

This type of permission/license, instead of the standard Terms and Conditions, is sent to you because no fee is being charged for your order. Please note the following:

- Permission is granted for your request in both print and electronic formats, and translations.
- If figures and/or tables were requested, they may be adapted or used in part.
- Please print this page for your records and send a copy of it to your publisher/graduate school.
- Appropriate credit for the requested material should be given as follows: "Reprinted (adapted) with permission from {COMPLETE REFERENCE CITATION}. Copyright (YEAR) American Chemical Society." Insert appropriate information in place of the capitalized words.
- One-time permission is granted only for the use specified in your RightsLink request. No additional uses are granted (such as derivative works or other editions). For any uses, please submit a new request.

If credit is given to another source for the material you requested from RightsLink, permission must be obtained from that source.

BACK CLOSE WINDOW

4) T. Ghosh et al., Adv. Opt. Mater. 2023, 2203126.

CCC RightsLink

Home ? Live Chat Tanushree Ghosh

Recipe for Fabricating Optimized Solid-State Electrochromic Devices and Its Know-How: Challenges and Future

Author: Rajesh Kumar, Anjali Chaudhary, Chanchal Rani, et al
 Publication: Advanced Optical Materials
 Publisher: John Wiley and Sons
 Date: Apr 4, 2023
 © 2023 Wiley-VCH GmbH

Review Order

Please review the order details and the associated [terms and conditions](#).

No royalties will be charged for this reuse request although you are required to obtain a license and comply with the license terms and conditions. To obtain the license, click the Accept button below.

Licensed Content		Order Details	
Licensed Content Publisher	John Wiley and Sons	Type of use	Dissertation/Thesis
Licensed Content Publication	Advanced Optical Materials	Requestor type	Author of this Wiley article
Licensed Content Title	Recipe for Fabricating Optimized Solid-State Electrochromic Devices and Its Know-How: Challenges and Future	Format	Print and electronic
Licensed Content Author	Rajesh Kumar, Anjali Chaudhary, Chanchal Rani, et al	Portion	Figure/table
Licensed Content Date	Apr 4, 2023	Number of figures/tables	1
Licensed Content Volume	0	Will you be translating?	No
Licensed Content Issue	0		
Licensed Content Pages	16		